

AD A051698

AD No.

DDC FILE COPY

SOLID STATE ELECTRONICS LABORATORY

2



STANFORD ELECTRONICS LABORATORIES

DEPARTMENT OF ELECTRICAL ENGINEERING

STANFORD UNIVERSITY · STANFORD, CA 94305

STUDY OF THE ELECTRONIC SURFACE STATE OF III-V COMPOUNDS

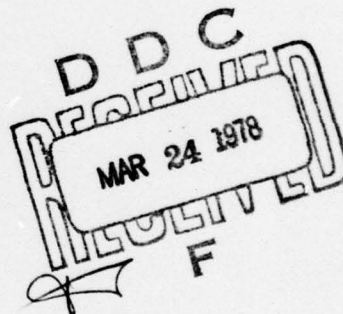
SEMI-ANNUAL TECHNICAL PROGRESS REPORT

W. E. Spicer, Principal Investigator

Telephone: (415) 497-4643

15 September 1977

NIGHT VISION LABORATORY
U.S. Army Electronics Command
Fort Belvoir, Virginia 22060



Sponsored by

DEFENSE ADVANCED RESEARCH PROJECTS AGENCY
DARPA ORDER NO. 2182
PROGRAM CODE NO. 4D10

CONTRACT NO. DAAK02-74-C-0069

The views and conclusions contained in this document are those of the authors and should not be interpreted as necessarily representing the official policies, either expressed or implied, of the Defense Advanced Research Projects Agency of the U.S. Government.

DISTRIBUTION STATEMENT A
Approved for public release;
Distribution Unlimited

⑥
STUDY OF THE ELECTRONIC SURFACE STATE OF III-V COMPOUNDS .

⑨
SEMI-ANNUAL TECHNICAL PROGRESS REPORT.

⑩ W. E. Spicer Principal Investigator

Telephone: (415) 497-4643

⑪ 15 September 1977

⑫ 131 p.

NIGHT VISION LABORATORY
U.S. Army Electronics Command
Fort Belvoir, Virginia 22060



Sponsored by

DEFENSE ADVANCED RESEARCH PROJECTS AGENCY
DARPA ORDER NO. 2182
PROGRAM CODE NO. 4D10

⑬ CONTRACT NO. DAAK02-74-C-0069

Effective: 1973 September 01

✓ DARPA Order-2182
Expiration: 1977 September 30 (\$564,360)

STANFORD ELECTRONICS LABORATORIES
STANFORD UNIVERSITY
STANFORD, CALIFORNIA 94305

4030575-
The views and conclusions contained in this document are those of the authors and should not be interpreted as necessarily representing the official policies, either expressed or implied, of the Defense Advanced Research Projects Agency of the U.S. Government.

332400

JB

CONTENTS

	<u>Page</u>
I. OVERVIEW	1
II. ANALYZED WORK	2
III. SUMMARY OF APPENDED PAPERS	3
IV. SUMMARY OF MOST RECENT RESULTS	6
V. FUTURE PLANS	8
Appendix A. EVIDENCE FOR A NEW TYPE OF METAL- SEMICONDUCTOR INTERACTION ON GaSb	9
Appendix B. VALENCE BAND STUDIES OF CLEAN AND OXYGEN EXPOSED GaAs (110) SURFACES	18
Appendix C. CHEMISORPTION AND OXIDATION STUDIES OF THE (110) SURFACES OF GaAs, GaSb, AND InP	62

ACCESSION for	
NTIS	White Section <input checked="" type="checkbox"/>
DDC	Buff Section <input type="checkbox"/>
UNANNOUNCED	<input type="checkbox"/>
for 50 on file.	
BY	
DISTRIBUTION/AVAILABILITY CODES	
SP CIAL	
A	

Chapter I

OVERVIEW

At the time of the last semiannual report, we had just started experiments at SSRP to study metal overlayers on the (110) cleavage faces of GaAs, GaSb, and InP. Since then, we have completed our first set of measurements which consisted of work on both the 8° ($9 \leq h\nu \leq 30$ eV) and 4° ($30 \leq h\nu \leq 600$ eV) lines at SSRP. In this work, we concentrated on studying Au on Ga and the (110) cleavage faces of GaAs, InP, and GaSb, as well as studying In on InP (110). We will not discuss our work on In-Au alloys since it was covered in our last Quarterly Report. We have analyzed the data dealing with Au on GaSb, and it is presented in Appendix A.

Activities during this period included the following. (1) We finished assembling and used our new vacuum system in a number of experiments. This system gives us the capability of doing photoemission, Auger spectroscopy, and LEED on a sample that can be prepared by cleaving, heat cleaning, or ion bombardment and annealing. We also have evaporators (gold and cesium) in the system (see section on future plans for planned additions to this system). (2) We started developing the software for our new computer system. This work is progressing quite well. (3) We continued our work on developing the capability of heat cleaning GaAs surfaces (~~see Chapter IV~~).

Chapter II

ANALYZED WORK

The metal-overlayer work proved to be quite exciting so that we have put a major part of our effort into quickly analyzing this data. The first result of this work has been a short paper emphasizing gold on GaSb (110) and GaAs (110) (see next section).

In our previous reports, we have emphasized the fact that the GaAs (110) surface is very strained and that rearrangements of the surface lattice could take place as the result of very small amounts of contaminants. We have now finished a paper where we compare the photoemission results for 16 cleaves from a total of four different samples. We correlated the results of photoemission, band bending, and partial yield measurements and tied them in with recent theoretical calculations of the valence band electronic structure for the relaxed and ideal surface.

Chapter III

SUMMARY OF APPENDED PAPERS

As mentioned in the previous chapters, our metal overlayer studies have proved to be quite exciting. In Appendix A, we present the first analysis of our data for gold on GaSb, GaAs, and InP with an emphasis on trying to understand the different Fermi-level pinning behavior seen in the Au-GaSb system compared to Au-GaAs on Au-InP. Gold pins the Fermi level of GaSb at the valence band maximum (VBM) and at about mid-gap for InP or GaAs. There have been some recent theoretical studies postulating that metal-induced extrinsic states are responsible for the pinning. However, these studies have assumed an ideal semiconductor-metal interface and have not given deep insights into how these states are induced.

In our work, we monitored the core levels and valence bands as gold was evaporated onto the surface of the sample. As mentioned in previous reports, the escape depth of the photoemitted electrons is very short. Therefore, we are able to monitor the composition of the interface layer at the same time as the Schottky barrier is being formed. Experimentally, we find that, as a gold layer is built up on the GaSb (110) surface, the emission from the Ga-3d level drops in proportion to the increase in emission from the Au-4f levels until the Ga emission completely disappears. The Sb emission, on the other hand, drops to about 0.6 of what it was on the clean surface and then remains almost constant, even for gold films thicker than (roughly) 50 Å. In the case of GaAs or InP, the emission from both the column III and column V elements drops simultaneously until a constant value is reached again for thick films of gold. Therefore, we have found that the GaSb surface dissociates upon addition of Au, resulting in a film of Sb that "floats" on the Au and a nonstoichiometric interface consisting of an excess of Ga. The excess Ga atoms create a large number of acceptor states which make the interface region p-type and pin the Fermi level at the valence band maximum. The InP and GaAs surfaces also dissociate upon addition of Au. However, since both the anion and cation come off together, possibly as a dimer, the resulting interface does not experience a large departure from

stoichiometric. These results will have a very significant impact on future theoretical considerations since now the nonstoichiometry of the Au-GaSb interface must be included. There are also implications in device tailoring: Now that we know the composition of the interface, it may be possible to alter this composition, for example, by heating or adding reactive materials to remove the pinning states and thus possibly to alter the barrier characteristics.

By studying the valence bands of GaAs in a photon energy region where direct transitions are still important (i.e., ~ 21 eV), we studied the effects of strain on the cleaved GaAs (110) surface and related this to possible rearrangements of the surface. As mentioned in Chapter II, recent theoretical calculations have shown that the valence band electronic structure at the surface is strongly affected by the surface lattice. Therefore, by looking for changes in the valence band as a function of cleavage or of oxygen coverage, it may be possible eventually to correlate these changes with changes in the rearrangements of the surface atoms. By correlating the photoemission results with band bending and partial-yield spectroscopy measurements from a large number of samples, we found that Fermi-level pinning at midgap of n-type GaAs (110) is caused by extrinsic states. The exact nature of these states is not yet clear, but the surfaces with Fermi-level pinning were strained as evidenced by a smeared valence-band emission. This smearing was removed by as little as one oxygen atom per 10^4 to 10^5 surface atoms. This implies that the oxygen has very long-range effects in causing spontaneous but small rearrangement of the surface lattice and removing surface strains. When about 5% of a monolayer of oxygen is adsorbed, a major change in the electronic structure takes place. Again, the oxygen coverage is very small, which suggests long range effects now leading to a fairly large rearrangement of the surface lattice. Furthermore, by comparing the oxygen-induced emission from exposures greater than 10^7 LO_2 with the spectra from gas-phase photoemission measurements on molecular oxygen, we propose that the oxygen is chemisorbed as a molecule on the (110) surface of GaAs.

Finally, in Appendix C, we present a detailed analysis of all our chemical shift results on the oxidation of GaAs, GaSb, and InP. Some

of the data have been presented in previous reports, but here we tie all our previous results together and give a ligand shift analysis for the observed chemical shifts.

When the cleaved GaAs (110) surface is exposed to molecular oxygen in the ground state, chemisorption onto only arsenic atoms results. No back bonds are broken even for large exposures. Room temperature oxidation of the surface can be induced by exciting the oxygen, e.g., by an ionization gauge. The adsorption of excited oxygen is initially the same as for unexcited, except 500 times faster. However, after >20% of a monolayer has been adsorbed, further exposure to excited oxygen causes back bonds to be broken; $\text{As}_2\text{O}_5/\text{AsO}_2$ and Ga_2O_3 are formed. Larger doses of excited oxygen result in the formation of thicker oxides composed primarily of Ga_2O_3 with small amounts of elemental As (or As bound to only one Ga) and As_2O_3 , most of which has sublimed from the surface. No $\text{As}_2\text{O}_5/\text{AsO}_2$ is seen in the thicker oxide because there is a deficiency of oxygen and any partially oxidized Ga present will reduce the arsenic oxides. The escape depth for GaAs (110) was measured for electron kinetic energies between 20 and 200 eV. This range includes the minimum in the escape depth which is about 6 Å at 60 eV. No chemical shift in the core levels between the atoms on the surface and in the bulk was observed. GaSb (110) and InP (110) surfaces were also studied. InP behaves like GaAs, whereas the GaSb is oxidized immediately even when exposed to only unexcited oxygen. The oxygen uptake curves for GaSb and GaAs were compared and found to be quite different, with a sticking coefficient at zero coverage, of 2×10^{-4} for GaSb and 8×10^{-10} for GaAs.

Chapter IV

SUMMARY OF MOST RECENT RESULTS

Our results on metal overlayers belong in this section, but they have already been described in the previous section and in Appendix A, so we will concentrate on our other work here.

As mentioned in Chapter I, we have assembled our new vacuum system and have tested it. In particular, we have done some preliminary work with the LEED apparatus in collaboration with Professor P. Mark, showing that the lattice rearrangement is similar for cleaved and ion sputtered-annealed GaAs. We are presently determining its applicability to our metal overlayer studies as described in Chapter V.

Our work on preparing GaAs surfaces by heat cleaning alone and by argon-ion bombardment and annealing has progressed to the stage where we can reproducibly obtain clean surfaces. We are now concentrating on trying to determine which cleaning procedures give the highest quality surfaces. At present, the quality of the surface is gauged by looking at the sharpness and relative amplitudes of the peaks in the energy distribution curves (EDC's) using $h\nu \sim 10$ eV. In the discussion that follows, we will summarize our results on both the heat cleaning and ion bombardment and annealing of the (110) and $(\bar{1}\bar{1}\bar{1})$ surfaces of GaAs.

We found, as expected, that heat cleaning alone does not remove the carbon contamination which was present on the crystal before it was put into the vacuum system. However, atmospheric oxides are removed from the (110) surface by heating to 550°C and from the $(\bar{1}\bar{1}\bar{1})$ surface by heating to 600°C. Subsequent heating at lower temperatures seems to improve the surfaces, possibly by annealing surface strains and defects more completely. Therefore, heat cleaning can be used if suitable chemical etchings and/or other preparations are found that can minimize the amount of carbon that is left on the surface.

If carbon is present on the surface, ion bombardment must be used to remove it. However, the straightforward procedure of ion bombardment at a fixed ion energy followed by annealing results in EDC's that are smeared out, indicating that the surface is not perfect. One procedure that does work is an ion bombardment in which the ion energy is gradually

reduced from about 700 eV to under 200 eV followed by immediate annealing or by exposing to oxygen and then annealing. The reason this procedure works can be explained as follows. First, the high energy ion bombardment removes the carbon and oxygen but damages the surface. The subsequent ion bombardments at lower energy remove the previous damage while introducing less damage of their own. The damage caused by the final bombardment can then be removed simply by annealing. Ion bombardment may result in an arsenic-rich surface. Therefore, exposing the surface to oxygen before annealing may facilitate the final cleaning since oxides of arsenic are more volatile than arsenic, gallium, or gallium oxide. This may allow any excess arsenic on the surface to easily come off as As_2O_3 .

We have also found that argon tends to implant itself in the sample and annealing temperatures are too low to drive it off. (Raising the temperature would simply serve to dissociate the crystal.) This effect may be minimized by ion bombarding at a small angle to the surface and by heating the sample during bombardment to decrease any ion-channeling effects. In addition, ion bombardment at shallow angles should help to insure that any damage will be confined to the topmost surface layers.

Chapter V

FUTURE PLANS

Our future plans are quite extensive, and we will list here the major projects we hope to undertake in the next six months. As mentioned above, we now have the capability of performing LEED. We hope to apply this technique to our study of metal overlayers (including Al, Au, and Cs) on GaAs, GaSb, and InP in order to observe possible changes in the surface structure taking place due to adsorption of the metal. We will also calibrate the coverage using Auger electron spectroscopy (AES). We are quite concerned about the effects of the electron beams on the surface. Consequently, we will monitor any possible electron beam effects by looking for changes in the top 5 eV of the valence bands using $h\nu = 21$ eV.

We will perform experiments similar to the ones described above in studying the oxidation of GaAs except that the oxygen adsorptions will be done as a function of temperature. This may enable us to discern any adsorption of oxygen onto surface Ga atoms and will also allow us to study annealing effects. If oxygen is adsorbed onto the surface Ga atoms, we expect the bonding to be weak, possibly enabling removal of oxygen from the Ga by gentle heating. Our end object is to develop passivation techniques.

We will also reinvestigate the valence bands of oxygen-covered GaAs. We have found that unexcited oxygen gives rise to three peaks in the valence band emission, as pointed out in Appendix B. We will study these peaks as a function of photon energy, from 15 to 40 eV, to try to determine whether the adsorbed oxygen is atomic or molecular.

In our future work on the heat-cleaned surfaces, we will try to characterize the quality of the surfaces in more detail. We will apply some of the techniques described in Appendix B (employing 21.2 eV radiation) to determine the nature of any possible strains on these surfaces. In addition, we will use LEED as an independent check of the surface perfection and AES to determine the surface stoichiometry. As soon as we are satisfied with this work, we will perform experiments at SSRP on these surfaces at $h\nu \sim 100$ eV to further study the chemistry of the surface layers.

Appendix A

EVIDENCE FOR A NEW TYPE OF METAL-SEMICONDUCTOR INTERACTION ON GaSb*

P. W. Chye, I. Lindau, P. Pianetta,
C. M. Garner, and W. E. Spicer
Stanford Electronics Laboratories
Stanford University
Stanford, California 94305

Abstract

The formation of Au-semiconductor Schottky barriers is studied using soft x-ray photoemission spectroscopy. The Au-GaSb interface is highly nonstoichiometric due to selective removal of Sb. This nonstoichiometry results in acceptor-like states which pin the Fermi level at the interface and determine the Schottky barrier height.

*Work supported by the Office of Naval Research Contract No. N00014-75-C-0289; by the Advanced Research Projects Agency of the Department of Defense monitored by Night Vision Laboratory, U.S. Army Electronics Command under Contract No. DAAK02-74-C-0069; by the National Science Foundation Contract No. DMR 73-07692 A02 in cooperation with the Stanford Linear Accelerator Center and the U.S. Energy Research and Development Administration.

Metal-semiconductor interfaces have been studied extensively both theoretically and experimentally. However, well established fundamental knowledge is still lacking, although certain empirical rules, e.g. the "two-thirds rule" of Mead and Spitzer,¹ or the more recent column V rule of McCaldin et al² have been suggested over the years. While these empirical rules have been useful, they offer little deep insight into the physics of the interface. Why, for example, is the Fermi level (E_f) pinned by metals at the valence band maximum (VBM) on GaSb and above midgap on InP? What causes the pinning? Recent studies³ led to general agreement that metal induced extrinsic states are responsible for the pinning; however, there is still insufficient understanding of how these states are induced. Andrews and Phillips⁴ have classified metal-nonmetal interfaces into four broad categories. In this paper, we present evidence for a new type of metal-semiconductor interaction not previously considered, and show, for the first time, how this interaction produces the pinning states on GaSb. The interaction is different in nature on InP and GaAs as are the pinning positions.

The experimental technique used was soft x-ray photoemission spectroscopy, using synchrotron radiation from the SPEAR storage ring at SLAC as the light source. The radiation was tuned by a monochromator such that the emerging photoelectrons have very short escape depths. Formation of the Schottky barrier was by repeated evaporation from a Au bead in ultrahigh vacuum ($<10^{-10}$ torr) onto a freshly cleaved (110) surface. Energy distribution curves (EDC's) were recorded after each evaporation using a double pass cylindrical mirror analyzer with a resolution of 0.3 eV. In this manner, the formation of the Schottky barrier was monitored as the Au layer was built up. For the first evaporations, the samples

were rotated rapidly through the evaporated Au stream. Evaporation times and currents were gradually increased so that by the last evaporations the samples were exposed to the evaporator for ~20 to 30 seconds. However, heating of the sample surfaces is expected to be small as relatively low evaporator currents were used. At this point, the crystal surfaces appear golden.

Figure 1 shows a set of EDC's of n-GaSb at $h\nu = 120$ eV, with E_f taken as the reference level. The photoelectrons originating from the Ga-3d and Sb-4d core levels have kinetic energies that lie within the broad minimum in the escape depth,⁵ so the probing depths for Ga and Sb should be close, i.e., within the last two molecular layers. The striking thing in Fig. 1 is that the Ga-3d emission decreases until it disappears altogether while the Sb-4d emission remains strong as increasing amounts of Au are deposited. Near saturation, the Sb emission has dropped to roughly two-thirds that of the cleaved surface and remains at that level. This may be contrasted with Fig. 2, where EDC's for Au-covered InP's are shown. The leading part of the EDC is taken at $h\nu = 120$ eV while the back portion (P-2p) is taken at $h\nu = 165$ eV. Both In and P emission decrease together as Au coverage is increased to a small fraction of the original amplitude. The simultaneous reduction of Ga and As emission is also observed on GaAs.

What the above suggests is the following: in GaSb, on Au deposition Sb breaks apart from the crystal and moves to the surface of the Au layer, leaving behind a highly nonstoichiometric interface rich in Ga. At saturation, the emission from the Sb suggests a layer "floating" on top of the Au. Thus, one observes almost constant Sb emission at a somewhat reduced level. Explanation of this data in terms of "clumping" of

Au to form islands is implausible since that would not lead to preferential decrease in Ga emission. In contrast, in InP or GaAs, there is no such strong preferential removal of one member of the 3-5 compound. However, neither core peak disappears after large Au deposition as does the Ga peak in GaSb. This suggests that both components may come to the surface in this case. Further work is called for here.

Based on the above, we propose the following model of Au Schottky barrier formation on GaSb. As Au is deposited on the GaSb surface, the Sb segregates out to the surface leaving behind an excess of Ga at the interface. The excess Ga creates a large number of acceptor-like states⁶ which makes the interface region p-type and pins E_f at the VBM. Whereas, there is no similar preferential removal of one element in InP and GaAs. E_f therefore is not pinned at the VBM in these materials. The mechanism for E_f pinning in InP and GaAs is probably different and may, for example, be surface rearrangement or relaxation. In GaSb, it is known that the highly electropositive Cs pins E_f at the VBM as well. Thus, pinning E_f through the mechanism of creating a nonstoichiometric interface in GaSb is probably not specific to a single metal. The highly electronegative Au and the highly electropositive Cs⁷ produce the same pinning position on GaSb--the metal used is irrelevant as long as it can selectively remove the Sb.

We have, in this letter, presented evidence for a new type of metal-semiconductor interaction. Au interacts strongly with GaSb, but not in the sense of strong chemical bonding which would give rise to large chemical shifts. Rather, it selectively removes the Sb atoms from the interface and creates a highly nonstoichiometric interface region which becomes p-like to pin E_f at the VBM. Theoretical calculations of the

electronic structure of the Au-GaSb interface must then take this non-stoichiometry into account. There are also implications in device "tailoring." For example, by using an alloy overlayer, one component of which reacts with the Ga to remove the pinning states, different barrier characteristics might be obtained, e.g. Sb may be evaporated with or before the Au. Another possibility is simultaneous oxidation to form Ga oxides. Heating of the interface may also alter the electrical characteristics by removing Ga from the interface through diffusion. It is clear that more work needs to be done to completely understand the many different metal-semiconductor interfaces.

Acknowledgment

We would like to thank Professor James Gibbons for helpful discussions.

References

1. C. A. Mead and W. G. Spitzer, Phys. Rev. 134, A713 (1964).
2. J. O. McCaldin, T. C. McGill, and C. A. Mead, Phys. Rev. Lett. 36, 56 (1976).
3. J. E. Rowe, S. B. Christman, and G. Margaritondo, Phys. Rev. Lett. 35, 1471 (1975); J. E. Rowe, J. Vac. Sci. Technol. 13, 798 (1976).
4. J. M. Andrews and J. C. Phillips, Phys. Rev. Lett. 35, 56 (1975).
5. I. Lindau and W. E. Spicer, J. Electron Spectro. 3, 409 (1974).
6. R. F. Brebrick, Treatise on Solid State Chemistry, Vol. 2, Ed., N. B. Hannay, Plenum Press, New York (1975).
7. P. W. Chye, T. Sukegawa, I. A. Babalola, H. Sunami, P. Gregory, and W. E. Spicer, Phys. Rev. B 15, 2118 (1977).

Figure Captions

1. EDC's for GaSb as Au is deposited. Note the strong emission from the Sb-4d even when the Ga-3d emission has disappeared.
2. EDC's for InP. Unlike GaSb, emission from both In and P decreases initially as Au is deposited. However, the emission does not completely disappear even for relatively thick Au layers as does the Ga emission in Fig. 1.

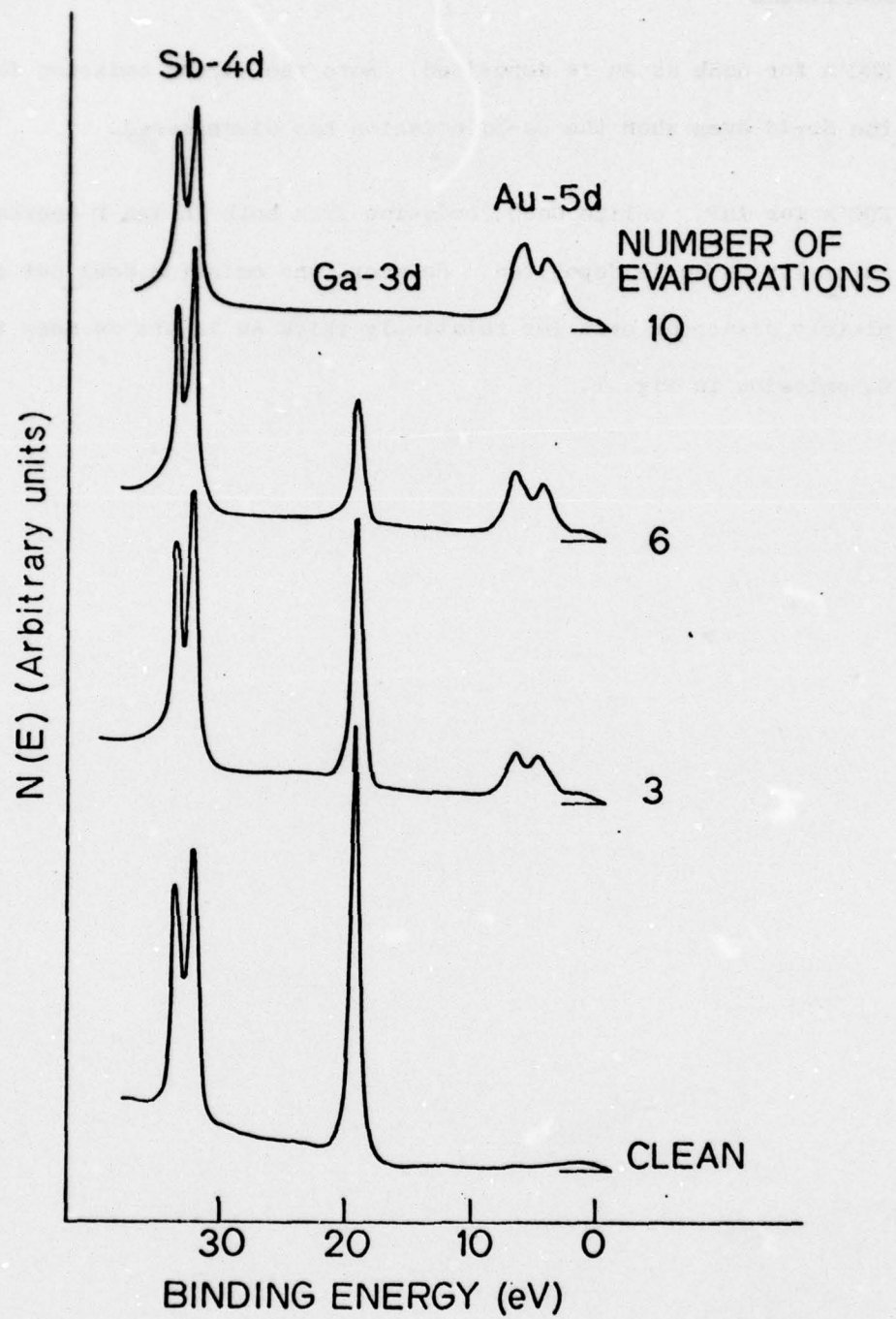


Fig. 1

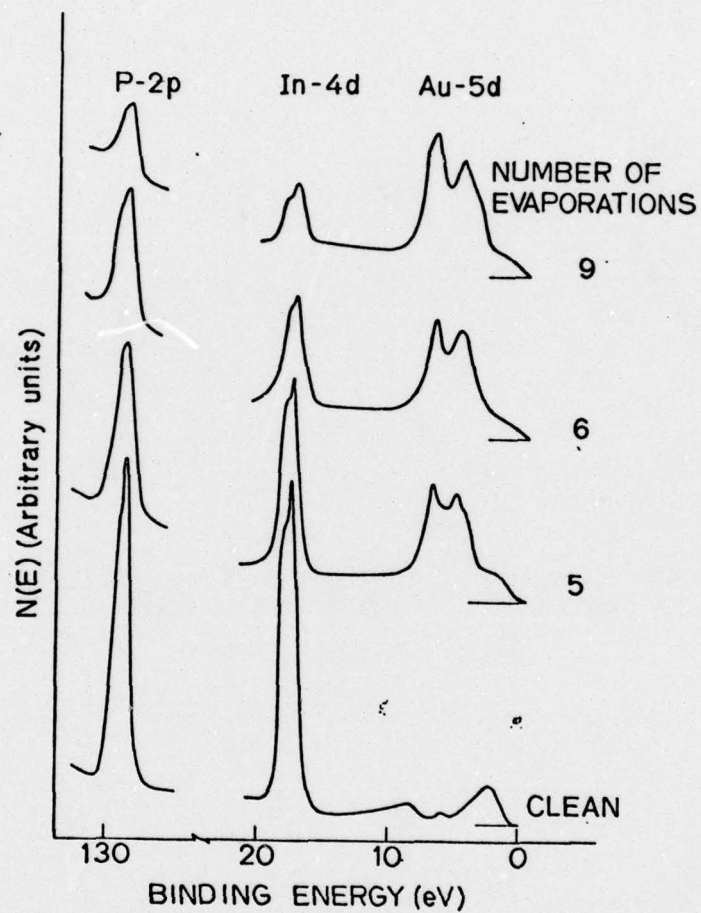


Fig. 2

Appendix B

VALENCE BAND STUDIES OF CLEAN AND OXYGEN EXPOSED GaAs (110) SURFACES*

P. Pianetta, I. Lindau, P. E. Gregory,**
C. M. Garner, and W. E. Spicer
Stanford Electronics Laboratories
and
Stanford Synchrotron Radiation Project
Stanford University
Stanford, California 94305

Abstract

We found, by correlating band bending, ultraviolet photoemission spectroscopy, and partial yield spectroscopy measurements, that Fermi level pinning at midgap of n-type GaAs (110) is caused by extrinsic states. The exact nature of these states is not yet clear, but the surfaces with Fermi level pinning were strained as evidenced by a smeared valence band emission. This smearing was removed by as little as one oxygen per 10^4 to 10^5 surface atoms. This implies that the oxygen has very long range effects in causing spontaneous but small rearrangement of the surface lattice and removing surface strains. When about 5% of a monolayer of oxygen is adsorbed, a major change in the electronic structure takes place. Again, the oxygen coverage is very small, which suggests long range effects now leading to a fairly large rearrangement of the surface lattice. Finally, from comparing the oxygen induced emission for exposures greater than 10^7 LO_2 , with the spectra from gas phase photoemission measurements on molecular oxygen, we suggest that the oxygen is chemisorbed as a molecule on the (110) surface of GaAs.

*Work supported by the Advanced Research Projects Agency of the Department of Defense monitored by Night Vision Laboratory, U.S. Army Electronics Command under Contract No. DAAK 02-74-C-0069; by the Office of Naval Research Contract No. N00014-75-C-0289; by the National Science Foundation Contract No. DMR 73-07692 A02 in cooperation with the Stanford Linear Accelerator Center and the U.S. Energy Research and Development Administration.

**Present address: Varian Associates, Palo Alto, California.

I. INTRODUCTION

The atomic structure of the GaAs (110) surface has been the object of numerous theoretical and experimental studies. LEED measurements¹ as well as theoretical predictions² have suggested that the GaAs (110) surface rearranges with the surface arsenic atoms moving out and the surface gallium atoms in. The exact values of these displacements are still under investigation. It is not clear how useful LEED is in detecting small changes in the surface rearrangement due to defects or oxygen adsorption. Recent calculations have shown that the valence band electronic structure of GaAs (110) surfaces depends markedly on the surface rearrangement.^{3,4} It is difficult, at this point, to correlate differences in the experimentally determined valence band electronic structures to actual lattice distortions since the calculations that have been performed consider only the extreme cases of the fully relaxed and ideal surfaces. Small displacements from these two extremes have not yet been considered. Consequently, we will not attempt detailed comparisons with calculated surface densities of states; instead, we will concentrate on looking at the differences in the surface valence band electronic structure, as determined by photoemission, between a large number of samples as well as the effects of exposure to oxygen.⁴

The valence band of GaAs consists of four bands extending approximately 14 eV below the valence band maximum (VBM).⁶ The lowest lying band (giving a peak 9 to 14 eV below the VBM) is primarily s-like and associated with the arsenic.^{7,8} The next band (giving a peak centered 6.75 eV below the VBM) is composed of s-like states around the gallium and p-like states around the

arsenic.^{7,8} The remaining two bands (giving the structure for the first 5 eV below the VBM and containing at least four peaks) are completely p-like around the arsenic.^{7,8} The structures associated with these bands can be seen in Figs. 1-4 where we show energy distribution curves (EDC's) for the cleaved GaAs (110) surface taken at 21 eV (see below for detailed discussion of these spectra; here, we will just use them as examples of the general GaAs valence band structure). All the peaks are easily seen except for the one 9-14 eV below the VBM, both because it is masked by the scattering tail and because the cross-section for this peak (s-like) is less than that of the p-like peaks at this photon energy. We should also note that the band structure of GaAs has a large number of critical points in the upper 5 eV of the valence band compared to the region 5-14 eV below the VBM.^{9,10} The critical points should be the part of the band structure that is the most sensitive to any changes in the surface lattice structure. Thus, we should expect the most significant changes to occur in the upper 5 eV of the EDC's. The calculations of Refs. 3 and 4 show that the top 5 eV of the valence band do indeed show the most changes due to a rearrangement of the surface.

Another very sensitive technique which can be used to characterize semiconductor surfaces is the measurement of band bending.^{11,12,13} The presence of band bending is seen as a difference in the position of the Fermi level at the surface with respect to that in the bulk which is determined by the doping. For GaAs (110), it has been recently shown from contact potential difference¹³ measurements and photoemission^{4,14} that the bands are flat all the way up to the surface within the experimental

uncertainty. This means that for p-type GaAs (110) the Fermi level is at the VBM, while for n-type it is at the conduction band minimum (CBM).

In earlier work,^{11,12} however, Fermi level pinning was detected in n-type GaAs (110). This pinning was attributed to the existence of an empty band of intrinsic surface states in the middle of the gap.¹¹ These results were reinforced by partial yield measurements¹⁵ showing strong transitions from the Ga-3d levels to states which seemed to be located in the middle of the gap (the partial yield results have since been reinterpreted to be consistent with the absence of band bending).¹⁶

The presence or absence of intrinsic states in the gap has important implications bearing on surface band structure calculations. For example, calculations based on the ideal surface result in an empty band of surface states in the gap,⁷ whereas, those based on the rearranged surface give an empty band of surface states whose center of gravity is in the conduction band.³ Therefore, it is important to clarify some of the present confusion as to the origin of the states that cause the Fermi level pinning in n-type GaAs (110). Some workers have assumed the pinning observed in the earlier work was always caused by surface roughness which was the result of bad cleaves.^{13,14,17} However, some of our previous work has shown that pinning is observed in macroscopically good cleaves as well.^{4,18} Thus, the Fermi level pinning could also be caused by states which are the result of surface strain or other microscopic defects in the crystal.

In order to investigate more systematically the possible relationship between the Fermi level pinning on clean n-type GaAs (110) with

surface defects or strains as well as the nature of the states causing the pinning (i.e., whether they are actually intrinsic or extrinsic), we performed a series of experiments where we studied photoemission and partial yield spectroscopy measurements from four different samples (16 total cleaves). We concentrated on the valence band electronic structure, particularly the top 5 eV, and correlated the changes in this structure with both the Fermi level pinning and partial yield for the clean and oxygen exposed surfaces.

II. EXPERIMENTAL

A. Apparatus and Procedure

The experimental apparatus has been described in detail elsewhere,⁵ and only details which are pertinent to this experiment will be described below.

We studied four separate samples from two suppliers. Three of the samples came from Laser Diode Corporation (LD). These will be designated samples LD1, LD2, and LD3. LD1 and LD2 were cut from the same boule. The third came from MCP Electronics in England (MCP). The samples were 5 mm \times 5 mm \times 12 mm with the (110) axis along the long dimension. All samples were n-type and had the following doping: LD1 and LD2, Te doped with $n = 0.5 \times 10^{18} \text{ cm}^{-3}$; LD3, Te doped with $n = 3.5 \times 10^{17} \text{ cm}^{-3}$; and, MCP, Te doped with $n = 1.7 \times 10^{18} \text{ cm}^{-3}$. The MCP sample was the same sample used by Gregory and Spicer in their earlier work.¹¹

The sample chamber consists of a stainless steel UHV bell jar, base pressure $< 1 \times 10^{-10}$ Torr. The pumping system is a 240 L/sec ion

pump plus titanium cryopump with a poppet valve for sealing the pump from the main chamber. The samples are mounted in a carousel being held at one end with a metal clamp which exerts a minimum amount of pressure on them. Four cleaves, each 2 mm thick, can be taken from each sample. The samples are cleaved by carefully squeezing them between an annealed copper anvil and a tungsten carbide blade. A cleave is judged to be "good" if it has a shiny, mirror-like surface. We have since performed preliminary optical measurements and found that the cleaves appear comparable to the "good" cleaves of Huijser and Van Laar in terms of step density.

All cleaves were performed at pressures $< 1 \times 10^{-10}$ Torr, and no hot filament or ionization gauges were used during the measurements or oxygen exposures except as specifically noted. Gas exposures were performed by admitting research grade oxygen into the vacuum system through a bakeable leak valve. For large exposures, an auxiliary pumping system was used to return the main chamber to pressures below $\sim 10^{-8}$ Torr.⁵ Binding energies were measured with respect to the VBM and the position of the Fermi level with respect to the VBM was determined by referencing to the Fermi level of a gold film evaporated in situ on a substrate in electrical contact with the sample.¹⁹

Synchrotron radiation in the range 9 to 30 eV from the "8°" line at the Stanford Synchrotron Radiation Project⁵ was used in this work. The radiation is first monochromated by a Seya-Namioka monochromator and then enters the chamber through a bakeable straight through valve. The energy of the photoemitted electrons is then determined by a double pass cylindrical mirror analyzer operated in the retarding mode. This mode insures a constant resolution which is equal to 0.6% of the electron pass energy. In these measurements, we used a pass energy of 25 eV,

giving an electron energy resolution of 0.15 eV. Counting rates over 2×10^4 C/sec in the GaAs valence band at $h\nu = 20$ eV were typical.

B. Results

In Figs. 1-4, we show EDC's taken at 21 eV (20 eV in Fig. 4) for several cleaves from each of samples LD1, LD2, LD3, and MCP. We will designate successive cleaves from a given sample as cleaves A, B, C, etc., and we will refer to cleave A from sample LD1 as "sample LD1A;" similarly, cleave A from sample MCP is "sample MCPA," and so on. The Fermi level at the surface is marked on each curve. The horizontal scale gives the energy below the VBM. The position of the Fermi level relative to the valence band maximum as well as to the peak at a binding energy of 6.75 eV is plotted in Fig. 5. (This figure will be discussed below.)

In Table I, we give a summary of the samples that were studied. This table includes the figure numbers where the spectra for the various samples are located, an indication as to the sharpness of the spectral features in the top 5 eV of the valence band for each sample and a classification of each sample based on the band bending.

The first thing we should notice from Figs. 1-4 is that the peak locations are constant from sample to sample and cleave to cleave. Relative peak heights, on the other hand, vary considerably. As an extreme example, compare sample LD1C, i.e., sample LD1, cleave C (Fig. 1) with samples MCPA & B (Fig. 4). In Sample LD1C, there is a large peak 1.75 eV below the VBM, whereas it is relatively small on MCPA. There is, however, better agreement in the shape of the valence band structure

when samples from the same boule are compared. For example, all cleaves from the same sample are similar and all cleaves from samples LD1 and LD2 (Fig. 2), which are different samples from the same boule, give similar results.

The next observation that will be made concerns the "sharpness" of the individual spectra for the clean samples. This is a very subjective judgement and open to question, but we feel that the observations are general enough that they should be of some use. In all cases, samples with the Fermi level located at the conduction band minimum are somewhat sharper, i.e., more structure can be resolved in the top 5 eV of the EDC. For example, compare LD1C to LD1A, B, or D; also, compare MCPA to MCPB or MCPC. LD3A, B, or C (Fig. 4) do not exhibit significant surface Fermi level pinning, and they have very well resolved structure in the top of the valence band. An exception is sample LD2. Cleaves A, C, and D from sample LD2 are as sharp as LD1C, yet they exhibit pinning while LD1C does not. Samples LD2B and E (not shown) had a very smeared out structure and exhibited Fermi level pinning. Thus, the most general statement we can make concerning these observations is that, if a sample has an unpinned Fermi level, the structure in the upper 5 eV of the valence band will be well defined. If the Fermi level is pinned, the majority of samples will have a smeared out valence band.

We should also note at this point that, in the case of LD1C, the structure in the top of the valence band became sharper after the sample had been in the vacuum system at 1×10^{-10} torr for 12 hours. In the case of MCPB, however, the structure did not change noticeably even after 20 hours at 10^{-10} torr. In both cases, there was movement of the

position of the Fermi level. We are not yet sure if the sharpening is due to some sort of surface lattice relaxation with time or if it is due to contamination. At a base pressure of $\sim 10^{-10}$ torr, the sharpened structure had an exposure of ~ 4 L to the residual gas in the chamber. As we will show below, definite effects in the valence band are observed with the addition of less than 100 L of oxygen (in some cases, effects are seen for exposures as low as 10 L). Consequently, the effect we are seeing could be due to contamination.

Before discussing the position of the Fermi level as a function of oxygen exposure, let us consider one more feature which all the samples have in common. In Figs. 6 to 14, we show the EDC's as a function of oxygen exposure for a representative number of cleaves from each sample. In all cases, changes take place in the top 5 eV of the valence band for exposures which are less than 10^3 L of O_2 . In some cases, the changes take place for exposures as small as 10 L O_2 (see, for example, Figs. 10 and 11). When the EDC for the clean sample is smeared out, these changes take the form of a sharpening of the structure in the top 5 eV of the valence band (see Figs. 8 and 10). In other cases, where the EDC's show well resolved valence band structure in that region, the changes are more subtle, i.e., there might be a small variation in relative peak heights as shown in Figs. 6, 9, 13, and 14.

Now that we have taken care of these general considerations, we will group the spectra together according to the Fermi level pinning, and then we will describe each group in detail. The first group contains samples LD1C,²⁰ MCPA, and LD3A, B, C. In all these samples, the Fermi

level was located approximately at the conduction band minimum, i.e., no surface Fermi level pinning is observed. We have complete exposure data only for samples LD1C and LD3C which are shown in Figs. 7 and 14, respectively. There is only one exposure for sample MCPA, and this is shown in Fig. 9.

The first thing to notice is that the Fermi level is about 1.4 to 1.6 eV above the valence band maximum, which is approximately the location of the conduction band minimum since the band gap of GaAs is 1.4 eV. Thus, the Fermi level is at the bulk position, and there is no pinning.

As the surface is exposed to more and more oxygen, the Fermi level moves closer and closer to midgap until it stops moving downward by about 10^6 L O₂ (Figs. 7 and 14). These points are plotted in the lowest curve of Fig. 5. After the initial sharpening of structure in sample LD1C, notice that no large changes occur in the EDC's until we reach this critical exposure at 10^5 to 10^6 L O₂. Up until this point, the only changes seen were the changes in the top 5 eV of the valence band and a possible splitting in the band structure feature located 10-12 eV below the VBM (this happened for sample LD1C in Fig. 7; no such splitting was seen for LD3C in Fig. 14). At 10^5 to 10^6 L O₂, a significant amount of emission is lost from the top 3 eV of the valence band, and most of the sharp structure in top 5 eV is gone. The valleys located 4.5 and 8.3 eV below the VBM start filling. No definite peak is seen yet in the 4.5 eV valley. However, for LD1C (Fig. 7), two peaks can be clearly resolved at 8.3 and 9.7 eV below the VBM and, for LD3C (Fig. 14),

one peak is seen at 8.3 eV below the VBM. The peak at 6.75 eV has so far been unaffected by the oxygen. By 10^9 LO_2 , the Fermi level has moved back towards the CBM by 0.15 eV (Fig. 5). The large exposures have led to a further decrease in the emission at the top of the valence band and an increase in emission from the adsorbed oxygen. Also, at 10^9 LO_2 , a more definite oxygen level begins to appear 5 eV below the VBM. The emission from the GaAs is still so large with respect to the new emission that it is very difficult to find the precise location of the new structure.

The second group contains those cleaves which exhibit Fermi level pinning at about midgap. This group is the largest and contains LD1A, B, D; LD2A, B, C, D, E; and MCPC, D (Figs. 6, 8; 13, 15; and, 11, 12, respectively). In the majority of these cleaves, the Fermi level is pinned 0.9 ± 0.15 eV above the VBM, and it remains within these limits for all exposures. In two cases, LD1D (Fig. 8) and LD1C (Fig. 15), the initial pinning was 0.6 eV above the VBM (these two samples have not been included in Fig. 5). The effect of oxygen on the valence states at the surface is the same as for the first group when exposures $\geq 10^6$ LO_2 are reached. Again, oxygen emission begins to be seen at 10^9 LO_2 as for the first group. For the lower exposures, especially below 10^3 LO_2 in all of the LD1 and MCP samples, the top 5 eV of the EDC sharpened dramatically even, in one case, for an exposure as low as 10 LO_2 . The LD2 samples, already somewhat being sharp, show more subtle effects.

The third "group" contains only one sample, MCPB,²⁰ and is shown in Fig. 10. In this case, the Fermi level for the just cleaved surface is located 0.7 eV above the VBM, putting it at midgap.

After being in the vacuum system at $\leq 1 \times 10^{-10}$ torr for 20 hours (giving an exposure of 7 L to residual gases), the Fermi level moves to 0.8 eV above the VBM. Upon exposure to oxygen, the Fermi level goes to the unpinned position (CBM) by 10 LO_2 , remains at that position until an exposure of 10^2 LO_2 , and then returns back to midgap by about 10^6 LO_2 . The structure at the top of the valence band sharpens dramatically for an exposure of less than 100 LO_2 , as for the group II samples, and the loss of intensity in the upper 5 eV of the EDC is seen as early as 10^5 LO_2 , even before a significant filling of either of the two valleys (4.5 and 8.3 eV below the VBM) has taken place.

This sample presents a unique situation. If we measure the position of the Fermi level relative to the VBM, we get the behavior described above and shown in the bottom curve of Fig. 5. If, however, we measure the Fermi level with respect to the peak 6.75 eV below the VBM (labeled peak "A" in the example EDC on the top of Fig. 5), we find that the Fermi level moves up 0.9 eV from freshly cleaved to 1 LO_2 exposure and then remains at this position until 10^3 L (see top curve in Fig. 5). If we measure the distance from the 6.75 eV peak to the VBM and plot it vs exposure, we get the middle curve of Fig. 5 (x's), where we have included the same plot for sample LD1C (solid circles) for comparison. It becomes very clear from these curves that the width of the valence band at the surface is changing as well as having a change in the pinning. The decrease in width upon addition of oxygen implies that structure at the top of the valence band is removed with oxygen. Furthermore, the 6.75 eV peak becomes noticeably narrower by 10^2 LO_2 . Neither effect was seen in the other samples. In those cases, the 6.75

eV peak remained constant in width, and the distance from the 6.75 eV peak and the VBM remained approximately constant for all oxygen exposures as can be seen from the example given for sample LD1C.

We can make a general comment with reference to Fig. 5, although the top and bottom sets of curves are consistent with each other. Less scattering was obtained between the data points in the top set. This indicates some of the problems in using the VBM as a reference. Since the top 5 eV of the VB change in shape, using the upper edge as a reference is clearly less reliable than using a constant structure such as the 6.75 eV peak.

We now turn our attention to what happens when we use the hot filament ionization gauge during an exposure. These results are shown (for sample LD2C) in the dashed curves of Fig. 15. The solid curves were obtained using unexcited oxygen on sample LD2A and are shown for comparison. The excited oxygen speeds up the rate of chemisorption, as can be seen by comparing the dashed curve at 10^5 L (excited oxygen) exposure with the solid curve at 10^6 L (unexcited oxygen) exposure. In fact, the first large effects with excited oxygen are seen at 5×10^4 L, while with unexcited oxygen, the first large effects are seen between 10^6 and 10^7 L, an increase in activity by about a factor of 100. We have discussed the increase in the rate of adsorption in References 5 and 21. As in the exposures with unexcited oxygen, we see the appearance of oxygen induced emission, associated with the O-2p level, at exposures $> 10^6$ L. In the case of excited oxygen, however, this emission is much more pronounced and eventually becomes the dominant feature of the EDC, located at approximately 5 eV below the VBM of the clean sample. With unexcited

oxygen, the oxygen emission is at most a shoulder at even 10^9 L. Also note that the position of the O-2p emission does not become well established until after an exposure of 10^7 L excited oxygen since, even at 10^5 L excited oxygen, it is not much bigger than the GaAs emission.

At 10^5 L, a peak is present at 8.2 eV below the VBM in both samples. A second peak at 9.9 eV below the VBM is seen for the sample exposed to excited oxygen, but does not appear for the sample exposed to unexcited oxygen until 10^7 LO₂. As can be seen from the figure, these two sets of peaks are the same for exposure to either excited or unexcited oxygen. We note, however, that at 10^7 L of excited oxygen, the two peaks at 8.2 and 9.9 eV below the VBM disappear and a single peak at 8.8 eV takes their place. The same sequence of exposures with excited oxygen for sample LD2C, taken at a photon energy of 25 eV, is shown in Fig. 16. This was done mainly to get a better look at any structure lower than 10 eV below the VBM which is obscured by the scattering peak for $h\nu = 21$ eV. By comparing Figs. 15 and 16, we see that the EDC's for the two photon energies are similar except for two major exceptions. First, the structure at 8.2 and 9.9 eV below the VBM is not visible at 10^6 L excited oxygen for the 25 eV spectrum, whereas it is present at 21 eV. The peak at 8.8 eV below the VBM is quite prominent at 10^7 L excited oxygen for both photon energies. Second, because of cross-section effects, the height of the O-2p derived emission relative to the GaAs valence band emission is much larger at 25 eV than 21 eV. Consequently, we are able to see direct emission from the oxygen more readily using 25 eV photons.

The next experimental results are those of partial yield spectroscopy measurements performed on samples LD1C, which shows no pinning and MCPB, which shows pinning at midgap. These spectra, shown in Figs. 17a and 17b, were performed concurrently with the data of Figs. 7 and 10. The two sets of spectra are essentially identical. There are some differences in relative peak heights and shapes, but the energy positions of all the peaks are identical. On the clean spectra, there are two sharp peaks at 19.7 and 20.2 eV and a third broad peak at 20.9 eV. Upon addition of oxygen, the three peaks remain unchanged in position and shape up to an exposure of 10^5 L of unexcited O_2 . At 10^6 L, the peaks are almost gone, but there has been no shift in energy position. At 10^7 L, the fine structure is completely gone, leaving one broad peak at 20.1 eV. The behavior of partial yield spectra for other samples and cleaves was identical to the spectra shown, irrespective of any differences in the initial Fermi level pinning or behavior with oxygen exposure.

III. DISCUSSION AND CONCLUSIONS

In the discussion that follows, we will first condense the information obtained from our valence band, Fermi level pinning, and partial yield studies, and then correlate these results.

We have seen three main things in our data. First, Fermi level pinning occurred on surfaces that could be classified as good cleaves. This implies that pinning is not necessarily caused by high step densities or surface roughness,^{13,14} but rather by more subtle types of defects. Exposure of the surface to oxygen caused the Fermi level to go

to midgap for unpinned samples and stay the same (at midgap) for the pinned samples.

Second, the top 5 eV of the EDC's were relatively sharp for unpinned samples, while for pinned samples the structure in this region was, in general, more smeared. The exposure of the surface to less than 10^3 LO_2 resulted in a sharpening of the smeared structure and more subtle changes in relative peak heights for the sharp EDC's. At exposures between 10^5 to 10^6 LO_2 , the top 5 eV of the valence band was again affected, exhibiting both a loss of emission and smearing. For exposures above 10^6 LO_2 , the top 5 eV of the EDC dropped even more and oxygen induced emission became noticeable. However, at 21 eV, the cross-sections are such that no clear peak from the oxygen can yet be seen 4 to 5 eV below the VBM. Through all this, the valence band structures lower than 5 eV below the VBM have remained essentially unchanged.

Third, the partial yield gave the same results for all samples, irrespective of the initial position of the Fermi level. Addition of as much as 10^5 LO_2 had no effect on the partial yield structure either in peak position or height. The peaks lose intensity at 10^6 LO_2 and disappear by 10^7 LO_2 , with no shift in the peak positions.

As we mentioned in the introduction, the top 5 eV of the valence band should be strongly affected by the surface lattice structure, so that movements in the positions of the surface atoms would appear as changes in the top 5 eV of the EDC. If a surface is strained, the surface atoms at the strain points will be somewhat displaced from their ideal positions. Consequently, the EDC's from such a surface would be smeared, since the EDC would have contributions from both

the ideal and strained parts of the surface. The fact that surfaces with unpinned Fermi levels have sharp structures in the top 5 eV of the EDC, while samples with pinned Fermi levels are initially smeared and sharpen with exposure to oxygen, indicates that the unpinned surfaces are more perfect. That is, the surfaces exhibiting Fermi level pinning are probably strained. Furthermore, since we see no difference in the partial yield results from the samples with and without Fermi level pinning, the pinning must be due to extrinsic states.^{4,13} Therefore by combining the photoemission and partial yield results, we can conclude that surface defects could be responsible for both the Fermi level pinning and the smearing of the valence band.

The sharpening of the EDC's with oxygen occurs for exposures less than 10^3 LO_2 . From previous work,⁵ we saw that at 10^6 LO_2 the coverage is only 5% of saturation. Assuming saturation at half monolayer (4.4×10^{14} oxygens/ cm^2), the oxygen coverage causing sharpening of the EDC's would be on the order of one oxygen per 10^4 to 10^5 surface atoms. These rather long range effects associated with the oxygen can be interpreted to mean that the surface strains are rather unstable so that rearrangements can be triggered quite easily by very few oxygens. One oxygen per 10^4 to 10^5 surface atoms gives a concentration on the surface of approximately 4×10^9 to 4×10^{10} oxygens/ cm^2 . The typical concentration of dopant on the surface is on the order of 10^{10} atoms/ cm^2 for a bulk doping of 10^{18} atoms/ cm^3 . It is interesting that these numbers are close enough to indicate a possible link between the dopant and the initial oxygen chemisorption. However, we should keep in mind that it does take at least 10^{12} to 10^{13} states/ cm^2 to pin the Fermi level at

midgap.^{11,12,13} Thus, although the dopant atoms at the surface could be responsible for triggering surface rearrangement upon oxygen chemisorption, they can not be the primary cause of the Fermi level pinning observed on the surfaces with the smeared EDC's. In addition, even though the already sharp EDC's (i.e., with no pinning) are affected by less than 10^3 LO_2 , the Fermi level does not start to move towards midgap until exposures larger than 10^3 LO_2 . This is more evidence which implies that the sites causing the pinning or strain and those that remove the strain are not necessarily the same.

Many of the conclusions that have been drawn so far have been rather speculative, but the most important point that must be reiterated is that the chemisorbed oxygen has long range effects on the surface, acting at coverages as small as one oxygen per 10^4 to 10^5 surface atoms. The fact that the oxygen has such large effects for very small coverages implies that oxygen stimulates spontaneous rearrangement of the surface by possibly removing strains. The cause of the pinning on the cleaved samples is extrinsic states whose source is not yet known. However, we suggest that surface defects cause both the pinning and the smearing of the EDC's.

Between 10^3 and 10^6 LO_2 , the coverage goes from 1 oxygen in 10^4 to 10^5 surface atoms to 5% of saturation, and the Fermi level goes from the CBM to midgap (for group I samples). This latter coverage corresponds to about 10^{13} oxygen atoms/cm² which is approximately the number of states needed at the surface to pin the Fermi level. Thus, it is easy to see the origin of the Fermi level pinning with exposure to oxygen, provided, of course, that every chemisorbed oxygen gives rise to one new interface state. Besides pinning the Fermi level at midgap, an

oxygen exposure of 10^6 IO_2 results in the complete smearing of the top 5 eV of the EDC's.⁴ Since the coverage is now only about one oxygen atom per 20 surface sites (i.e., 5% of saturation), the effects of the oxygen are again long range. The large changes in the EDC's imply a relatively large rearrangement of all the surface atoms, not just the ones at the strain sites, as was the case before.

With these large changes taking place in the valence band, we should also expect significant changes in the local dielectric constant (or screening properties) at the surface. Such changes would explain the disappearance of the partial yield peaks in going from 10^5 to 10^7 IO_2 . If the screening at the surface changes, the excitonic binding energy, which determines the position of the peaks in the partial yield could change. If this happened, the partial yield from the clean surface would drop and new structure representative of the new excitonic binding energy would grow. We could not, however, see such new structure if it was too close to the valence band. Thus, the loss of the partial yield peaks could possibly be due to a rearrangement of charge in the surface layer rather than a direct interaction of the oxygen with the surface gallium atoms. The same arguments could be applied to explain the disappearance of the structure in electron energy loss measurements.²²

With exposure to large amounts of oxygen, we saw further decrease in the intensity from the top 5 eV of the valence band with two new peaks 9.9 and 8.2 eV and a shoulder 4 to 5 eV below the VBM. Similar peaks are present during the initial stages of exposure to excited oxygen. This fits in with other data from chemical shift measurements

where it was shown that the result of exposure to excited or unexcited oxygen started in the same way, i.e., with a chemisorption stage.⁵ However, in the case of excited oxygen, the surface is oxidized for exposures above 10^6 L. Thus, the peaks we see in the curves for exposures of 10^7 L of excited oxygen (Fig. 15) at 8.8 and 5 eV below the VBM should be oxide peaks. If the excited oxygen was found to be atomic rather than excited molecular oxygen, the similarity in the initial adsorption of the excited and the molecular oxygen would indicate that the molecular oxygen adsorbed dissociatively on the GaAs (110) surface. Thus, it would be very interesting to perform an experiment to determine the nature of the excited oxygen, as well as an adsorption experiment with atomic oxygen.

The simultaneous appearance and growth of the peaks 9.9, 8.2, and 4 to 5 eV below the VBM indicates that all three are due to a single adsorption process. The splitting between the shoulder and second peak is 3.2 to 4.2 eV and between the second and third peaks is 1.7 eV. It is interesting to compare these peaks to those seen in gas phase photoemission from molecular oxygen. The first three peaks in that case are the π_g , π_u , and ${}^4\Sigma_g$ levels with splittings of 4 eV (π_g and π_u) and 2 eV (π_u and ${}^4\Sigma_g$).^{23,24} If we associate the shoulder in our data with the π_g level and the next two peaks with the π_u and ${}^4\Sigma_g$ levels, respectively, we see that the agreement is rather good. The first splitting between the π_g and π_u is within the range of values we see, and the second splitting is 0.3 eV larger than what is seen in our results. This is, by no means, conclusive evidence that the oxygen adsorbs as a molecule. However, the evidence is strong enough that the suggestion must be made.

The studies presented in this paper are rather exploratory in nature, and their importance lies, not only in what we have learned so far but, also, in suggestions for new work that will clarify some of the questions that remain unanswered. For example, more work must be done to correlate the pinning on clean surfaces with actual physical defects, such as, impurities or cleavage steps. LEED studies should be performed along with the photoemission to see if we can detect any change in the LEED I-V curves when we have changes in the EDC's. In order to gather more evidence as to the nature of the adsorbed oxygen, the three oxygen induced levels should be studied as a function of photon energy to see if their cross sections are the same as for molecular oxygen, and electron energy loss experiments to detect any molecular vibrational levels that might be present should also be undertaken.

Finally, since theoretical calculations on the rearranged GaAs (110) surface are starting to be published,³ it should not be long until until we can start making more detailed comparisons between our photoemission data and the calculated surface densities of states.

REFERENCES

1. A. R. Lubinsky, C. B. Duke, B. W. Lee, and P. Mark, Phys. Rev. Letters 36, 1058 (1976); C. B. Duke, A. R. Lubinsky, B. W. Lee, and P. Mark, J. Vac. Sci. Technol. 13, 761 (1976); A. R. Lubinsky, J. Vac. Sci. Technol. 14, 910 (1977).
2. W. A. Harrison, Surface Sci. 55, 1 (1976); J. Vac. Sci. Technol. 14, 883 (1977).
3. S. G. Louie, J. R. Chelikowsky, and M. L. Cohen, J. Vac. Sci. Technol. 13, 790 (1976); J. R. Chelikowsky, S. G. Louie, and M. L. Cohen, Phys. Rev. B (in press); C. Calandra, F. Manghi, and C. M. Bertoni (to be published).
4. Some preliminary work has been published in W. E. Spicer, I. Lindau, P. E. Gregory, C. M. Garner, P. Pianetta, and P. W. Chye, J. Vac. Sci. Technol. 13, 780 (1976) and W. E. Spicer, P. Pianetta, I. Lindau, P. W. Chye, J. Vac. Sci. Technol. 14, 885 (1977).
5. P. Pianetta, Ph.D. thesis, Stanford University (1976).
6. L. Ley, R. A. Pollak, F. R. McFeely, S. P. Kowalczyk, and D. A. Shirley, Phys. Rev. B 9, 600 (1974).
7. J. D. Joannopoulos and M. L. Cohen, Phys. Rev. B 10, 5075 (1974).
8. D. J. Chadi and M. L. Cohen, Phys. Stat. Sol. (b) 68, 405 (1975).
9. J. Chelikowsky, D. J. Chadi, and M. L. Cohen, Phys. Rev. B 8, 2786 (1973).
10. J. R. Chelikowsky and M. L. Cohen, Phys. Rev. B 14, 556 (1976).

11. P. E. Gregory and W. E. Spicer, Phys. Rev. B 13, 725 (1976);
P. E. Gregory, W. E. Spicer, S. Ciraci, and W. A. Harrison,
Appl. Phys. Letters 25, 511 (1974).
12. J. H. Dinan, L. K. Galbraith, and T. E. Fischer, Surface Sci.
26, 587 (1971).
13. J. van Laar and A. Huijser, J. Vac. Sci. Technol. 13, 769 (1976);
A. Huijser and J. van Laar, Surface Sci. 52, 202 (1975).
14. W. Gudat and D. E. Eastman, J. Vac. Sci. Technol. 13, 831 (1976)
and references contained therein.
15. D. E. Eastman and J. L. Freeouf, Phys. Rev. Letters 34, 1624 (1975).
16. G. J. Lapeyre and J. Anderson, Phys. Rev. Letters 35, 117 (1975).
17. Here, we are discussing only clean cleaved GaAs (110) surfaces
since contamination can also cause pinning as will be discussed
below.
18. The surfaces studied in Reference 11 showed Fermi level pinning
but were not the result of "bad" cleaves, i.e., there was no
surface roughness nor was there a large amount of microscopic
steps.
19. For a detailed explanation of the justification for this method,
see Reference 11 or G. F. Derbenwick, D. T. Pierce, and W. E.
Spicer, Methods of Experimental Physics (Academic Press, New York,
1974), Vol. 11, pp. 89-92.
20. LD1C was called sample II cleave A, and MCPB was called sample III
cleave B in Reference 4.
21. P. Pianetta, I. Lindau, C. M. Graner, and W. E. Spicer, Phys. Rev.
Letters 37, 1166 (1976).

22. R. Ludeke and A. Koma, Crit. Rev. Solid State Sci. 5, 259 (1975);
and J. Vac. Sci. Technol. 13, 241 (1976).
23. K. Siegbahn, C. Nordling, G. Johansson, J. Hedman, P. F. Hedén,
K. Hamrin, U. Gelius, T. Bergmark, L. O. Werme, R. Manne, and
Y. Baer, ESCA Applied to Free Molecules (North Holland, Amsterdam,
1969), pp. 69-73.
24. D. W. Turner, C. Baker, A. D. Baker, and C. R. Brundle, Molecular
Photoelectron Spectroscopy (Wiley, New York, 1970), pp. 36-37, 52.

Table I

LIST OF SAMPLES. Entries include Fermi level location for each sample immediately after cleavage, classification of samples according to location of the Fermi level, and an indication as to the relative sharpness of the valence band before and after exposure to oxygen.

Sample		E_F Position ^a	Valence Band Structure ^b		Group ^c	Data Shown in Figure Numbers	
			After Cleavage	After $\lesssim 10^2$ LO_2		(Clean)	(+O ₂)
LD1	A	midgap	smeared	sharpened	II	1	6
	B	midgap	smeared	no data	II	1	not shown
	C	CBM	sharp	same	I	1	7
	D	midgap	smeared	sharpened	II	1	8
LD2	A	midgap	sharp	sharper	II	2	13,15
	B	midgap	smeared	sharpened	II	not shown	not shown
	C	midgap	sharp	same	II	2	15,16
	D	midgap	sharp	same	II	2	not shown
	E	midgap	sharp	no data	II	not shown	no data
LD3	A	CBM	sharp	same	I	3	not shown
	B	CBM	sharp	same	I	3	not shown
	C	CBM	sharp	sharper	I	3	14
MCP	A	CBM	sharp	sharper	I	4	9
	B	midgap	smeared	sharpened	III	4	10
	C	midgap	smeared	sharpened	II	4	11
	D	midgap	no data	sharp	II	not shown	12

a. Approximate position, see Figs. 1-5 for exact position.

b. See text for discussion of what is meant by sharpness.

c. Group I indicate E_F at CBM, group II at midgap, group III at midgap then going to CBM with addition of oxygen.

FIGURE CAPTIONS

- Fig. 1. EDC's taken at a photon energy of 21 eV for four cleaves from Sample LD1. The solid curve for sample LD1C was taken 12 hours after cleaving, whereas the dotted curve was taken within 45 minutes after cleaving.
- Fig. 2. EDC's taken at $h\nu = 21$ eV for three cleaves from Sample LD2.
- Fig. 3. EDC's taken at $h\nu = 20$ eV for three cleaves from Sample LD3.
- Fig. 4. EDC's taken at $h\nu = 21$ eV for three cleaves from Sample MCP. The solid curve for sample MCPB was taken 20 hours after cleaving, whereas the dotted curve was taken within 30 minutes after cleaving.
- Fig. 5. Summary of Fermi level movement versus exposure for some of the samples shown in Figs. 1 - 4. Here, we show the position of the Fermi level, E_F , with respect to both the valence band maximum, VBM (in the bottom set of curves) and peak "A" (in the top set of curves). The middle set of curves show the position of the VBM with respect to peak "A". Samples in group I show no Fermi level pinning after cleavage. Pinning is seen from group II and III samples, but, for the group III sample, it is removed by exposure to oxygen (see text).
- Fig. 6. EDC's for Sample LD1A, i.e., Sample LD1 cleave A, as a function of oxygen exposure ($h\nu = 21$ eV).

- Fig. 7. EDC's for Sample LD1C as a function of oxygen exposure ($h\nu = 21$ eV).
- Fig. 8. EDC's for Sample LD1D as a function of oxygen exposure ($h\nu = 21$ eV).
- Fig. 9. EDC's for Sample MCPA as a function of oxygen exposure ($h\nu = 21$ eV).
- Fig. 10. EDC's for Sample MCPB as a function of oxygen exposure ($h\nu = 21$ eV).
- Fig. 11. EDC's for Sample MCPC as a function of oxygen exposure ($h\nu = 21$ eV).
- Fig. 12. EDC's for Sample MCPD as a function of oxygen exposure ($h\nu = 21$ eV). No spectra were taken of the clean sample.
- Fig. 13. EDC's for Sample LD2A as a function of oxygen exposure ($h\nu = 21$ eV).
- Fig. 14. EDC's for Sample LD3C as a function of oxygen exposure. Note, here, $h\nu = 21$ eV, but $h\nu = 20$ eV in Fig. 3, so the clean spectra will be somewhat different due to direct transition effects.
- Fig. 15. Comparison of Sample LD2A, exposed to molecular unexcited oxygen, with Sample LD2C, exposed to excited oxygen.
- Fig. 16. EDC's for Sample LD2C exposed to excited oxygen ($h\nu = 25$ eV).
- Fig. 17. Partial yield measurements for (a) Sample MCPB and (b) Sample LD1C as a function of oxygen exposure.

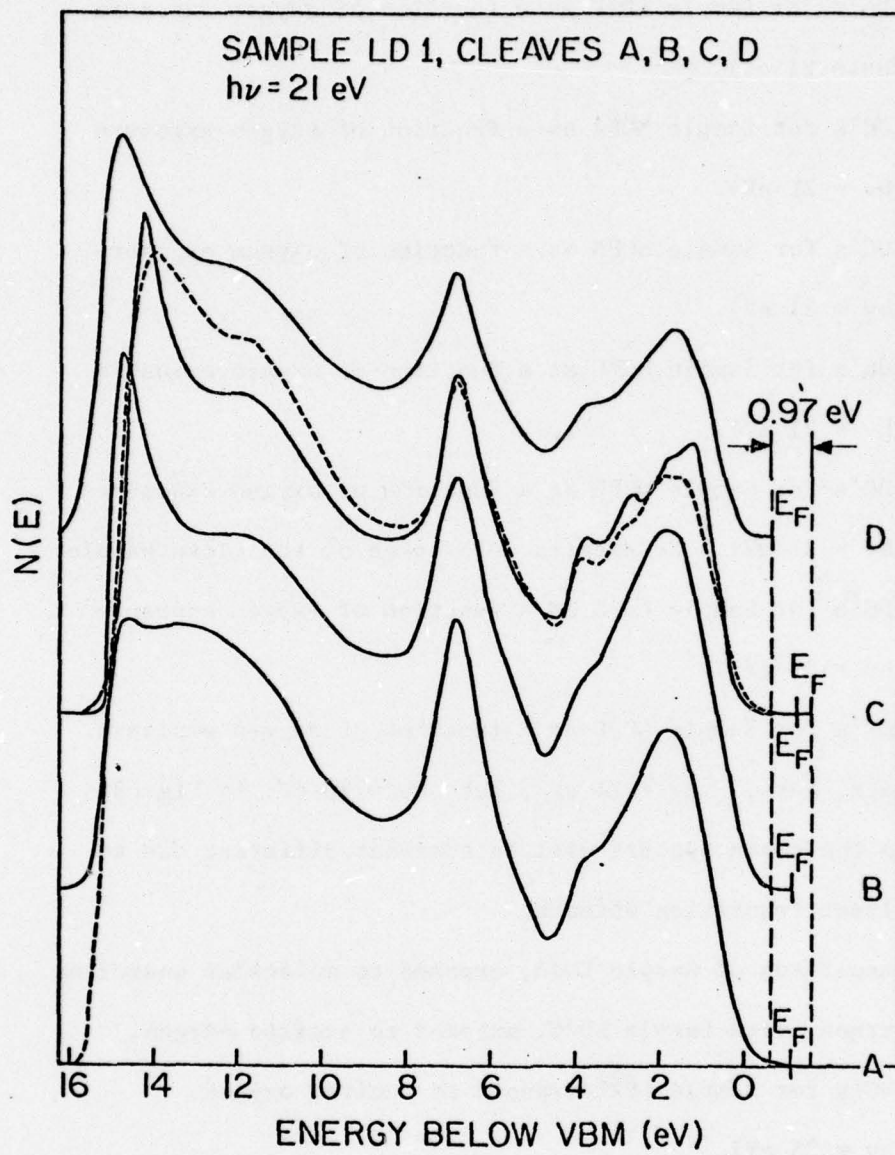


Fig. 1

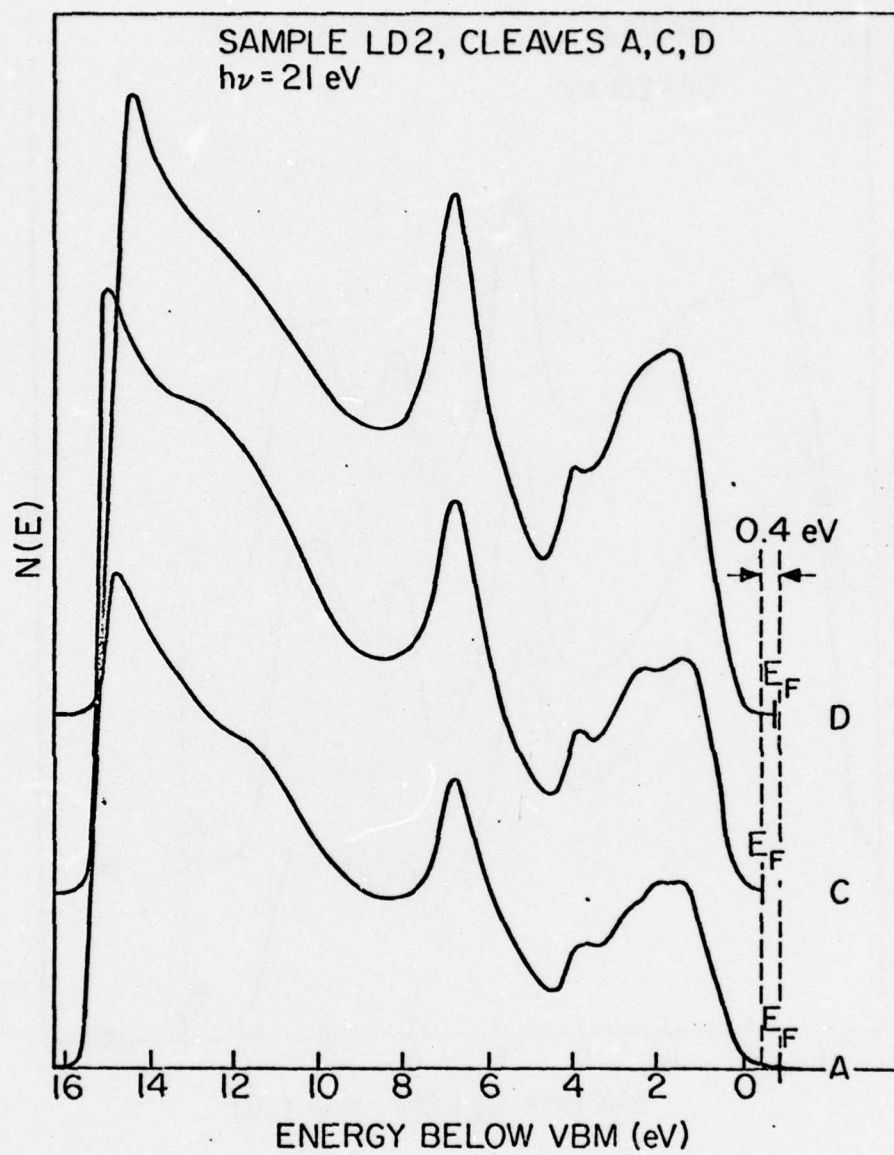


Fig. 2

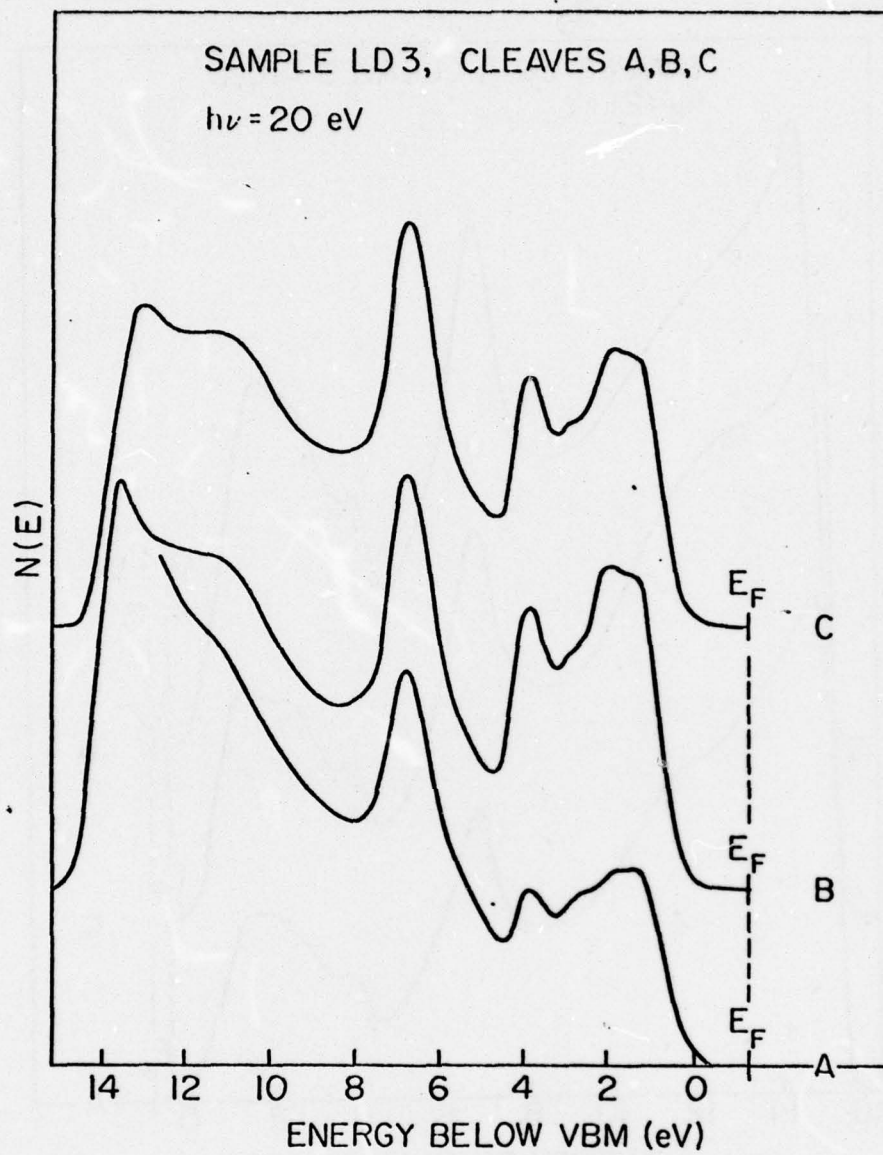


Fig. 3

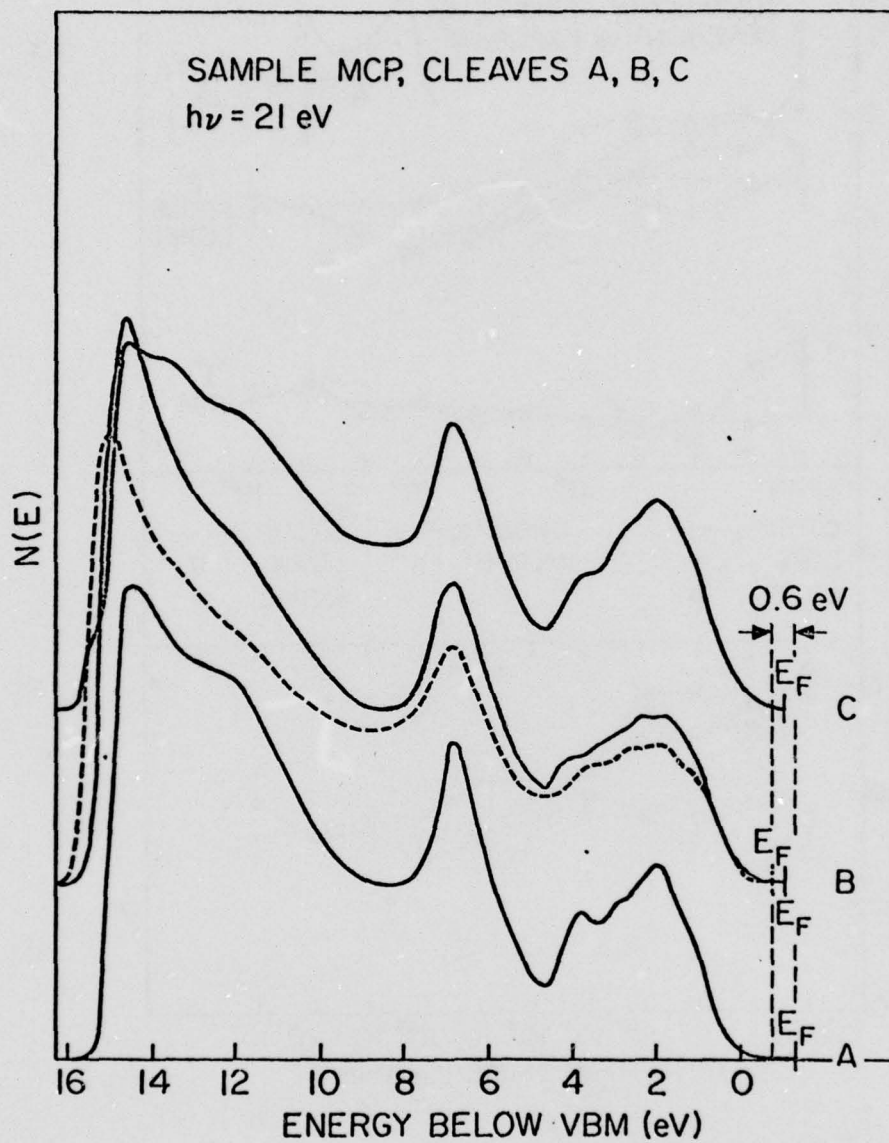


Fig. 4

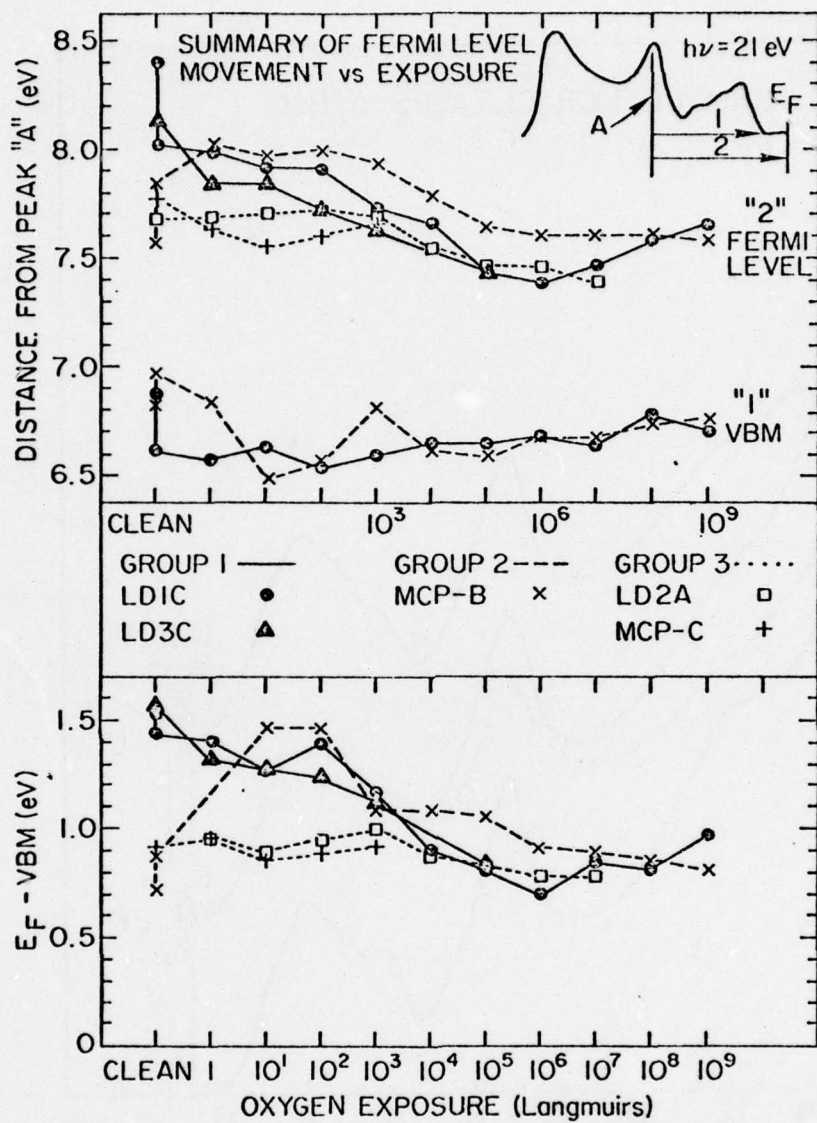


Fig. 5

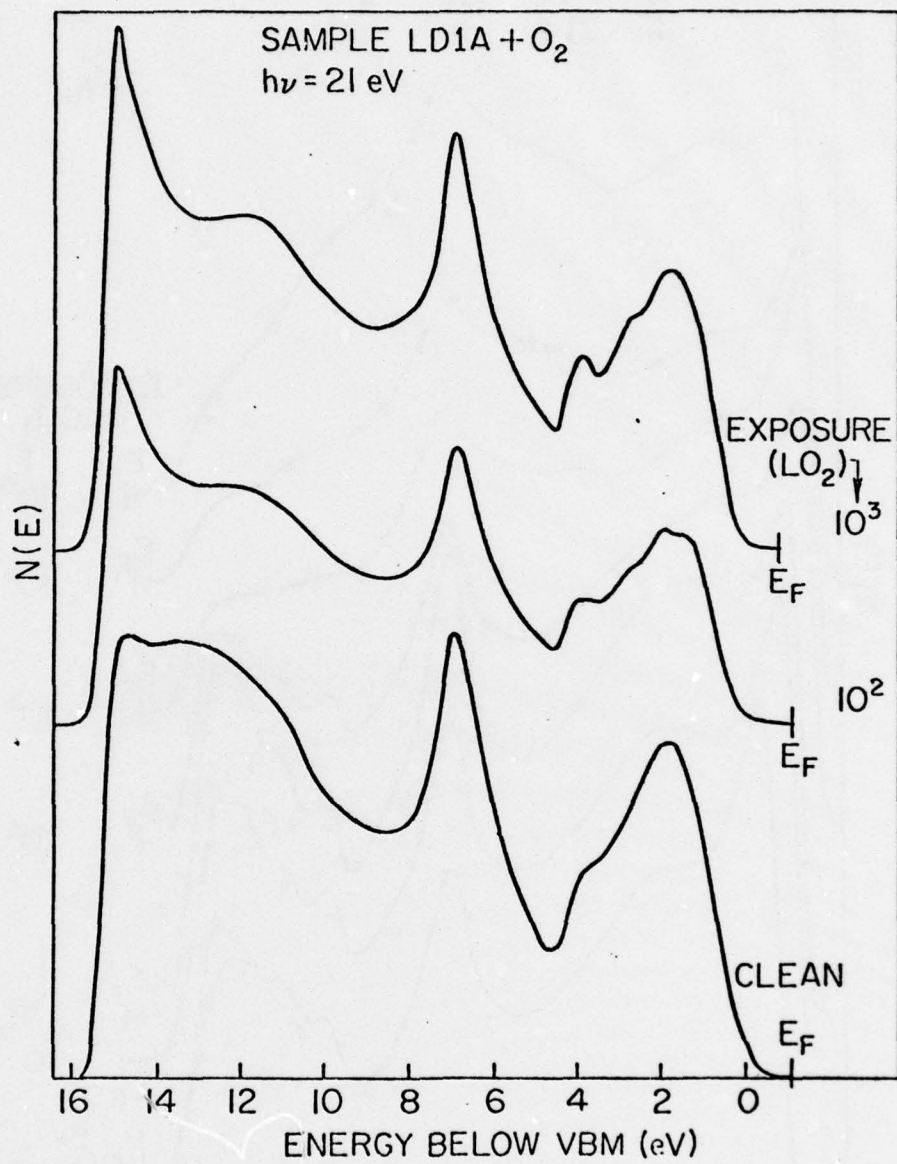


Fig. 6

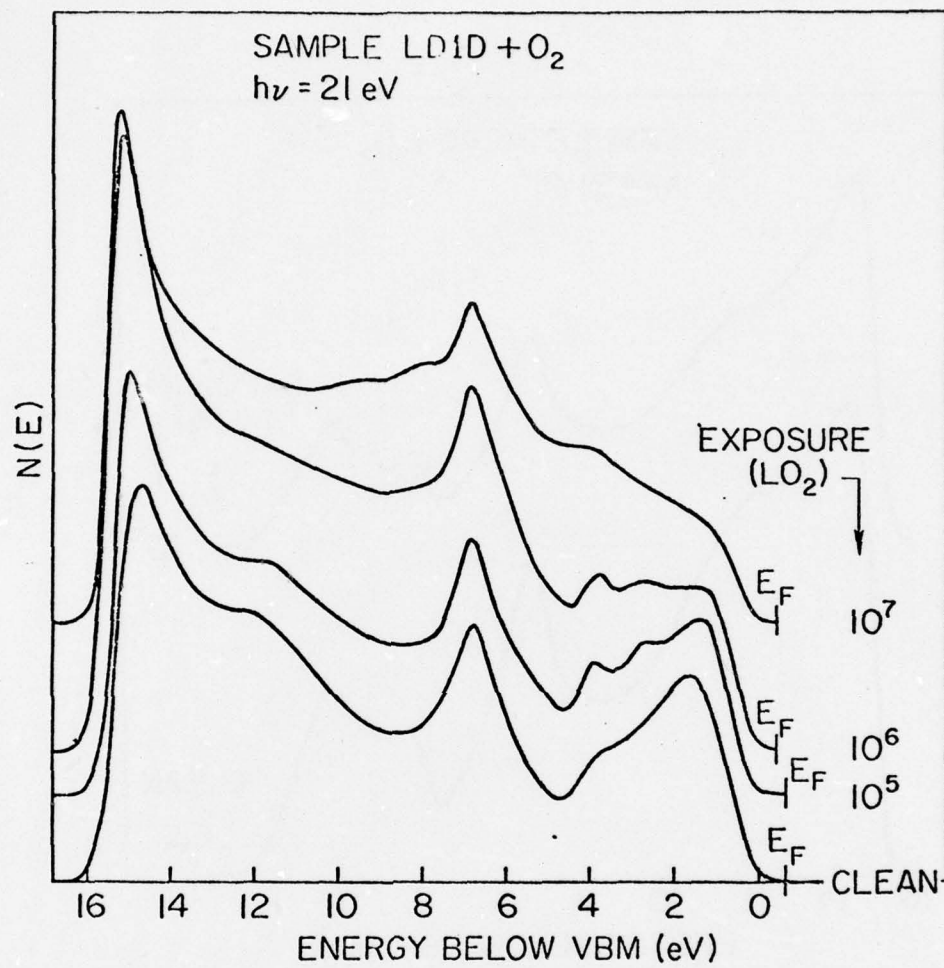


Fig. 8

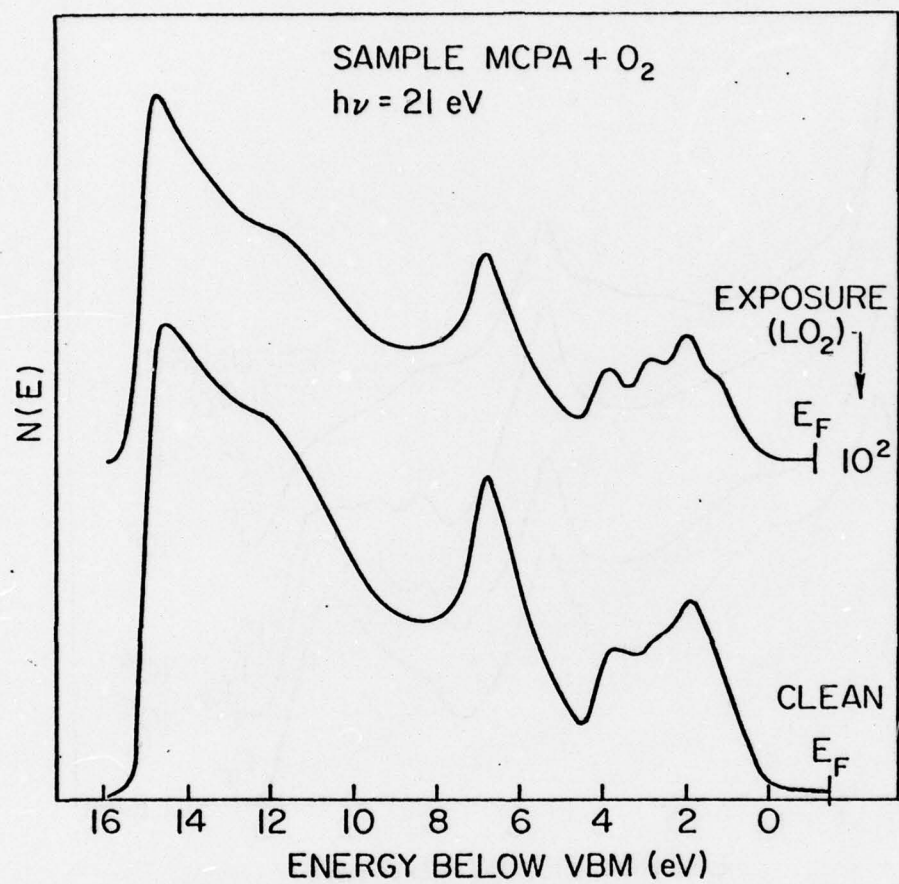


Fig. 9

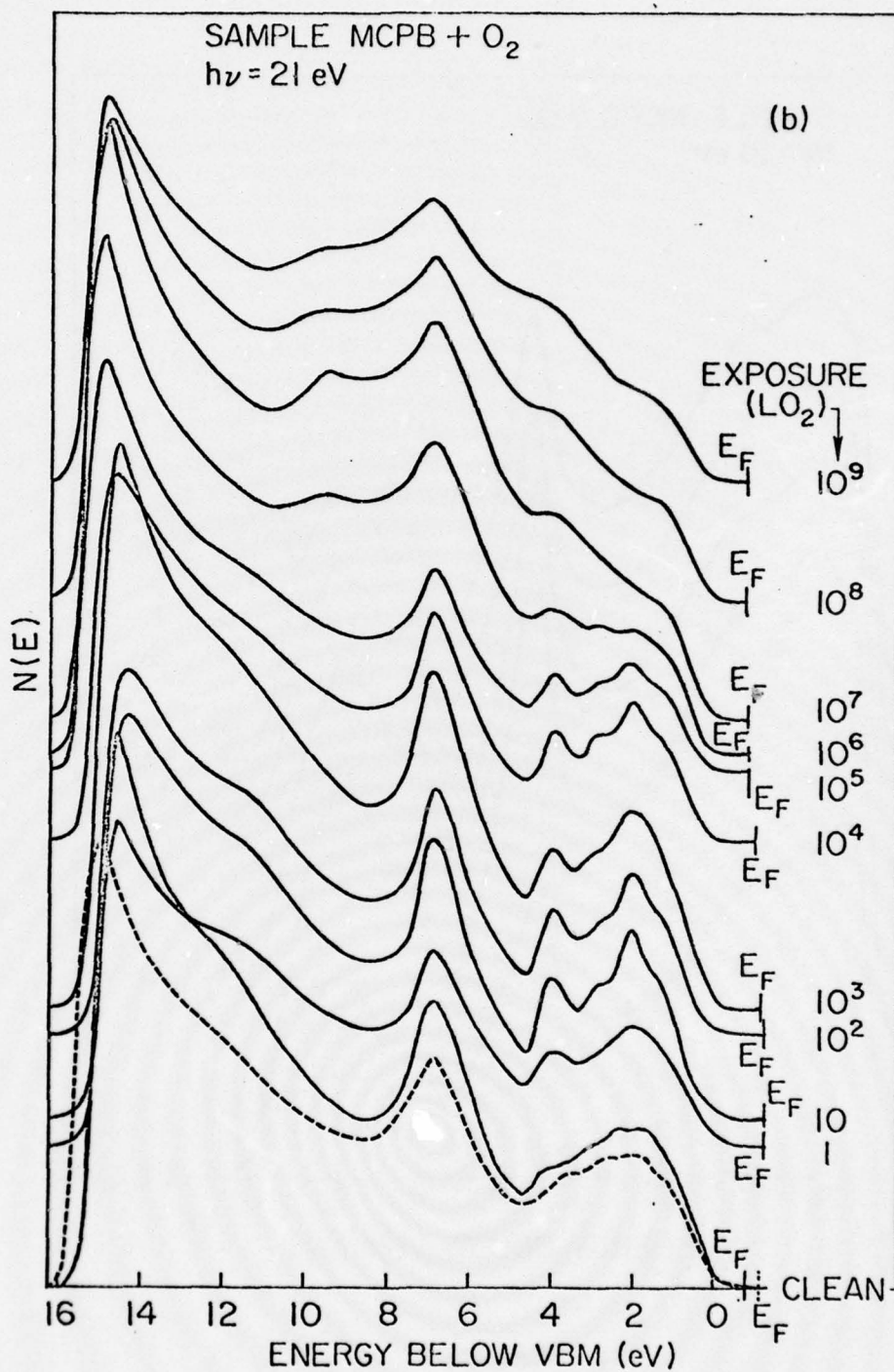


Fig. 10

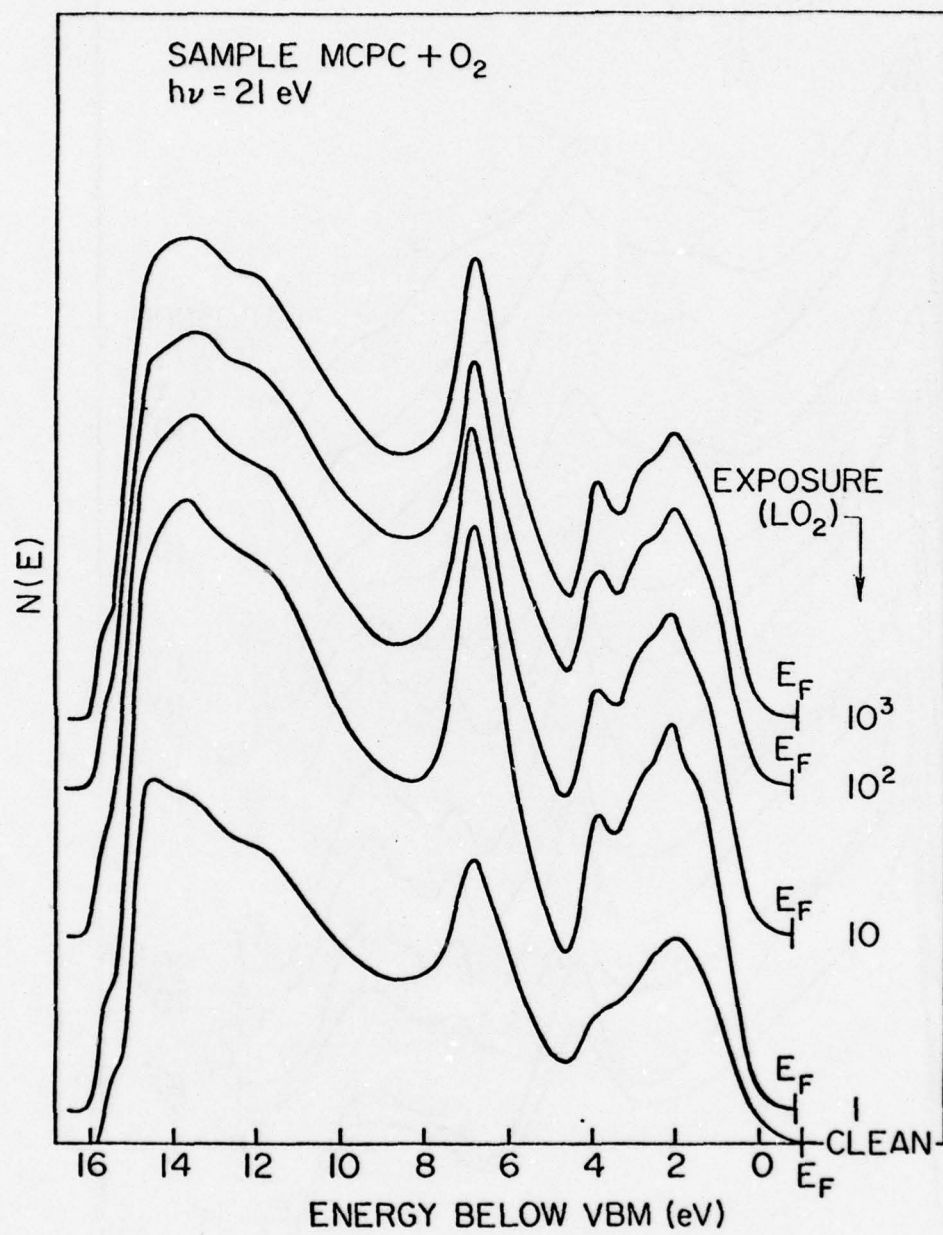


Fig. 11

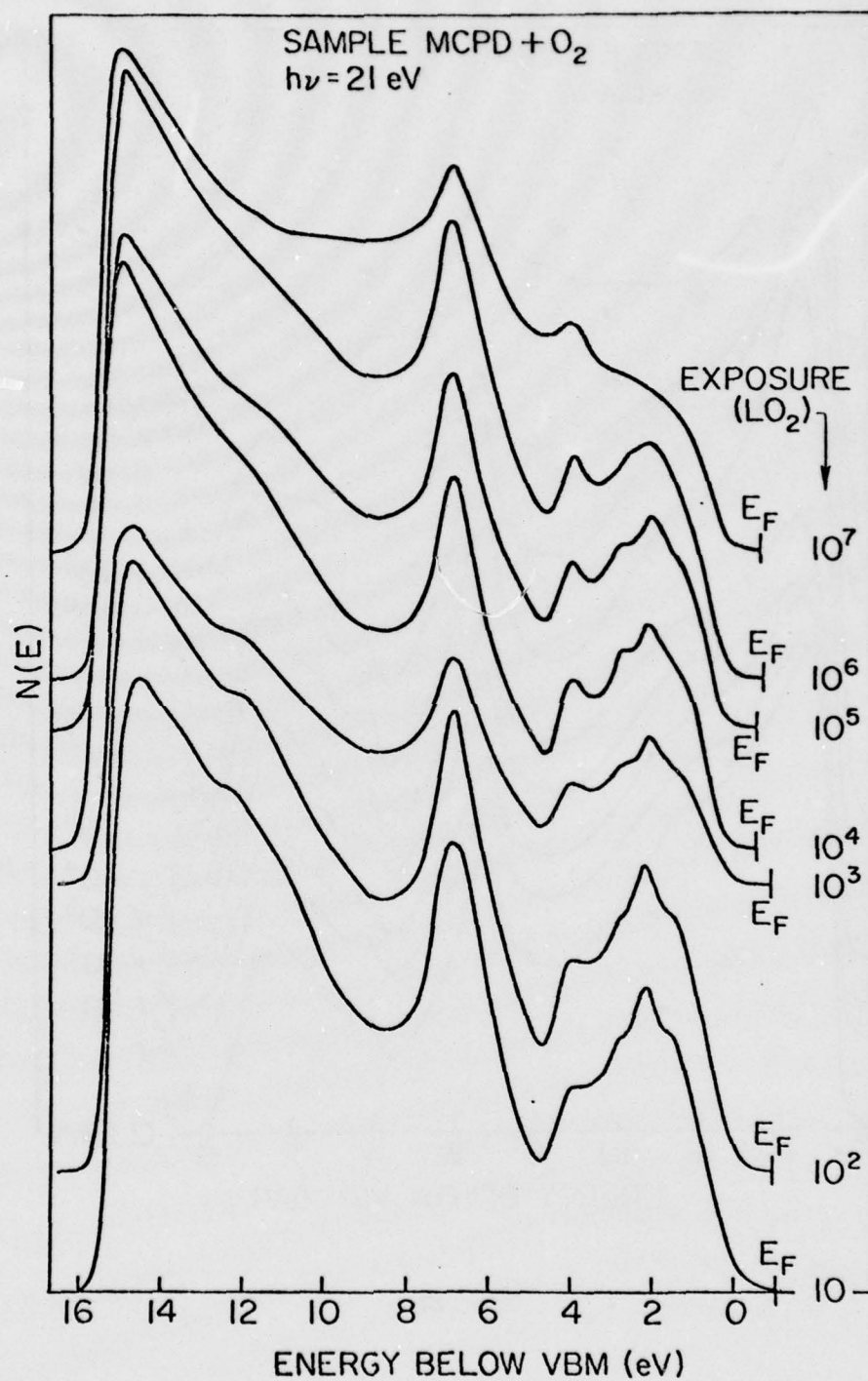


Fig. 12

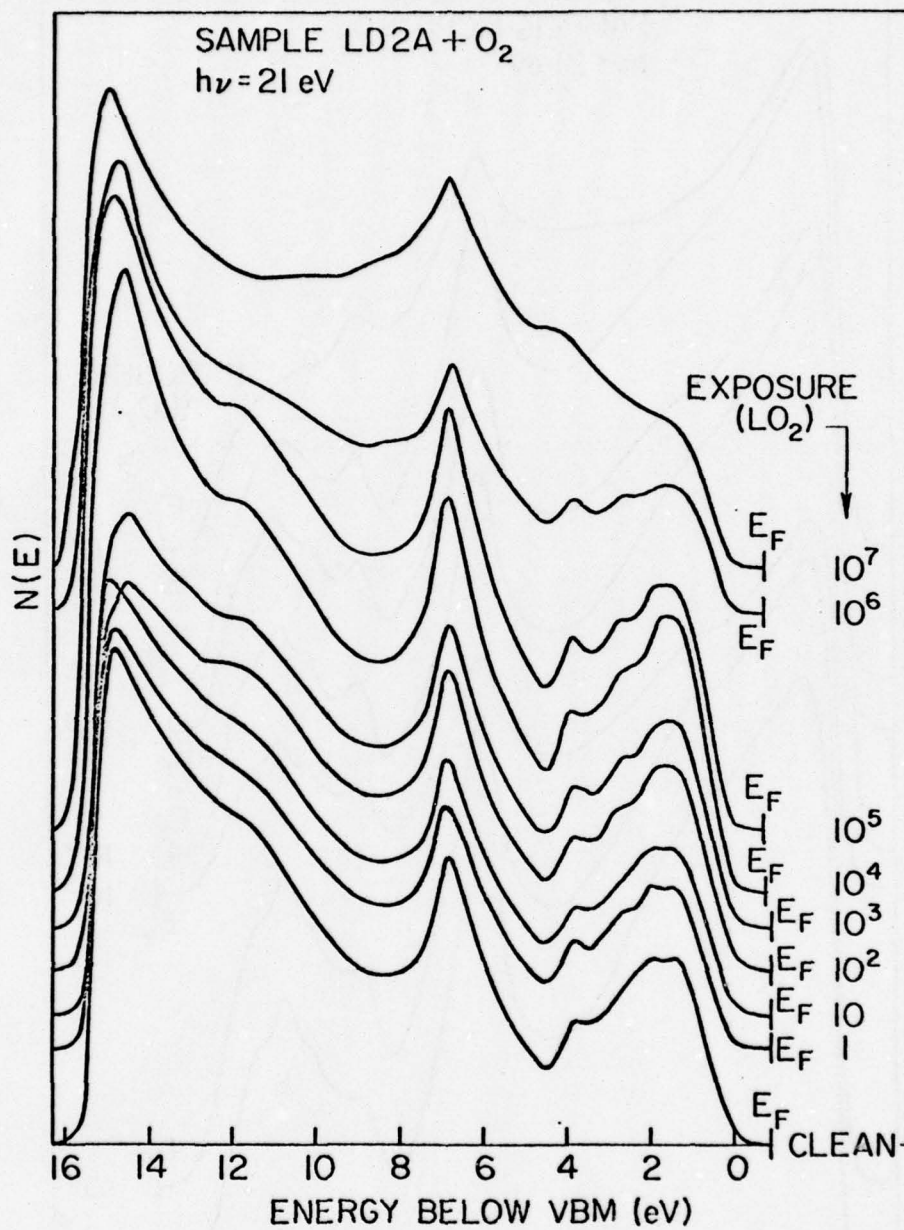


Fig. 13

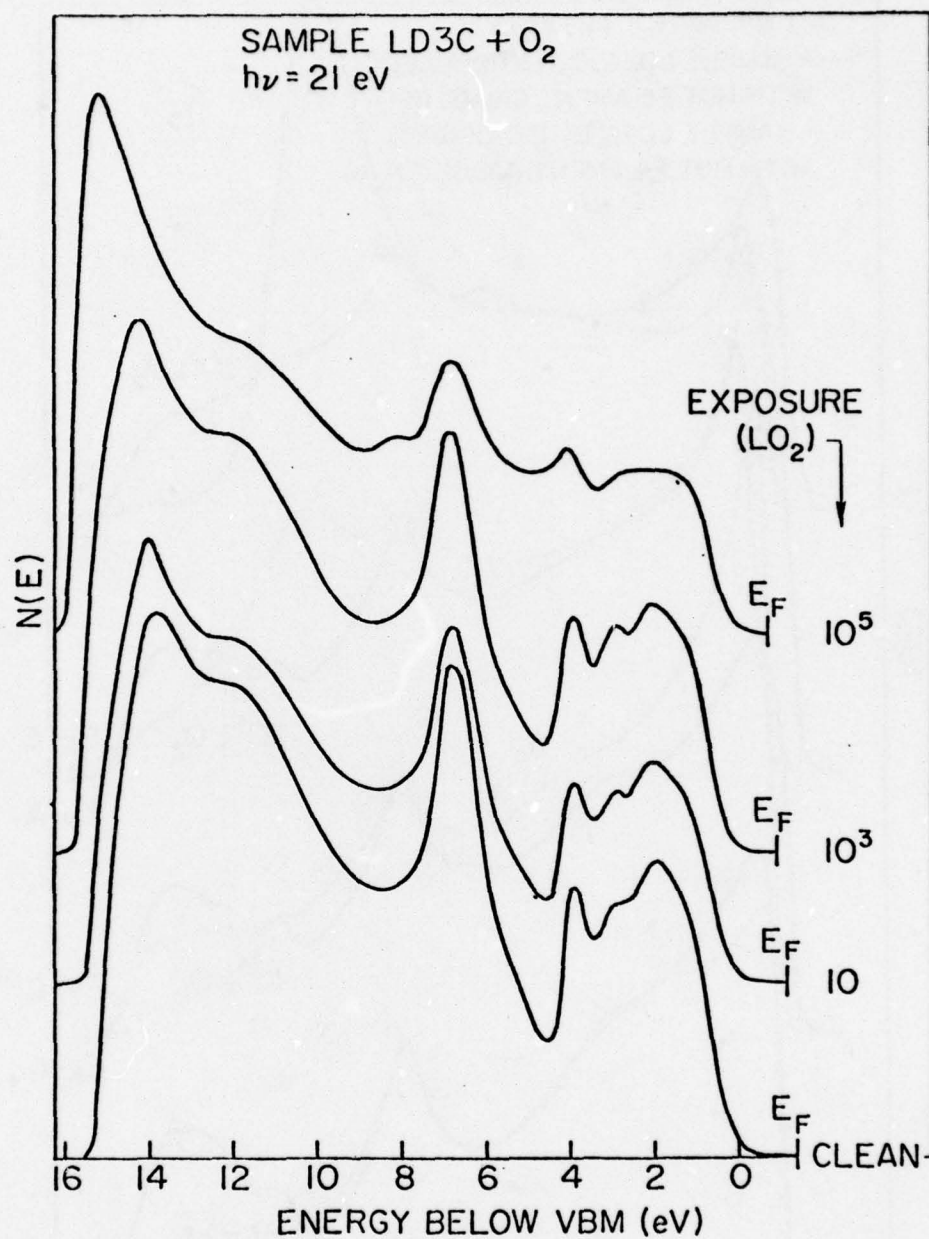


Fig. 14

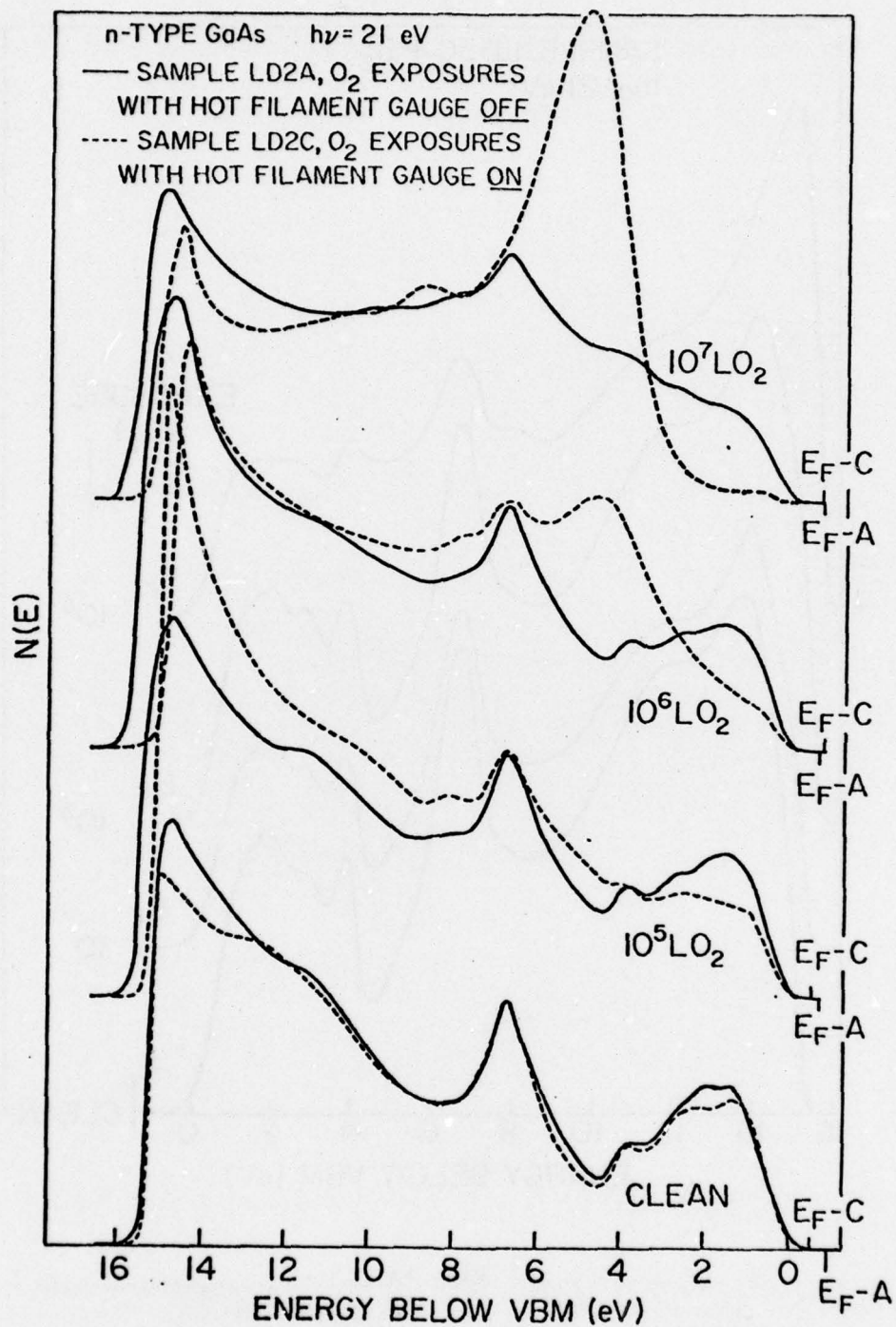


Fig. 15

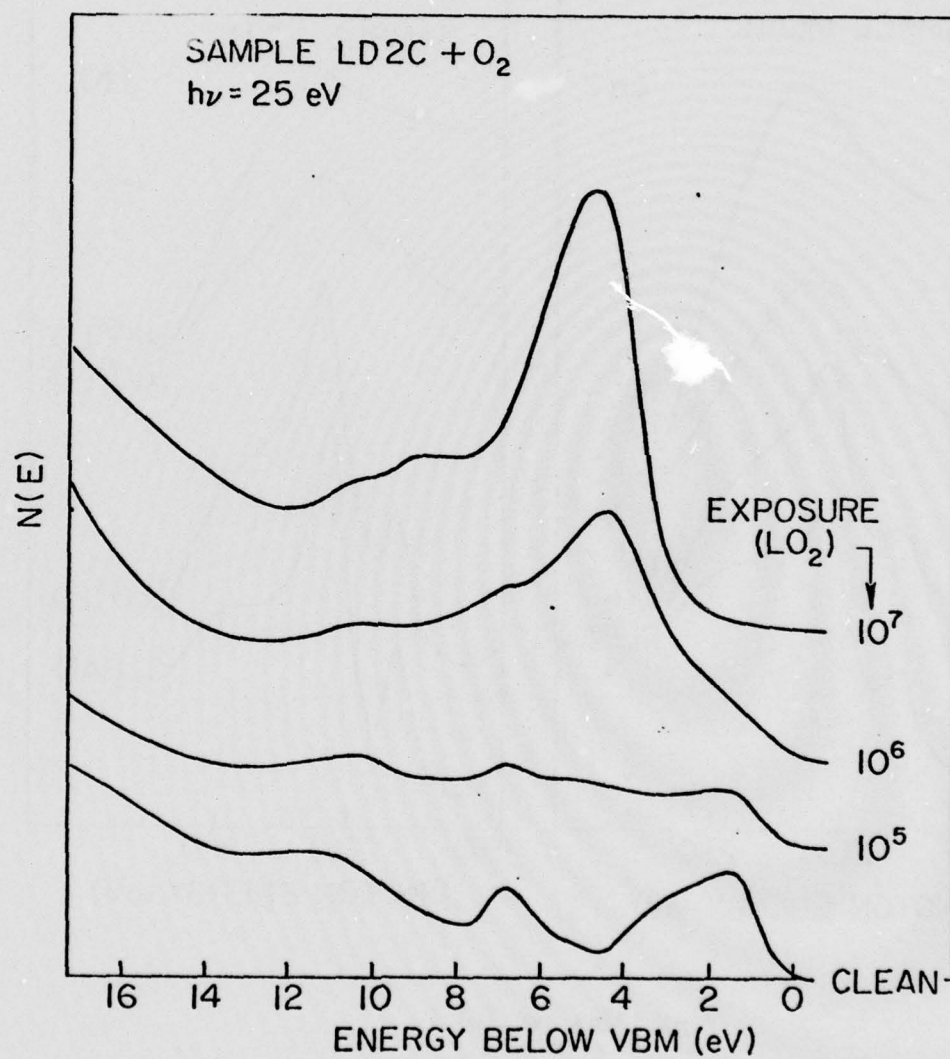


Fig. 16

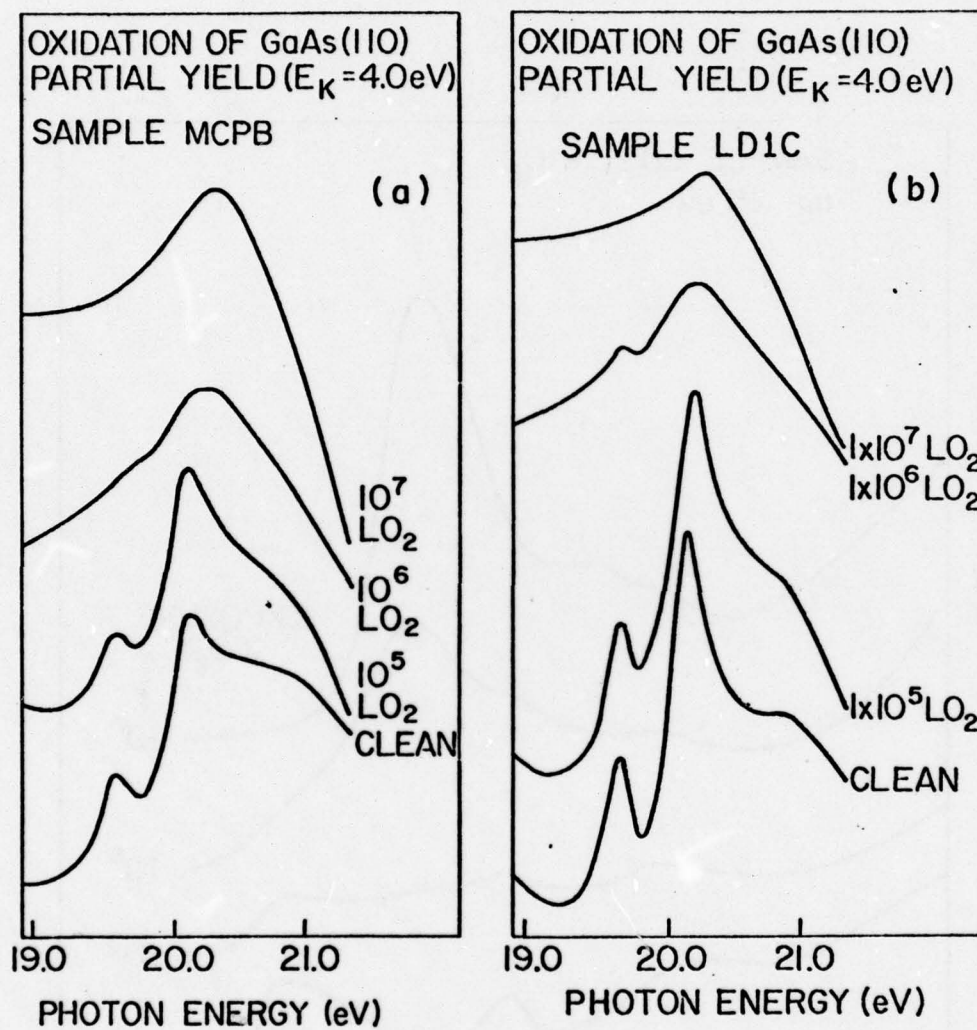


Fig. 17(a) and (b)

Appendix C

CHEMISORPTION AND OXIDATION STUDIES OF THE (110) SURFACES OF GaAs, GaSb, AND InP*

C. M. Garner, and W. E. Spicer
Stanford Electronics Laboratories
Stanford University
Stanford, California 94305

The surface chemistry of cleaved GaAs (110) (and, to a lesser extent, InP and GaSb) is studied as a function of oxygen exposure (both unexcited and excited) with soft X-ray photoemission spectroscopy. When the cleaved GaAs (110) surface is exposed to molecular oxygen in the ground state, chemisorption to only the arsenics takes place. No back bonds are broken even for large exposures. Room temperature oxidation of the surface can be induced by exciting the oxygen, e.g., by an ionization gauge. The adsorption of excited oxygen is initially the same as for the unexcited, except 500 times faster. However, after $>20\%$ of a monolayer has been adsorbed, further exposure to excited oxygen causes back bonds to be broken and $\text{As}_2\text{O}_5/\text{AsO}_2$ and Ga_2O_3 are formed. Larger doses of excited oxygen result in the formation of thicker oxides composed primarily of Ga_2O_3 with small amounts of elemental As (or As bound to only one Ga) and As_2O_3 , most of which has sublimed from the surface. No $\text{As}_2\text{O}_5/\text{AsO}_2$ is seen in the thicker oxide because there is a deficiency of oxygen and any partially oxidized Ga present will reduce the arsenic oxides. The escape depth for GaAs (110) was measured for electron kinetic energies between 20 and 200 eV. This range includes the minimum in the escape depth which is about 6 Å at 60 eV. No chemical shift in the core levels between the atoms on the surface and in the bulk was observed. GaSb (110) and InP (110) surfaces were also studied. InP

behaves like GaAs, whereas the GaSb is oxidized immediately even when exposed to only unexcited oxygen. The oxygen uptake curves for GaSb and GaAs were compared and found to be quite different with a sticking coefficient, at zero coverage, of 2×10^{-4} for GaSb and 8×10^{-10} for GaAs.

* Work supported by the Advanced Research Projects Agency of the Department of Defense monitored by Night Vision Laboratory, U. S. Army Electronics Command under Contract No. DAAK 02-74-C-0069 by the Office of Naval Research Contract No. N00014-75-C-0289; by the National Science Foundation Contract No. DMR 73-07692 A02 in cooperation with the Stanford Linear Accelerator Center and the U. S. Energy Research and Development Administration.

I. INTRODUCTION

The surface physics and chemistry of III-V compound semiconductors have attracted considerable interest, both experimental and theoretical. One of the things that makes III-V compounds such as GaAs so interesting from a fundamental point of view is the effect of the polar nature of the fundamentally covalent Ga-As bond on the surface properties of the crystal. III-V compounds also have important practical applications such as infrared detectors, high frequency MOS devices, and light emitting diodes. One of the major obstacles in fabricating GaAs MOS devices, as well as in many other applications, is that it is very difficult to passivate the surface. Much work has been done in this area, but no oxides with the favorable properties characteristic of silicon based devices have yet been developed. Thus, it is very important to gain more insight into the chemistry of the oxide semiconductor interface.¹

Crystals of the III-V compounds have the zincblende structure, illustrated in Fig. 1, where we give a view of the lattice along the $(1\bar{1}0)$ axis and terminate it on the ideal (110) , (111) , and $(\bar{1}\bar{1}\bar{1})$ faces. We should note that in terminating the lattice to create the ideal surfaces, one covalent bond per surface site has been broken, leaving three intact.²

On the (110) surface, which is the cleavage face of the III-V semiconductors, a rearrangement of charge takes place and it becomes energetically favorable for the surface atoms to seek a bonding configuration more characteristic of their covalent bonding in small molecules. To be more precise, a simplified version of the currently accepted model is that the surface Ga now has only three electrons (in an sp^2 configuration), all involved in back bonding, while the As has five electrons (in a p^3s^2 configuration), three of these electrons take part in the

back bonds (p^3) and the remaining two (s^2) are the "dangling bond orbitals."²⁻⁴ This charge rearrangement has two important consequences. First, the change in the bonding configuration of the surface atoms results in a distortion of the lattice at the surface consistent with the planar sp^2 Ga back bonds and the prismatic p^3 As back bonds, Fig. 2 (we should note this relaxation is not total).^{3,5,6} Secondly, since all of the electrons on the surface Ga are used in forming the back bonds, the Ga has no filled surface state orbitals. The surface As atoms, on the other hand, have two available electrons to contribute to the filled surface state band which lies well below the valence band maximum.^{1,2} The position of the filled and empty surface states on an energy level diagram is also shown in Fig. 2 after Gregory et al.^{2,3,7-10}

The basic aspects of this model can also be applied to the polar faces in order to explain the greater chemical activity of the As-terminated ($\overline{111}$) face with respect to the Ga-terminated (111) face. However, the experimental situation for the polar faces is not as well defined as for the cleaved (110) surface since the surface atoms on the polar surfaces probably have some unsaturated bonds. This situation could be caused by deficiencies in the available surface preparation techniques or fundamental problems arising from the polar nature of these surfaces.^{3,4,11,12}

One of the major predictions of the model of Fig. 2 is that, for the (110) surface, oxygen is adsorbed preferentially on the arsenic atoms by interacting with the filled surface states. Furthermore, since all the bonding electrons associated with the surface gallium atoms are involved in the back bonds, the oxygen will bond to the gallium only after one or more of the back bonds are broken.^{2,7,13} The oxidation of

GaAs has been studied extensively by ultraviolet photoemission spectroscopy (UPS),^{2,14} ellipsometry,¹⁵ electron energy loss spectroscopy (EELS),^{16,17} Auger electron spectroscopy (AES),^{12,14,15,18} and low energy electron diffraction (LEED).^{5,15} The early experimental work on the cleaved (110) surface gave results that were consistent with the predictions outlined above,^{2,15,16} whereas recent results on the polar surfaces have been interpreted to mean that the oxygen sticks preferentially to the surface Ga atoms.^{12,17} However, the conclusions from one of the studies¹⁷ on the polar surfaces are based on indirect evidence whose interpretation is open to question.¹⁹ The interpretation given in the second set of studies¹² is probably correct, but the polar faces used had unsaturated Ga bonds so that adsorption on the Ga sites does not necessarily disagree with the model of Fig. 2 (this point will be discussed at the end of Section III.F).

In our recent work^{7,13} on the GaAs (110) surface, we showed definitively that there is a charge transfer from surface As atoms to chemisorbed oxygen. We interpreted this to mean that the oxygen is bound preferentially to surface As atoms, in agreement with the earlier work cited above. We have also shown that InP behaves in the same way as GaAs, whereas the oxidation of GaSb proceeds in an entirely different manner. In GaSb, the oxygen bonds both species breaking the Ga-Sb back bonds.⁷ This latter effect can then be compared to the situation when the GaAs (110) surface is exposed to excited oxygen.²⁰

In this paper, we will present a detailed analysis of our previously reported results and new data on the very heavily oxidized surface of GaAs (110) which gives us greater insight into the oxidation of GaAs.

All the results presented here were obtained with soft X-ray photoemission spectroscopy (SXPS) using synchrotron radiation from the "4° line" at the Stanford Synchrotron Radiation Project in the photon energy range $32 \text{ eV} \leq h\nu \leq 350 \text{ eV}$.²¹ This photon energy range is interesting because, first of all, it allows us to observe both the valence band and several core levels from both the Ga and As at high resolution (0.25 eV). In Fig. 3, we show a typical electron energy distribution curve (EDC) for the clean, cleaved GaAs (110) surface for $h\nu = 240 \text{ eV}$. The spectral features of interest for this work are the As and Ga core levels located 19.0 and 40.8 eV below the valence band maximum as well as the valence band (s-p derived levels) which occupy the top 12 eV of the spectrum. Besides these one electron lines, we are also able to see Auger transitions and plasmon losses.

By tuning through the available photon energies, we are able to adjust the kinetic energies of the various levels to be roughly between 20 and 200 eV. This is possibly the most significant aspect of our experiments because the escape length of electrons in a material is strongly dependent on the electron kinetic energy, and this escape depth goes through a minimum of $\sim 10 \text{ \AA}$ for kinetic energies between 50 and 150 eV for most materials.²² Thus, we are indeed able to observe the surface electronic structure.

The experimental methods, such as LEED, AES, and UPS, that were used in the earlier oxidation studies all have high surface sensitivity. However, they lack the chemical information which can be obtained from X-ray photoemission (XPS) studies of core level shifts.²³ AES can be used to look at chemical shifts, but the use of an e-beam as the excitation source can desorb the oxygen or destroy the integrity of the surface.^{18,20,24}

This damage is minimized when using UV light or X-rays. However, conventional XPS ($h\nu = 1486.7$ or 1253.6 eV) lacks the necessary surface sensitivity.²² With SXPS, not only can we study the chemical shift of core levels upon forming a chemical bond, but we can also perform these studies at submonolayer coverages due to the inherent surface sensitivity of the technique.^{7,13} In our experiment, we adsorb oxygen on GaAs, GaSb, or InP and observe any core level shifts that take place upon adsorption. We then measure the magnitude of the core level shifts and correlate these shifts with chemical shift measurements made on bulk oxides using conventional XPS. This correlation allows us to determine the type of oxides forming at the surface in a relatively straightforward way, obviating the need to perform complicated calculations.²³ The ratio of the area of the shifted to unshifted peaks can be used to determine coverages versus exposure as well as escape depth information. All these points will be treated in detail here.

In Section II, we will discuss the experimental apparatus, procedure, and results. Section III will contain the discussion. In this section, we will correlate the chemical shifts obtained from the surface oxidation of GaAs (110) to the shifts obtained from ESCA measurements of bulk oxides. These correlations will then be used to give a model for the oxidation of GaAs (110), starting from surface chemisorption and ending with the formation of actual bulk oxides. We will also determine the escape depth for GaAs as a function of photon energy as well as show a difference in adsorption kinetics between GaAs (110) and GaSb (110).

II. EXPERIMENTAL

A. Apparatus

The experimental chamber consists of a stainless steel UHV bell jar, base pressure $<1 \times 10^{-10}$ torr, and is shown schematically in Fig. 4. The pumping system is a 240 L/sec ion pump plus titanium cryo-pump with a poppet valve for sealing the pump from the main chamber. The chamber contains a double pass cylindrical mirror analyzer (Physical Electronics), a cleaver, and a sample manipulator capable of holding 4 samples for cleaving, one sample for heat cleaning ($T_{\text{max}} \approx 2000^\circ\text{C}$) and a substrate upon which Au or Cu may be evaporated for Fermi level (and thus binding energy) determinations.²⁵ An evaporator which contains copper and gold beads is also housed in the chamber.

Research grade oxygen was admitted into the vacuum system through a bakeable leak valve. For large exposures (pressures up to 750 mm O_2) an auxiliary pumping system was used to return the main chamber to pressures below $\sim 10^{-8}$ torr. This system consisted of vacuum pumps, an ion pump, and all the necessary gauging to measure pressures for the gas exposures.

Pressures between 10^{-11} and 10^{-5} torr were measured by a Red-head cold cathode ionization gauge (NRC) located in the main vacuum system. This pressure range was used for exposures up to 10^4 L (1 L = 10^{-6} torr/sec) where the exposure time was no longer than 10^3 sec. A hot filament ionization gauge with Thoria coated iridium filaments (Varian) was also located in the main vacuum system. This gauge was used initially to check the cold cathode gauge and more importantly as a source of excited oxygen when used during a gas exposure. The effect of the ion gauge on the oxidation will be treated in a later section.

Pressures between 10^{-5} and 0.6 torr were measured by a millitorr gauge (Varian) located in the auxiliary pumping system. This pressure range gives exposures between 10^4 L and $\approx 10^9$ L. A thermocouple gauge (Hasting DV-4) again in the auxiliary pumping system, was used for pressures between 1 and 20 torr, giving exposures between 10^9 L and 2×10^{10} L. For larger exposures of up to 10^{12} L, a mechanical vacuum gauge (Wallace and Tiernen) was used, measuring pressures up to 800 torr.

The synchrotron radiation is monochromatized by a grazing incidence monochromator (resolution 0.2 \AA) with a refocusing mirror located after the exit slit.²⁶ The radiation enters the chamber through a bakeable straight through valve and strikes the sample as indicated in Fig. 4. The energy of the photoemitted electrons is then determined by the double pass cylindrical mirror analyzer operated in the retarding mode. This mode insures a constant resolution which is equal to 0.6% of the electron pass energy through the analyzer. In these experiments, we used a pass energy of 25 eV, giving an electron energy resolution of 0.15 eV. At $h\nu = 100 \text{ eV}$, typical counting rates on the Ga 3d levels are about 5×10^3 counts per second for a circulating electron current in SPEAR of 20 ma.

The signals from the electron energy analyzer are amplified and fed into a 2048 channel signal averager (Tracor Northern) used as a multichannel scaler. The energy of the detected electrons was controlled by the signal averager through a voltage ramp synchronized with the memory sweep.

The samples that were studied in these experiments are Te doped, n-type GaAs ($n = 3.5 \times 10^{17} \text{ cm}^{-3}$ and $n = 0.5 \times 10^{18} \text{ cm}^{-3}$)²⁷ and Zn doped p-type GaAs ($p = 6 \times 10^{18} \text{ cm}^{-3}$) from Laser Diode (LD) Corporation;

Te doped n-type GaSb ($n = 1.1 \times 10^{18} \text{ cm}^{-3}$) from Asarco;²⁸ and Zn doped p-type InP ($p = 2 \times 10^{18} \text{ cm}^{-3}$) from Varian Associates. The GaAs and GaSb samples were rectangular prisms $5 \times 5 \times 10 \text{ mm}^3$, and the InP was $2 \times 5 \times 10 \text{ mm}^3$. In all the samples, the (110) axis was along the long dimension.

B. Procedure

First, the samples were cleaved along the (110) planes by slowly squeezing the sample between the annealed copper anvil and tungsten-carbide knife of the cleaver. The cleaved sample is then inspected visually to ensure the cleave had a mirror-like finish. A set of spectra is taken for $32 \leq h\nu \leq 300$. Now the sample is ready to be exposed to oxygen. The pump is valved off from the main chamber with the poppet valve, partially for exposures below 10^4 L and completely for larger exposures. The gas is admitted and the pressure monitored. After the desired exposure is reached, the majority of the gas is removed with the auxiliary pumping system. When the chamber reaches a pressure below $\sim 10^{-8}$, the poppet valve is opened and the main pump takes the chamber to pressures below $5 \times 10^{-10} \text{ torr}$ for all gas exposures that were performed. During these exposures, the straight through valve into the grazing incidence monochromator has been closed and is not opened until the pressure in the chamber $< 1 \times 10^{-9} \text{ torr}$. With this scheme for making the gas exposures, the chamber is returned to its base pressure very quickly. Using the technique described above, the majority of the gas is pumped out in the first 15 sec and working pressure is achieved within 10 to 15 minutes, giving a minimum of down time between spectra. A set of spectra is then taken after each exposure as mentioned above.

The majority of the pressure gauges are located in the auxiliary pumping system, 60 cm away from the main chamber, separated by two right angle bends. Calibration runs were made to insure that the pressure measured in the auxiliary system matched the actual pressures in the main system.

The exposures with excited oxygen are performed with the ion gauge in the main chamber turned on.²⁹ This gauge is out of line of sight of the sample so that the gas molecules must strike at least 2 surfaces before hitting the sample. However, for the larger exposures, it is also possible that the oxygen is deflected to the sample through collisions with other gas molecules since the mean free path of the molecules is between 1 and 10 cm for the pressures used in the ion gauge exposures (10^{-2} to 10^{-3} torr). Two different ion gauge emission currents were used in the exposures. One emission current setting was 4.0 ma (for pressures below 10^{-4} torr), and the other was 0.4 ma (for pressures between 10^{-2} and 10^{-3} torr). We did not directly determine if there was a tenfold increase in the amount of excited oxygen in going from the 0.4 to 4.0 ma emission currents, but the results of the oxidation indicate that this should be the case.³⁰

The binding energies in these studies are measured relative to the valence band maximum of the clean surface. Binding energies with respect to the Fermi level can be determined by referring the unknown binding energies to either the 4f levels of Au (binding energy = 84.0 eV) or the Fermi level of a gold film evaporated in situ on a substrate in electrical contact with the sample.²⁵

In all the figures that follow, in which we show spectra for clean and oxidized samples on the same graph, the horizontal binding

energy scale refers to the clean spectrum. The spectrum of the oxidized samples are adjusted so that the various unshifted peaks line up consistently. This must be done because the Fermi level pinning for these samples changes as a function of oxygen exposure so that binding energies referenced to the Fermi level vary.^{7,31} Furthermore, the structure in the valence band also changes considerably with oxidation so that the unshifted core levels must again be used as standards. Beyond 10^7 LO_2 , the position of the Fermi level has stopped moving so that we may use the measured energy positions of the peaks as a consistency check.

C. Results

In this section, we will present our photoemission results for oxygen adsorption on the (110) surface of GaAs, GaSb, and InP. These results include measurements of the chemical shifts of the substrate core levels upon oxygen adsorption and the determination of the oxygen coverage as a function of exposure. We also present results for the exposure of GaAs (110) to excited oxygen and measure the resulting substrate core level shifts.

In Fig. 5, we show spectra for the clean and oxidized GaAs (110) surface at $h\nu = 100$ eV. As we expose the surface to oxygen, we see a single peak ($E_B = 43.7$ eV) growing 2.9 eV below the As-3d peak ($E_N = 40.8$ eV) with a proportionate decrease in the As-3d intensity. This is a chemically shifted peak indicating a transfer of charge from the surface As atoms to the adsorbed oxygen. Concurrent with the appearance of the shifted arsenic peak, we see the O-2p resonance level at a binding energy of about 5 eV.

As we go to higher exposures, the shifted As-3d peak and O-2p level grow simultaneously until saturation is reached between 10^9 and 10^{12} LO_2 . An estimate of the relative amount of oxidized As atoms on the surface can be obtained by comparing the areas under the shifted and unshifted peaks. This is done in Fig. 6, where we plot the area in relative units under the shifted and unshifted peaks as a function of exposure. Here, the sum of the areas under the shifted and unshifted peaks were normalized to unity. As expected, the amount of oxidized arsenic increases while the unoxidized decreases for increasing exposure. At 10^6 LO_2 , where we first start to see the effect of oxygen in the valence band as well as seeing a chemically shifted As-3d level, the coverage is only about 2% of saturation.

If we consider only the points up to an exposure of 5×10^9 LO_2 in Fig. 6, saturation seems to have been reached at about 10^9 LO_2 . If, however, we include the point at 10^{12} LO_2 , which gives a 1.7 times increase in coverage over that at 10^9 LO_2 , the apparent saturation exposure is increased by three orders of magnitude. At present, we will not place too much emphasis on this one point because the spectrum for 10^{12} LO_2 was obtained from sample LD1, whereas the other spectra in Fig. 5 came from sample LD3.

It is also possible that cleave quality could affect oxygen uptakes by as much as a factor of two. On the other hand, we could be seeing a real effect indicating a change in adsorption kinetics between 10^{10} and 10^{12} LO_2 . In any case, the question of oxygen uptake versus exposure merits further experimental investigation before we can make quantitative statements on the adsorption kinetics.

Information on relative oxygen coverages can also be obtained by measuring the area under the O2p resonance in the valence band. The major drawback to this technique is that the valence band and the O2p signal overlap so that it is difficult to get reliable coverage information below exposures of about $5 \times 10^7 \text{ LO}_2$. Even above this exposure, the GaAs valence band is still a significant fraction of the total emission, so care must be used in separating out the oxygen contribution from that of the GaAs. These problems are seen rather clearly in Fig. 7 where we show a blow-up of the GaAs valence band for various oxygen exposures.

We should also note at this point that the coverage, as determined from the shifted arsenic level, gives a measure of the relative amount of oxygen that has chemically combined with the surface arsenic atoms. The coverage obtained from the O2p signal gives a measure of the total amount of oxygen sticking to the surface. Thus, comparison of the oxygen uptake determined in these two ways can be used to give additional information on the kinetics of the adsorption as well as the nature of the adsorbate. Our initial studies on sample LD3 indicate that the two methods give similar results. However, as mentioned above, more experimental work needs to be done on exposures between 10^{10} and 10^{12} LO_2 before definitive conclusions may be drawn.

The significance of the curve for 10^{12} LO_2 is that, even for this very large exposure (this corresponds to an exposure of one atmosphere of O_2 for 20 minutes!), no shift in the gallium 3-d level is observed. The only effect on the gallium peak is a 0.4 eV broadening. Part of this broadening may be due to a nonuniformity in work function across the face of the sample since the unshifted arsenic peak is

broadened by 0.1 eV. Also, notice that no asymmetric broadening is seen in the Ga 3d level for the exposures below 10^{10} LO_2 .

The oxidation of the GaSb (110) surface is shown in Fig. 8 for $h\nu = 100$ eV. As in the case of GaAs, all the spectral features of interest can be obtained at the same photon energy and in one spectrum, thus facilitating comparisons. The valence band extends approximately 12 eV below the valence band maximum. The Ga-3d level is at a binding energy of 19.4 eV, the Sb-4d doublet is at 32.1 eV ($4d_{5/2}$) and 33.2 eV ($4d_{3/2}$). We are able to clearly see the spin orbit splitting in the Sb-4d levels, whereas we were not able to see it at these energies for the Ga and As levels, primarily because the splitting of the Sb-4d levels is much larger than that of the 3d levels of As or Ga. We should also note that the As and Ga levels are 3d's, while that of Sb is a 4d. This point is important for the choice of photon energy since the variation of cross-section for the 4d levels versus photon energy is rather dramatic, as indicated in Fig. 9. Here, we show spectra of oxidized GaSb for several different photon energies. Notice that almost all the intensity is lost from the 4d levels over a very small photon energy range. The variation in cross-section of the 3d's is not as dramatic, but is nevertheless also large.³² Consequently, we are forced to use photon energies below about 120 eV.

As we oxidize the GaSb surface, we start to see changes in the spectra at about 5×10^5 LO_2 . This is about a factor of two sooner than with the GaAs. But, more importantly, as we increase the exposure to 5×10^7 LO_2 , we start to see a definite broadening of the Ga-3d level toward higher binding energy. In fact, even by 5×10^8 LO_2 , a definite shifted Ga-3d peak is seen ($\Delta E_B = 1.1$ eV). Of course, the shifted

Sb-4d ($\Delta E_B = 2.5$ eV) level has also been growing at the expense of the unshifted level. The shifted peaks for both Sb and Ga completely dominate the unshifted peaks for exposures above 5×10^9 LO_2 . In Figs. 10(a) and 10(b), we can see the obvious differences between the oxidation of GaAs and GaSb. In GaAs, only the As peak is shifted while the Ga peak is broadened. In GaSb, both the Sb and Ga are definitely shifted, indicating that charge transfer from both surface Sb and Ga atoms to the oxygen has taken place. This implies that bonds are broken between neighboring surface Ga and Sb atoms.

Another striking difference is seen if the coverage (area under shifted Sb peak or O-2p level) is plotted with respect to exposure (Fig. 11). The rate of oxygen adsorption from Fig. 11 does not show the saturation behavior which is characteristic of the GaAs surface as seen in Fig. 6.

Spectra for the clean and oxygen exposed p-type InP (110) surface are shown in Fig. 12. In this case, we used two different photon energies to optimize the surface sensitivity and cross-section for the levels of interest. The P-2p levels are measured at $h\nu = 160$ eV and the In-4d levels at $h\nu = 80$ eV. The indium levels, being 4d levels, have the same general behavior versus photon energy as the Sb-4d levels. Therefore, they too have a rather large variation in cross section forcing us to choose a photon energy not too high above threshold. As seen from Fig. 12, the InP (110) surface behaves like GaAs (110), with possible differences in the adsorption kinetics which will not be dealt with here. One subtle difference is that we are able to resolve the spin orbit splittings in both the phosphorous and indium levels for the clean surface. However, they smear out upon oxygen adsorption. No shifts are

observed in the In-4d levels, and a shifted P-2p level ($\Delta E_B = 4.4$ eV) is observed which grows with oxygen exposure. Similar results have been seen in InAs by Gudat and Eastman.³⁴

All the previous exposures were done with unexcited molecular oxygen. In the section that follows, we will consider the effect of excited oxygen on the adsorption process.²⁰ In Fig. 13, we show what happens when the GaAs (110) surface is exposed to excited oxygen. In these spectra, the exposure was carried out in exactly the same way as the previous exposures except that the ion gauge was on during the exposure with an emission current of 4 ma (the exposures at 10^6 and 10^7 L used an emission current of 0.4 ma). Comparing these spectra to those in Fig. 5, we see that the sticking probability has become much larger. It only takes an exposure of 10^5 L excited oxygen to give the same effect as an exposure of 5×10^7 IO_2 . This is an increase in oxygen adsorption by a factor of 500! The fact that oxygen, which has been excited in some way, will stick more readily to semiconductor surfaces has been documented in the literature.^{15,33} What has not been seen before is the change in chemical state due to bonding of such excited oxygen.²⁰ As we expose the surface to even more excited oxygen, a rather striking thing happens. At an exposure of 5×10^5 L excited oxygen, the first shifted peak ($\Delta E_B = 2.9$ eV) stops growing, and a second shifted peak with a binding energy shift of 4.5 eV starts to grow and soon dominates the first shifted peak. But, what is even more striking is that the gallium peak starts to broaden also at 5×10^5 L excited oxygen. At higher exposures, we can see that the initial broadening at 5×10^5 L excited oxygen is due to a shifted gallium peak ($\Delta E_B = 1.0$ eV) which grows concurrently with the second shifted

arsenic peak.¹³ This simultaneous growth is very much like what was seen for the oxidation of GaSb in Fig. 8. We also see in these spectra the O-2s at 24 eV and the O-2p at 5 eV below the valence band maximum.

In Fig. 14, we give examples of the effects of very large doses of excited oxygen on the GaAs (110) surface. The top two curves are spectra for clean GaAs (110) and for the clean surface plus 10^{12} IO_2 . The spectrum labeled "heavily oxidized" was obtained by exposing the surface, which had previously been exposed to 10^{12} IO_2 , to 5×10^5 L excited oxygen with the ion gauge running at 0.4 ma emission current. Notice that the binding energies of the peaks in this spectrum are the same as those of Fig. 13. There are two oxidation states of As, and there is a shifted gallium peak. The fourth spectrum of Fig. 14 labeled "very heavily oxidized" was obtained by exposing clean GaAs (110) to 5×10^5 L excited oxygen with the emission current of the ionization gauge set at 4.0 ma (giving a significantly larger amount of excited oxygen than in the previous case). In this case, we see no unshifted gallium peak; only the shifted one. There is no unshifted arsenic peak, but there are two other peaks shifted 0.4 and 3.2 eV with respect to the unshifted peak (if it were present). Note the drastic decrease in emission from the arsenic derived levels. Notice also that the emission from the O-2p and O-2s levels has gone down with respect to that in the second and third spectra.

The significance of these observations will be discussed in the next section, where we will present a model for the oxidation of the GaAs (110) surface from the chemisorption stage to the formation of bulk oxides. In Tables I and II, we summarize the binding energies and chemical shifts (for GaAs) discussed above.

III. DISCUSSION

A. Introduction

Now that we have described our experimental results, we will first identify the chemical species that appear on the surface when the GaAs (and to a lesser extent InP and GaSb) is exposed to oxygen, both excited and unexcited. Since this surface chemistry determines the kinetics of the reaction, we will be able to comment on the differences between the oxygen uptake curves for GaAs and GaSb shown in Figs. 6 and 11.

In the third part of this section, we will use the photon energy dependence of the spectra to determine the relative escape depth of GaAs for $20 \text{ eV} \leq h\nu \leq 240 \text{ eV}$. We will then be able to determine the absolute escape depth by estimating the thickness of the chemisorbed oxygen layer. With this information, we can set an upper limit on any chemical shift between the surface and bulk atoms in GaAs. Finally, we will combine all the above information to give, for GaAs, a description of what happens when the clean surface is first exposed to molecular, unexcited oxygen and then fully oxidized by exposure to excited oxygen.

B. Interpretation of Chemical Shifts

In this section, we will concentrate on trying to determine which oxidation states of the As and Ga give rise to the chemically shifted peaks that are observed in the photoemission spectra.

Considerable information can be obtained from the chemical shift measurements by assuming that ligands of any given type each shift the core levels of the central atom by the same amount.²³ Thus,

the total shift, ΔE_{tot} , is simply given as the sum of the individual ligand shifts, ΔE_{ligand} , i.e.,

$$\Delta E_{\text{tot}} = \sum_{\text{all ligands}} \Delta E_{\text{ligand}} \quad (1)$$

The magnitude of the ligand shift may be determined by measuring the binding energies of several compounds containing different numbers of these ligands. In our case, this is very useful for the case of non-stoichiometric oxides. For stoichiometric oxides, the obvious thing to do is to use the bulk oxides as standards. Here, we will do both in order to determine the chemical species present on the surface after initial chemisorption and further oxidation.

In Table III, we present binding energy shifts for the Ga and As 3d levels in the compounds that will be used as standards. These values are taken from the literature and, rather than give absolute binding energies, we choose instead to give the binding energy differences between the levels in the various compounds. This, in effect, avoids many of the problems in choosing an appropriate reference level when comparing the results from several sources. Through the work of Bahl et al.,³⁵ we were able to determine the 3d level binding energy shifts for As_2O_5 and As_2O_3 with respect to As. We then calculated the difference between the Ga and As 3d levels of As_2O_3 , Ga_2O_3 , GaAs, and Ga by referring to the work of Leonhardt et al.³⁶ The $\text{Ga}_2\text{O}_3/\text{Ga}$ shift was found to agree with Schön's measurements to within 0.1 eV.³⁷ By this method, we obtained all of the binding energy differences listed in Table III except for those of GaAsO_4 (gallium arsenate). These

binding energies were measured for us by an independent laboratory (using a Hewlett-Packard 5950A ESCA spectrometer)³⁸ and were referenced to the Ga-3d level in Ga_2O_3 which was also measured. The GaAsO_4 sample outgassed considerably upon introduction into the vacuum system and showed a marked arsenic deficiency. The Ga:As ratio is about 3:1 in the GaAsO_4 compared to 1:1 in GaAs, indicating that the outgassing was probably due to sublimation of As_2O_3 from the material. We included this data in Table III, even though the original compound had probably dissociated, because the core level shifts match those which we measured for the AsII peak for oxidized GaAs (see Table II). To avoid confusion, we will refer to this compound as GaAsO_4 (dissociated).

The ligand shifts for the standard compounds may be calculated from the chemical shifts given in Table III. This is done in Table IV. In the first column of Table IV, we list the compounds. In the second column, we list the shifts of the As or Ga 3d levels in these compounds with respect to their binding energy for the free element. A positive chemical shift is defined as a shift to higher binding energy. Columns 4 and 5 give the number and type of ligand for the compounds in the first column. See Fig. 15³⁹ for an illustration of the molecules or lattices that give rise to the entries in columns 4 and 5. The GaAs structure is shown schematically in Fig. 15(a). Here, we show that each gallium (or arsenic) has four arsenic (or gallium) ligands. In Fig. 15(b), we show the As_4O_6 molecule which is the molecular arrangement for As_2O_3 . Here, we have three single oxygen single bonds per arsenic atom. Ga_2O_3 (not shown) is coordinated by six oxygens. In Fig. 15(c), we show the As_4O_{10} molecule which is the molecular form of As_2O_5 ; here, we have three oxygen single bonds and one oxygen double bond per arsenic.

Ideal GaAsO_4 has a quartz-like structure with the silicon atoms replaced by alternating Ga and As. This results in each gallium and arsenic having four oxygen ligands as shown in Fig. 15(d) (the shifts for ideal GaAsO_4 are discussed below). In Table IV, we have listed the As in GaAsO_4 (dissociated) as having four oxygen ligands while the Ga has six. This was done because, as mentioned above, the compound had decomposed, and we were probably looking at a mixture of Ga_2O_3 and As surrounded by four oxygens. This point will become clearer when we use the ligand shifts from column 3 to discuss the possible origins of the AsII peak of Fig. 14.

The ligand shifts, ΔE_j , are the shifts due to the particular ligand j and are obtained most simply by dividing the total shift (column 2) by the number of ligands (column 4). When there are two types of ligands in the compound in question, such as As_2O_5 which has three $-\text{O}$ and one $=\text{O}$, we use another compound, As_2O_3 in this case, to determine one set of the shifts and then we solve for the second.

In the last two rows of Table IV, we have calculated, using the experimentally determined shifts with Eq. (1), the shifts that we would expect from ideal GaAsO_4 , GaO_2 , and AsO_2 . All three of these structures have an As or Ga with four $-\text{O}$ ligands; thus, the shifts for the As or Ga in each compound should be the same. We should note, in comparing the ligand shifts of Table IV with those given in Table V of reference 35, that the shifts quoted here are only 3-d shifts, whereas those used by Bahl et al are the average of the shifts of all the core levels. Thus, there will be a slight discrepancy if this point is not realized.

Now we are in a position to compare these chemical shifts to the chemical shifts observed in our measurements.

As mentioned in the previous discussion, when the GaAs (110) surface is exposed to unexcited oxygen, only one shifted arsenic peak, AsI, is seen for all coverages. This implies that only a single site is involved in the chemisorption of unexcited oxygen. Thus, we must conclude that the AsI peak, with a shift of 2.9 eV with respect to GaAs (2.3 eV with respect to elemental As), is due to one oxygen atom or molecule bonded to a surface arsenic atom. The shift of the AsI peak is much larger than either the shift due to a single As-O bond ($\Delta E_B = 0.87$ eV with respect to GaAs) or of an oxygen-arsenic double bond ($\Delta E_B = 1.7$ eV with respect to GaAs). In fact, the experimentally determined shift of 2.9 eV is closer to the shift expected from three oxygens singly bonded to each surface arsenic atom, necessitating the breaking of back bonds. However, this latter situation implies that three, not one, chemically shifted As 3-d peaks (ΔE_B with respect to GaAs $\approx -0.87, -2.04$, and -3.06 eV) should be observed corresponding to the three possible oxidation states which the surface arsenic atoms would then have. We would expect to see the -0.87 and -2.04 eV peaks for low and intermediate coverages and the -3.06 eV peak almost exclusively for the high coverages. This is clearly not what we observe experimentally. Therefore, we must conclude that the AsI peak is due to a single arsenic oxygen bond that gives a binding energy shift three times larger than what is expected from an As-O bond in an arsenic oxide. In the case of As_2O_3 , the oxygens are more electronegative than the arsenic, so there is an equal transfer of charge away from the arsenic along each ligand. In the case of oxygen chemisorbed to the GaAs surface, the gallium back bonds transfer charge

to the arsenic so the oxygen is the only ligand in which there is charge transfer away from the arsenic. That is, the single oxygen ligand does not have any competition for the charge on the arsenic. Consequently, the oxygen ligand in this case could give a much larger shift than would be predicted by a simple ligand shift analysis where the different electronegativities of the various ligands have not been taken into account. These same arguments, now used to estimate the shift of the Ga-3d due to a chemisorbed oxygen, would imply that the shift should be less than 0.33 eV (the ligand shift due to a single oxygen ligand in Ga_2O_3). Consequently, we would not expect to see a distinct chemically shifted peak for the case of oxygen chemisorption on the surface gallium atoms. We would, however, expect to see an asymmetric broadening of the Ga-3d level. For exposures below 10^{10} LO_2 , the Ga 3-d broadens symmetrically by $\pm 0.12 \text{ eV}$ and the shift to higher binding energy is less than 0.03 eV. If oxygen did attach itself to the surface gallium atoms, there would be little charge transfer and the resulting bond would be weak. We can also exclude the possibility of bonding oxygen to the surface gallium atoms by breaking back bonds, because in this situation we should definitely see an asymmetric broadening of the Ga 3-d level along with intermediate oxidation states of the arsenic atoms, neither of which is observed experimentally.

The AsII peak, also labeled " As_2O_5 or AsO_2 ," in the "heavily oxidized" curve of Fig. 14 is shifted 4.6 eV with respect to the arsenic in GaAs (or 4.0 eV with respect to elemental As). This value is bracketed by the experimentally determined value of 4.9 eV (4.3 eV with respect to elemental As) for As_2O_5 and the calculated value of 4.1 eV (3.5 eV with respect to elemental As) for AsO_2 . The average of these two

shifts gives 4.5 eV (3.9 eV with respect to elemental As), very close to the value measured in this work. This seemingly fortuitous result may be interpreted as follows. There are three single bonds and one double bond in As_2O_5 , whereas AsO_2 contains four single bonds. The fact that the shift we measure lies between these two shifts is significant because, first, it indicates there are four oxygens bound to the As and, secondly, these bonds must have some double bond character. We should note at this point that the same arguments could be applied to what we see in the experimental shifts for GaAsO_4 (dissociated),³⁸ since the shifts are identical to those for the AsII and GaI peaks (compare Tables II and III). There are, however, no peaks in the spectra corresponding to the ideal GaAsO_4 structure of Fig. 15(d).

As mentioned above, with reference to Fig. 13, the gallium peak starts to shift as soon as the AsII peak appears. The magnitude of the gallium shift is 1 eV which corresponds to Ga_2O_3 (compare Tables II and III). The fact that we start forming oxides of Ga and As at the same time clearly indicates that back bonds are being broken and true oxidation of the surface is occurring. We should note again that we do not observe any intermediate oxidation states for the gallium.

In the "very heavily oxidized" spectrum of Fig. 14, the gallium peak, GaI, is still shifted by 1 eV, indicating the presence of bulk Ga_2O_3 . But, now, the peak labeled AsIII is shifted 0.4 eV with respect to the unshifted arsenic peak, Ga(As). The shift we expect between free arsenic and arsenic in GaAs is 0.6 eV. Thus, this peak could be due to

free As or, equally likely, arsenic bound to only one gallium atom (see the -Ga ligand shifts in Table IV for Ga(As)). The latter case would give a shift of about 0.4 eV. Therefore, it is plausible that this peak is due to either free arsenic or arsenic bound to at most one gallium atom. The second arsenic peak in this spectrum, labeled AsIV, is shifted 2.6 eV with respect to the As in GaAs. This is exactly the same as the shift observed for bulk As_2O_3 (Table III).

In the above discussion, we have identified the chemical species present on the GaAs (110) surface during the initial chemisorption stages as well as when we go well into the formation of bulk oxides. We will now turn our attention to InP and GaSb. As mentioned above, InP behaves exactly like GaAs in the chemisorption stage. As in the case for the AsI peak, the chemical shift in the P-2p ($\Delta E_B = 4.4$ eV) is much larger than one would expect by simply adding an -O or =O group. The shifts in these two cases are 0.24 and 1.58 eV, respectively.⁴⁰ This larger shift is again probably due to increased charge transfer from the phosphorous to the oxygen because of the low electronegativity of the surrounding indium atoms. Thus, the same arguments used above for GaAs may be used here.

The case of GaSb (110) is much simpler than that of InP or GaAs. Both the Ga and Sb peaks shift simultaneously. Therefore, bonds are being broken in order to allow charge transfer from both the gallium and antimony atoms, resulting in the simultaneous formation of both gallium and antimony oxides.

C. Determination of the Escape Depth

The relative escape depth for electrons with kinetic energies between 20 and 200 eV may be determined from our experimental results quite simply and elegantly by merely plotting the ratio of the areas under the shifted and unshifted arsenic peaks, A_s/A_{sI} , as a function of photon energy. This curve is given in Fig. 16. The horizontal scale gives the kinetic energies of the electrons in the crystal. The photon energies that were used for each point are obtained by adding 40 eV (the approximate As-3d binding energy) to the given kinetic energies. The right-most vertical scale gives the actual ratio of the areas of the unshifted to shifted As-3d peaks as measured from the spectra of GaAs (110) + 10^{12} IO_2 for various photon energies. The minimum in the escape depth curve occurs around 60 eV kinetic energy ($h\nu = 100$ eV). The error bars associated with the points are due to the uncertainties in measuring the areas under the peaks.

One assumption that allows us to calculate the absolute escape depth is that there is one oxygen molecule (or atom, for this discussion the nature of the adsorbed species is irrelevant) per surface arsenic atom by an exposure of 10^{12} IO_2 . It seems adequately clear that saturation is reached at 10^{12} IO_2 , but we have yet done no measurements to determine the actual oxygen coverage at this exposure. However, from the oxidation data of Fig. 5, it does seem to be a reasonable assumption. The major source of error is introduced into the calculation when we try to fix the absolute value of the escape depth. This entails estimating the thickness of the topmost GaAs plus chemisorbed oxygen layer. This one thickness will then allow us to give an absolute value to the escape depth.

Consider the situation depicted in Fig. 17 where we assume a system composed of two uniform layers, surface and bulk. Here, we neglect the fact that the surface layer is only one molecular layer and thus not uniform. But, in the spirit of the calculation, this assumption will not introduce an unreasonable amount of error. The fraction of electrons that are excited from a small volume element in the surface layer and then emitted into the vacuum is given by

$$dN_s = ndx e^{-x/\lambda_1}, \quad 0 \leq x \leq x_1$$

where ndx is the number of electrons excited in the surface layer, λ_1 is the escape length in the surface layer, and x is the depth into the sample. The excited electron density n will be assumed to be constant through the material. Upon integration, this gives

$$N_s = n \int_0^{x_1} e^{-x/\lambda_1} dx = n\lambda_1 \left(1 - e^{-x_1/\lambda_1}\right)$$

where x_1 is the thickness of the surface layer. For this calculation to be valid, the attenuation length for the exciting radiation must be much larger than the electron escape depth, which definitely is the case here. Similarly, the fraction emitted into the vacuum from the bulk is

$$dN_B = \left(ndx e^{-x'/\lambda_2} \right) e^{-x_1/\lambda_1} \quad 0 \leq x' \leq \infty,$$

where λ_2 is the escape depth in the bulk, x' is the variable of integration, and the attenuation by the surface layer has been explicitly taken into account by e^{-x_1/λ_1} . For simplicity, we will assume $\lambda_1 = \lambda_2 \equiv L(E)$. Upon integration,

$$N_B = nL(E) e^{-x_1/L(E)}$$

Assuming, as we did in originally making Fig. 16, that the number of emitted electrons is proportional to the area under the appropriate peak in the photoemission spectrum, we may write

$$\frac{A_s}{A_{sI}} = \frac{N_B}{N_s} = \frac{1}{e^{x_1/L(E)} - 1}$$

or

$$L(E) = \frac{x_1}{\ln (A_s/A_{sI})^{-1} + 1} \quad (2)$$

Using tabulated values for the radii of arsenic and oxygen, we let $x_1 = 4 \pm 1.5 \text{ \AA}$.⁴¹ This, with Eq. (2), gives the $L(E)$ scale on the left-hand side of Fig. 16. The second scale on the right of Fig. 16 giving the molecular layers is obtained by dividing the nominal escape depth by the distance between the (110) planes which is approximately 4 \AA . At the minimum, the escape depth is $5.8 \pm 1.5 \text{ \AA}$ or approximately 1.5 molecular layers, substantiating our claims of a very large surface sensitivity. With this value for the escape depth, simple calculations show that a spectral feature from the bulk can no longer be seen if it is more than five molecular layers from the surface (this assumes a detectability limit of about 2% for well separated peaks; if the peaks are close together, we must assume a higher detectability limit).

D. Surface Chemical Shift⁴²

During the course of this work, we have studied the Ga-3d levels from the clean GaAs (110) surface over a wide range of photon

energies ($35 \text{ eV} \leq h\nu \leq 240 \text{ eV}$). This photon energy range enables us to probe between approximately 1.5 and 3 molecular layers, giving, first, primarily surface and, second, more bulk contributions to the spectra. If an appreciable chemical shift in the core levels between the atoms on the surface and in the bulk were present, it would definitely show up as a change in the full width at half maximum of the Ga-3d levels when a photon energy corresponding to a different escape depth was used. The fact is that we see no such effect to better than $\pm 0.1 \text{ eV}$. In view of the surface state model of Fig. 2, these results indicate that there must be enough redistribution of charge along the back bonds, possibly involving several molecular layers, to keep the total charge densities around the surface atoms the same as in the bulk. This charge redistribution may, in fact, be one of the reasons for the smearing of the spin orbit splitting of the Ga and As 3-d levels.

The lack of chemical shift between the surface and bulk atoms also implies that the ligand shifts due to each back bond, i.e., the bonds connecting the surface layer to the rest of the crystal, will be $4/3$ larger than the shifts due to the bonds in the bulk. The reason for this is, of course, that the same shift is due to three bonds for the atoms at the surface compared to four in the bulk. This again fits in well with the surface state model of Fig. 2 since the arsenic atoms at the surface must have more charge and the gallium atoms less than the corresponding atoms in the bulk.

E. Adsorption Kinetics

The difference in the adsorption kinetics between GaAs and GaSb is most clearly seen by comparing the oxygen uptake curves of Figs. 6 and

11. We can immediately make two observations. First, the shapes of these two curves for oxygen coverage versus exposure are rather different and, secondly, the GaSb adsorbs oxygen more readily than the GaAs. The second observation can be understood by considering the ionicities of Ga, As, and Sb. There is a larger electronegativity difference between Ga and As than between Ga and Sb. This would imply that the GaAs bond is stronger than that of GaSb, giving a surface that is more resistant to chemisorption of oxygen. In view of this argument, we would expect that InP would behave like GaAs since the electronegativity difference between In and P is also large. This is indeed the case, as was shown above in Fig. 12. The dependence of oxygen uptake with electronegativity difference that we see here agrees with the work of Mark and Creighton⁴³ in which they observe a decrease in oxygen uptake with increasing bonding ionicity.

We will defer a detailed analysis of the adsorption kinetics for GaAs and GaSb until a future publication,⁴⁴ at which time we will have more detailed information on the coverage as a function of exposure. However, as mentioned above, the difference in shape between the two curves in Figs. 6 and 11 is striking and deserves some attention drawn to it. This difference in shape seems to be very closely tied to the fact that oxygen chemisorbs to the GaAs surface, leaving it intact, while, for GaSb, the oxygen actually breaks back bonds and forms oxides. Thus, for GaAs, we expect saturation at half monolayer coverage with the rate of oxygen uptake being a function of the coverage. For GaSb, on the other hand, the coverage does not stop at half monolayer, as seen by the vertical scale of Fig. 11 (this scale was determined by comparing the oxygen coverages on the GaAs and GaSb spectra from the O2p intensity

and assuming half monolayer coverage at saturation for GaAs). In fact, the oxygen uptake for GaSb should be controlled mainly by diffusion of oxygen through the oxide layer to the unoxidized substrate. These possibilities will be explored in detail after we perform additional experiments on the oxygen coverage as a function of exposure.

Discussion of the behavior of the sticking coefficient, which can be obtained from the curves of coverage versus exposure,^{15,45,46} will also be deferred. However, at zero coverage, the approximate sticking coefficient is 2×10^{-4} for the GaSb surface and 8×10^{-10} for the GaAs surface. The measured sticking coefficient for GaAs is about five orders of magnitude smaller than what is reported in the literature for the cleaved GaAs (110) surface.¹⁵ The larger sticking probability reported in the literature could possibly be due to the fact that the precautions exercised¹⁵ to avoid effects of excited oxygen²⁰ were not sufficient or that the surfaces used were not perfect enough.^{12,24} Furthermore, in the other studies, saturation is seen at 10^6 LO_2 , whereas at this exposure we see less than 10% of saturation coverage (see Fig. 6).

F. Model for Oxidation of GaAs (110)

The sequence of events leading to the formation of a thick oxide layer on GaAs may be summarized as follows: (1) the (excited or unexcited) oxygen is first chemisorbed on the surface As atoms with no breaking of back bonds; (2) addition of excited oxygen leads to the breaking of bonds between the first and second layers in the crystal and the formation of less than two layers of $\text{As}_2\text{O}_5/\text{AsO}_2$ and Ga_2O_3 ; (3) further exposure to oxygen (excited) causes the oxidation to proceed

further into the bulk, allowing the newly formed arsenic oxides to sublime and leave an oxide layer mainly composed of Ga_2O_3 with small amounts of bulk As_2O_3 and free As. In the discussion that follows, we will elaborate on these points.

The chemisorption step, which is identical for both excited and unexcited oxygen, seems to be a necessary precursor to the breaking of back bonds. In order to break the Ga-As back bonds, we not only need excited oxygen, but also the presence of an oxygen chemisorbed to the arsenic dangling bond. Therefore, the energy carried to the surface by the excited oxygen must be coupled to the strain energy due to the previously chemisorbed oxygen. In fact, if a saturation coverage of oxygen is preadsorbed on the surface and then that surface is exposed to excited oxygen, two layers of GaAs can be oxidized by an exposure 20 times less than was necessary to gradually oxidize only the top layer (compare the top curve of Fig. 13 with the "heavily oxidized curve" of Fig. 14).

The initial oxidation results in the formation of the most oxygen rich oxide of arsenic, satisfying all four of the possible arsenic bonds. This oxide rather than As_2O_3 is formed because the part of the substrate being oxidized is in direct contact with the gaseous oxygen present in the chamber during exposure and enough oxygen is present to fully oxidize both the surface arsenic and gallium atoms. If the surface is oxidized even further, the substrate peaks are no longer visible, indicating that more than three or four molecular layers of oxide have been formed. This step in the oxidation is then the start of true oxide formation in which there is no longer a direct bonding between the GaAs lattice and most of the oxide and interface layer. In such a situation, as soon as a gallium or arsenic atom has broken its bonds to the underlying

lattice due to oxidation of a neighboring site, it is no longer constrained to follow the chemistry of the GaAs surface. Instead, the gallium and arsenic atoms are now free to follow their elemental chemistries. In the case of gallium and arsenic, the formation of Ga_2O_3 is favored over arsenic oxide formation, as seen by comparing their respective heats of formation.⁴⁷ Consequently, elemental gallium is oxidized more readily than elemental arsenic. Since there is now a layer of oxide through which the oxygen must diffuse in order to reach the substrate crystal, the amount of oxygen available for oxidation is limited and, consequently, the gallium will be oxidized first and then the arsenic. This is indeed the case, as seen by the fact that the thick oxide contains elemental arsenic as well as bulk As_2O_3 . No elemental Ga is seen in the spectrum for "very heavily oxidized" surface, indicating that the Ga may even be able to reduce As_2O_3 to elemental As. This could explain the presence of elemental As and no elemental Ga in the thick oxide. No $\text{As}_2\text{O}_5/\text{AsO}_2$ is present because oxygen is now scarce and the formation of the lower oxide of arsenic is more favorable. If the substrate were heated, resulting in a greater oxygen mobility through the oxide and, thus, a greater oxygen concentration at the interface, the situation would be much like that for the "heavily oxidized" spectrum, so $\text{As}_2\text{O}_5/\text{AsO}_2$ should then be present in the oxide layer.

Finally, there is very little arsenic (elemental or oxide) present in the thick oxide, indicating that the volatile As_2O_3 does sublime from the surface leaving an oxide rich in Ga_2O_3 with small amounts of As_2O_3 and elemental arsenic.

Caution should be exercised in trying to generalize these results to the polar faces or even (110) faces prepared by different techniques. For example, the work of Ranke and Jacobi¹² on the polar faces prepared either by ion bombardment and annealing or molecular beam epitaxy suggests that oxygen sticks to the surface gallium atoms. However, the sticking coefficients reported in those studies were significantly higher than those for the cleaved (110) surface. These larger sticking coefficients were attributed to the presence of Ga atoms on the polar surface with unsaturated bonds.¹² From our results on the oxidation of GaAs (110) with excited oxygen, we saw that as soon as a Ga-As bond is broken, i.e., as soon as an unsaturated Ga bond is created, the Ga atom immediately becomes oxidized. Thus, if the polar surfaces studied by Ranke and Jacobi do indeed have unsaturated Ga bonds, it is not at all surprising that oxygen bonds preferentially to the Ga atoms. In fact, it would be entirely consistent with the results of our work. Therefore, it seems clear that the chemisorption properties of the various faces are very dependent on the integrity of the surface which is a function of both the fundamental properties of the particular face as well as the surface preparation technique. The resistance to oxidation exhibited by the cleaved GaAs (110) surfaces compared to the other surfaces or (110) surfaces prepared by techniques other than cleavage implies that the cleaved surfaces are more intact, i.e., all the surface atoms have saturated bonds, since the resistance to oxidation is characteristic of a low density of unsaturated bonds.

IV. SUMMARY

In the preceding discussions, we have shown that, when the cleaved (110) surface of GaAs is exposed to molecular, unexcited oxygen, only chemisorption to the surface arsenic atoms takes place. Oxygen either does not bind or is very loosely bound to the surface gallium atoms. No back bonds are broken even for very large exposures. Bulk oxide formation can be induced by exciting the oxygen. Initially, the chemistry of adsorption with excited oxygen is the same, though 500 times faster, as for the unexcited oxygen, i.e., only chemisorption taking place. However, after an appreciable fraction of a monolayer is on the surface ($\sim 10^5$ L excited O_2), further exposure causes the surface to truly oxidize, forming both arsenic and gallium oxides. Upon further doses of excited oxygen, a small amount of free arsenic is seen along with the gallium oxide and a diminished amount of arsenic oxide. This indicates that, with the formation of thicker oxides, the gallium and arsenic revert to their elemental chemistries in which the gallium will oxidize more readily than arsenic and that the arsenic oxide, because of its volatility, sublimates from the surface, leaving behind a film consisting mainly of gallium oxide.

We have also studied the oxidation of InP (110) and GaSb (110). Consistent with electronegativity arguments, the InP behaves like the GaAs, whereas the GaSb behaves quite differently. In GaSb, oxidation takes place even with exposure to only unexcited oxygen, without the intermediate chemisorption step characteristic of the GaAs and InP. The rates of oxygen uptake for GaAs and GaSb were compared and found to be quite different.

The escape depth of GaAs was measured for electron kinetic energies between 20 and 200 eV. At the minimum, which is at 60 eV electron kinetic energy ($h\nu = 100$ eV), the escape depth was found to be 5.8 ± 1.5 Å. Even with this high surface sensitivity, no appreciable chemical shift between the surface and bulk could be detected.

Thus, by using this very surface sensitive photoemission technique, we have been able to study, inobtrusively, the chemistry at the surface of several III-V semiconductors from the chemisorption stage right up to the formation of thick oxide films.

ACKNOWLEDGMENT

We would like to thank Prof. W. A. Harrison for helpful discussions and the staff of the Stanford Synchrotron Radiation Project for their

REFERENCES

1. For a review of the latest developments in the field of GaAs surfaces and devices, consult the Proceedings of the 3rd Annual Conference on the Physics of Compound Semiconductor Interfaces in J. Vac. Sci. Technol. 13, No. 4 (1976).
2. P. E. Gregory, W. E. Spicer, S. Ciraci, and W. A. Harrison, App. Phys. Lett. 25, 511 (1974); P. E. Gregory and W. E. Spicer, Phys. Rev. B 13, 725 (1976) and Surf. Sci. 54, 229 (1976); W. E. Spicer and P. E. Gregory, Crit. Rev. Solid State Sci. 5, 231 (1975).
3. W. A. Harrison, Surf. Sci. 55, 1 (1976).
4. H. C. Gatos and M. C. Lavine, J. Electrochem. Soc. 107, 427 (1960); H. C. Gatos, J. Appl. Phys. 32, 1232 (1961); H. C. Gatos, J. Electrochem. Soc. 122, 287C (1975).
5. A. U. Mac Rae and G. W. Gobeli, in Semiconductors and Semimetals, Vol. 2, Physics of III-V Compounds, Eds., R. K. Willardson and A. C. Beer (Academic Press, New York, 1966), pp. 115-137; A. U. Mac Rae, Surf. Sci. 4, 247 (1966).
6. A. R. Lubinsky, C. B. Duke, B. W. Lee, and P. Mark, Phys. Rev. Lett. 36, 1058 (1976); C. B. Duke, A. R. Lubinsky, B. W. Lee, and P. Mark, J. Vac. Sci. Technol. 13, 761 (1976).
7. W. E. Spicer, I. Lindau, P. E. Gregory, C. M. Garner, P. Pianetta, and P. W. Chye, J. Vac. Sci. Technol. 13, 780 (1976).
8. J. D. Levine and S. Freeman, Phys. Rev. B 2, 3255 (1970).
9. D. J. Miller and D. Haneman, Phys. Rev. B 3, 2918 (1971).
10. R. Ludeke and L. Esaki, Phys. Rev. Lett. 33, 653 (1974) and R. Ludeke and A. Koma, Phys. Rev. Lett. 34, 817 (1975).

11. R. W. Nosker, P. Mark, and J. D. Levine, *Surf. Sci.* 19, 291 (1970).
12. W. Ranke and K. Jacobi, *Surf. Sci.* (in press), and references given therein.
13. P. Pianetta, I. Lindau, C. M. Garner, and W. E. Spicer, *Phys. Rev. Lett.* 35, 1356 (1975), and P. Pianetta, Ph.D. Thesis, Stanford University, 1976 (unpublished).
14. K. Jacobi and W. Ranke, *J. Elect. Spectrosc.* 8, 225 (1976).
15. R. Dorn, H. Lüth, and G. J. Russell, *Phys. Rev. B* 10, 5049 (1974).
16. H. Froitzheim and H. Ibach, *Surf. Sci.* 47, 713 (1975).
17. R. Ludeke and A. Koma, *Crit. Rev. Solid State Sci.* 5, 259 (1975), and *J. Vac. Sci. Technol.* 13, 241 (1976).
18. W. Ranke and K. Jacobi, *Surf. Sci.* 47, 525 (1975).
19. The objections to the interpretation presented in Ref. 17 are explained in: P. W. Chye, P. Pianetta, I. Lindau, and W. E. Spicer, 4th Annual Conference on the Physics of Compound Semiconductor Interfaces, Princeton, New Jersey, Feb 1977.
20. P. Pianetta, I. Lindau, C. M. Garner, and W. E. Spicer, *Phys. Rev. Lett.* 37, 1166 (1976), and references given therein.
21. S. Doniach, I. Lindau, W. E. Spicer, and H. Winick, *J. Vac. Sci. Technol.* 12, 1123 (1975).
22. I. Lindau and W. E. Spicer, *J. Electron Spectrosc.* 3, 409 (1974); M. Klasson, J. Hedman, A. Berndtsson, R. Nilsson, and C. Nordling, *Physica Scripta* 5, 93 (1972).
23. K. Siegbahn, *J. Electron Spectrosc.* 5, 3 (1975); U. Gelius, *Physica Scripta* 9, 133 (1974); T. D. Thomas, *J. Am. Chem. Soc.* 92, 4184 (1970); J. M. Hollander and D. A. Shirley, *Ann. Rev. Nucl. Sci.* 20, 435 (1970).

24. H. Ibach, *Surf. Sci.* 53, 444 (1975).
25. G. F. Derbenwick, D. T. Pierce, and W. E. Spicer, Methods of Experimental Physics (Academic Press, New York, 1974), Vol. 11, pp. 89-92.
26. F. C. Brown, R. Z. Bachrach, S. B. M. Hagstrom, N. Lien, and C. H. Pruett, in Vacuum Ultraviolet Radiation Physics, Eds., E. E. Koch, R. Haensel, and C. Kunz (Pergamon, New York, 1974), pp. 785-787.
27. The sample with $n = 0.5 \times 10^{18} \text{ cm}^{-3}$ will be referred to sample LD1. It was used in the work of Refs. 7 and 20. In Ref. 7, it was called sample II. The sample with $n = 3.5 \times 10^{17} \text{ cm}^{-3}$ will be called sample LD3; it was used in the work of Refs. 7 (Fig. 1), 13, and 20.
28. This sample was also used in the work described in Refs. 7, 20, and the work of P. W. Chye, I. A. Babalola, T. Sukegawa, and W. E. Spicer, *Phys. Rev. Lett.* 35, 1602 (1975).
29. The Thoria-coated iridium filament in the ion gauge allows lower filament temperatures ($< 800^\circ\text{C}$) for a given emission current, relative to a Tungsten filament, so that no CO is generated by the hot filament.
30. In all the discussions that follow, we will refer to the molecular, unexcited oxygen simply as oxygen or O_2 . We will refer to the oxygen excited by the ion gauge only as excited oxygen since the detailed nature of excited oxygen has never been established. Certainly, many forms must be considered, e.g., oxygen ions, atomic oxygen, ozone, molecular oxygen in excited form, etc.
31. A. Huijser and J. van Laar, *Surf. Sci.* 52, 202 (1975), and J. van Laar and A. Huijser, *J. Vac. Sci. Technol.* 13, 769 (1976).

32. I. Lindau, P. Pianetta, and W. E. Spicer, Phys. Lett. 57A, 225 (1976), and Proceedings of the International Conference on the Physics of X-ray Spectra, 30 Aug-2 Sep 1976, National Bureau of Standards, Gaithersburg, Maryland.
33. H. Ibach, K. Horn, R. Dorn, and H. Lüth, Surf. Sci. 38, 433 (1973); R. J. Archer and G. W. Gobeli, J. Phys. Chem. Sol. 26, 343 (1965).
34. W. Gudat and D. E. Eastman, J. Vac. Sci. Technol. 13, 831 (1976).
35. M. K. Bahl, R. O. Woodall, R. L. Watson, and K. J. Irgolic, J. Chem. Phys. 64, 1210 (1976).
36. G. Leonhardt, A. Berndtsson, J. Hedman, M. Klasson, R. Nilsson, and C. Nordling, Phys. Stat. Sol. (b) 60, 241 (1973).
37. G. Schön, J. Electron Spectrosc. 2, 75 (1973).
38. Surface Science Laboratories (Palo Alto, Ca.), ESCA Analytical Service Report #9-576.
39. R. W. G. Wyckoff, Crystal Structures (Interscience, New York, 1965) Volumes 2 and 3.
40. J. Hedman, M. Klasson, R. J. Lindberg, and C. Nordling, Electron Spectroscopy, D. A. Shirley, Ed. (North Holland, Amsterdam, 1972), p. 681.
41. Handbook of Chemistry and Physics, R. C. Weast, Ed. (The Chemical Rubber Company, Cleveland, Ohio, 1972), p. E-55.
42. J. E. Houston, R. L. Park, and G. E. Laramore, Phys. Rev. Lett. 30, 846 (1973), and references contained therein for other studies on surface chemical shifts.
43. P. Mark and W. F. Creighton, Appl. Phys. Lett. 27, 400 (1975).
44. P. Pianetta, I. Lindau, and W. E. Spicer (in preparation).

45. D. O. Hayward and B. M. W. Trapnell, Chemisorption (Butterworths, London, 1964), pp. 86-107.
46. R. Gomer, Solid State Phys. 30, 93 (1975).
47. Ref. 42, p. D-45.

Table I

EXPERIMENTAL BINDING ENERGIES REFERENCED TO THE VALENCE BAND MAXIMUM. The experimental accuracy is estimated to be ± 0.05 eV with the largest uncertainty being in the determination of the valence band maximum. See text for discussion on difficulties in determining the binding energies with respect to the Fermi level.

Compound	Level	E_B (eV)
GaAs	Ga 3d	19.0
	As 3d	40.8
GaSb	Ga 3d	19.4
	Sb 4d 5/2	32.1
	Sb 4d 3/2	33.2
InP	In 4d	17.7
	P 2p	128.4

Table II

EXPERIMENTAL BINDING ENERGY DIFFERENCES (eV), FROM THIS WORK,
BETWEEN THE SHIFTED AND UNSHIFTED Ga AND As 3d LEVELS FOR THE
CLEAN AND OXIDIZED GaAs (110) SURFACE. The entries were
obtained by subtracting the binding energies of the levels
in the top row from those in the left most column.

ΔE_B (eV)	AsIII	AsII	AsI	Ga(As)	GaI	(Ga)As
AsIV ^a	2.8	-1.4 ^c	0.3	3.2	24.0	25.0
AsIII		-4.2	-2.5	0.4	21.2	20.2
AsII			1.7	4.6	25.4	26.4
AsI				2.9	23.7	24.7
Ga(As) ^b					20.8	21.8
GaI						1.0

- (a) The designations AsI, AsII, etc. refer to the labeling of Fig. 14.
- (b) Ga(As) refers to As in GaAs; similarly, (Ga)As refers to Ga in GaAs.
- (c) The negative shift means that AsII has a larger binding energy than AsIV.

Table III

EXPERIMENTAL BINDING ENERGY DIFFERENCES (eV), FROM THE REFERENCES CITED, BETWEEN THE SHIFTED AND UNSHIFTED Ga AND As 3d LEVELS FOR VARIOUS COMPOUNDS OF Ga AND As.

The data is presented in the same format as that of Table II.

ΔE_B (eV)	As ₂ O ₅ 35	As ₂ O ₃ 35,36	Ga(As) 36,38,40,41	As 35,36	Ga ₂ O ₃ 36,37,38	(Ga)AsO ₄ 38	(Ga)As 36,38,40,41	Ga 36,37
Ga(As)O ₄ ^a	-0.3	1.4	4.6	4	25.4	25.4	26.3	27.4
As ₂ O ₅		1.7	4.9	4.3	25.7	25.7	26.6	27.7
As ₂ O ₃			3.2	2.6	24.0	24.0	24.9	26.0
Ga(As) ^b				-0.6	20.8	20.8	21.7	22.8
As					21.4	21.4	22.3	23.4
Ga ₂ O ₃						0	0.9	2
(Ga)AsO ₄ ^a							0.9	2
(Ga)As								1.1

(a) This compound outgassed considerably during initial pumpdown (see text for discussion of the relevance of the shifts measured for this compound).

(b) See text for the discussion about reliably determining the shifts between the semiconductor compounds and the other compounds in this table.

Table IV

EXPERIMENTAL LIGAND SHIFTS OF THE Ga AND As 3d LEVELS FOR
THE COMPOUNDS WHOSE SHIFTS WERE GIVEN IN TABLE III

Compound	ΔE_e (eV) ^a	ΔE_j (eV) ^b	n_j^c	Ligand
Ga(As)O ₄ ^d (dissociated)	4.0	1.0	4	(-/=) O ^e
As ₂ O ₅	4.3	0.87	3	- O
		1.7	1	= O
As ₂ O ₃	2.6	0.87	3	- O
Ga(As)	-0.6	-0.15	4	- Ga
Ga ₂ O ₃	2.0	0.33	6	- O
(Ga)AsO ₄ ^d (dissociated)	2.0	0.33	6	- O
(Ga)As	1.1	0.28	4	- As
Ga(As)O ₄ ^f (ideal)	3.5	0.87	4	- O
or AsO ₂				
(Ga)AsO ₄ ^f (ideal)	1.3	0.33	4	- O
or GaO ₂				

- (a) ΔE_e is the binding energy shift with respect to the free element.
- (b) ΔE_j is the ligand shift referenced to the free element where $\Delta E_e = n_j \Delta E_j$, summed over all j .
- (c) n_j is the number of ligands of the given kind.
- (d) This compound decomposed in the spectrometer, so it is a mixture of As with four oxygen ligands and Ga₂O₃ (see text for details).
- (e) These ligands are assumed to be single bonds with some double bond character (see text); thus, this ligand shift is larger than the ligand shift for a single As-oxygen bond.
- (f) Note these are not experimentally determined shifts; these shifts are calculated for the ideal structures using the ligand shifts given in the rest of the table.

FIGURE CAPTIONS

- Fig. 1. Schematic of the GaAs lattice terminated on the ideal (110), (111), and $(\bar{1}\bar{1}\bar{1})$ surfaces. The view is along the $(1\bar{1}0)$ direction.
- Fig. 2. The reconstructed (110) surface with an energy level diagram showing the location of the filled (As-derived) and empty (Ga-derived) surface states.
- Fig. 3. Electron energy distribution curve for cleaved GaAs (110) taken at a photon energy of 240 eV showing the core levels and many-electron lines that are accessible in these studies.
- Fig. 4. Diagram of the photoemission spectrometer showing the electron energy analyzer, sample carousel, Au evaporator, light port, and sample cleaver. The anvil support bars on the cleaver, which are fastened to the stationary part of the linear motion feedthrough, have been cut away to show the wedge-shaped, tungsten-carbide blade.
- Fig. 5. EDC's of clean and oxygen exposed n-type GaAs (110) at $h\nu = 100$ eV. The exposure of 1×10^{12} LO_2 ($1 \text{ L} = 10^{-6}$ torr-sec) was made on sample LD1 while the smaller exposures were all on sample LD3.
- Fig. 6. The relative oxygen uptake of the GaAs (110) surface as a function of exposure determined from the area under the shifted As-3d levels (Δ). The area of the unshifted As-3d levels (∇) is also plotted. The scale on the right assumes saturation is reached at 10^{12} LO_2 .

- Fig. 7. The valence band of clean n-type GaAs (110) and the same surface exposed to the indicated exposures. These curves are blow-ups of the valence band region of Fig. 5.
- Fig. 8. EDC's of clean and oxygen exposed n-type GaSb (110) at $h\nu = 100$ eV. Notice that both the Ga and Sb shift simultaneously with increasing oxygen exposure.
- Fig. 9. EDC's of GaSb exposed to $5 \times 10^8 \text{ LO}_2$ for three photon energies showing the variation in the cross-section of the Sb-4d levels versus photon energy.
- Fig. 10. a) Comparison of clean GaSb (110) and GaSb (110) + $2 \times 10^{10} \text{ LO}_2$.
b) Comparison of clean GaAs (110) and GaAs (110) + 10^{12} LO_2 .
- Fig. 11. The relative oxygen uptake of the GaSb (110) surface as a function of exposure, determined from the area under the O-2p level. The vertical scale is obtained by comparing the areas under the O-2p in the spectra of Fig. 8 to the areas under the O-2p in Fig. 5 for GaAs.
- Fig. 12. EDC's of clean and oxygen exposed p-type InP (110). The In-4d level was measured at $h\nu = 80$ eV and the P-2p at $h\nu = 160$ eV.
- Fig. 13. EDC's of clean p-type GaAs (110) and the clean surface exposed to excited oxygen at $h\nu = 100$ eV.
- Fig. 14. EDC's of n-type GaAs (110), LD1, for the clean surface, the clean surface + 10^{12} LO_2 , the previous surface + $5 \times 10^5 \text{ L}$ excited oxygen with a 0.4 ma ion gauge emission current ("HEAVILY OXIDIZED"), and the clean surface exposed to $5 \times 10^5 \text{ L}$ excited oxygen with 4.0 ma ion gauge emission current ("VERY HEAVILY OXIDIZED").

Fig. 15. Bonding schemes for the As and Ga compounds in Table IV:

- (a) GaAs lattice; (b) As_4O_6 molecule; (c) As_4O_{10} molecule;
(d) GaAsO_4 lattice (see text).

Fig. 16. Plot of the ratio of the unshifted to shifted As-3d levels as a function of electron kinetic energy for the GaAs (110) surface + 10^{12} IO_2 (right-most scale). The other two scales give the escape depth in Angstroms and molecular layers (see text).

Fig. 17. Model of GaAs (110) surface plus saturation coverage of chemisorbed oxygen. N_S (N_B) is the number of electrons emitted into the vacuum from the surface (bulk).

IDEAL GaAs LATTICE

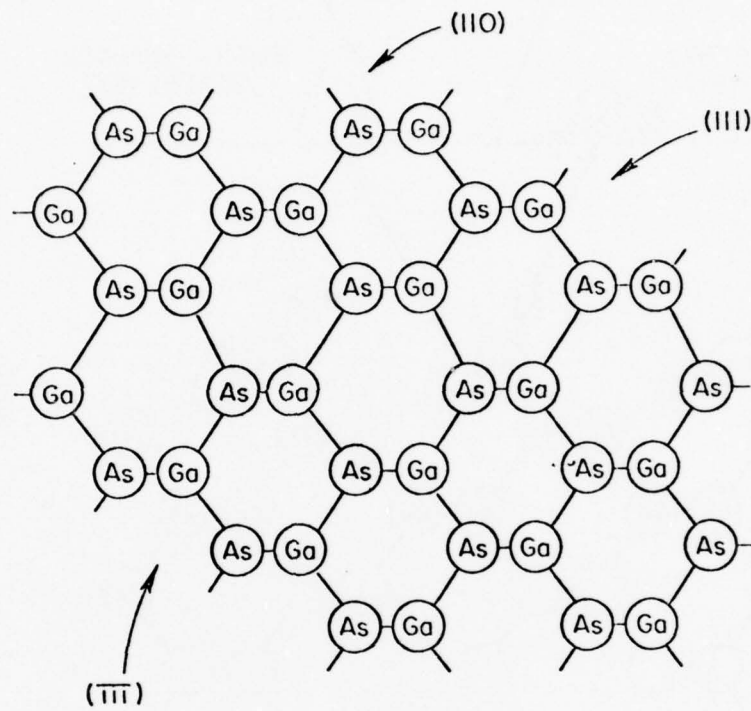
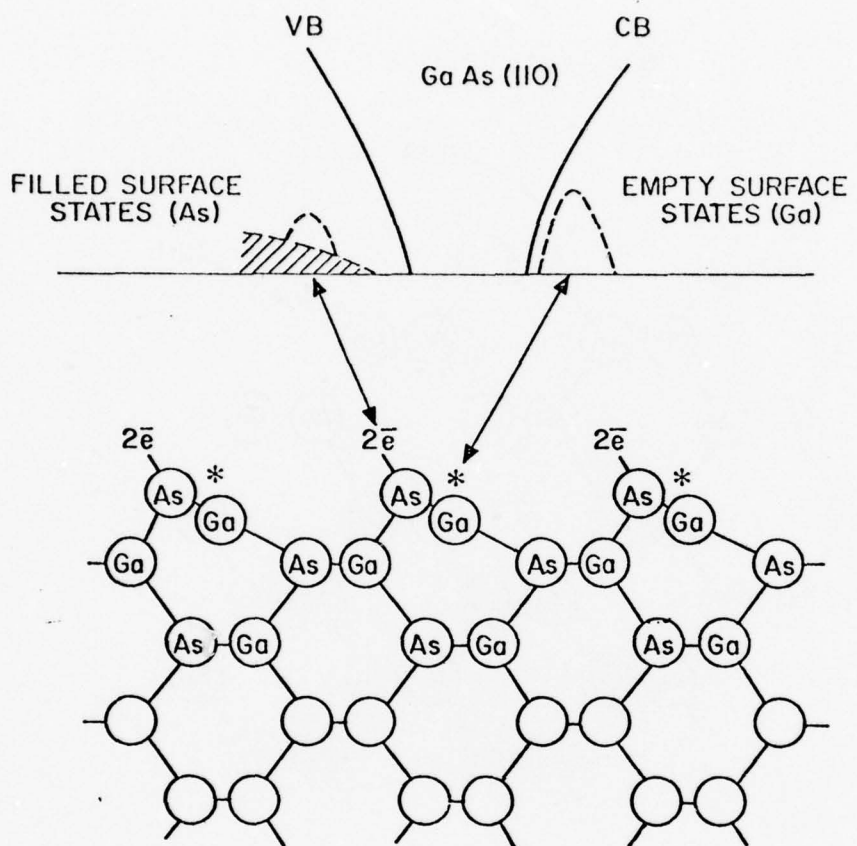


Fig 1.



* LOCATION OF EMPTY SURFACE STATE

Fig 2

5%
New York

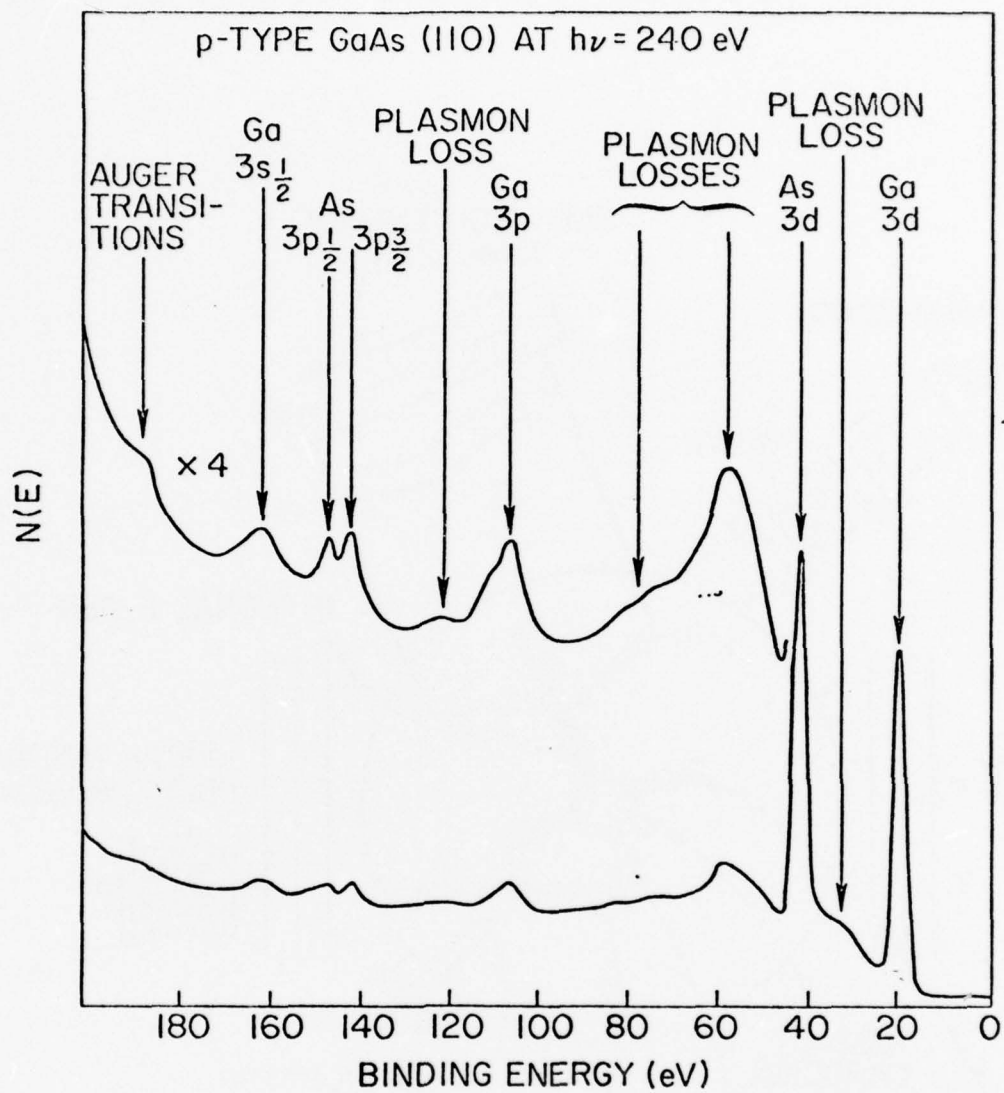


Fig 3

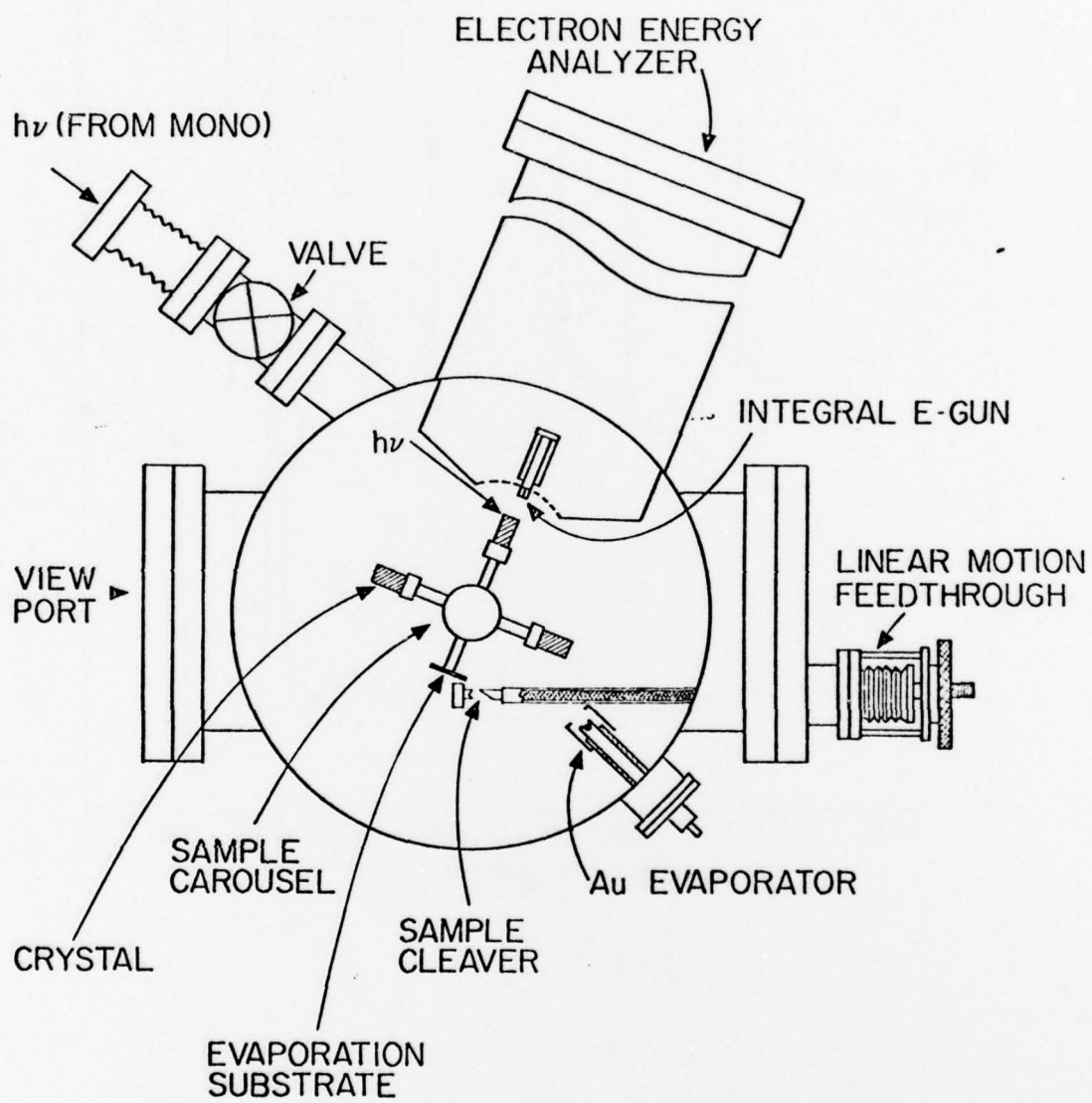


Fig 4

OXIDATION OF n-TYPE GaAs(110) AT $\hbar\omega=100$ eV

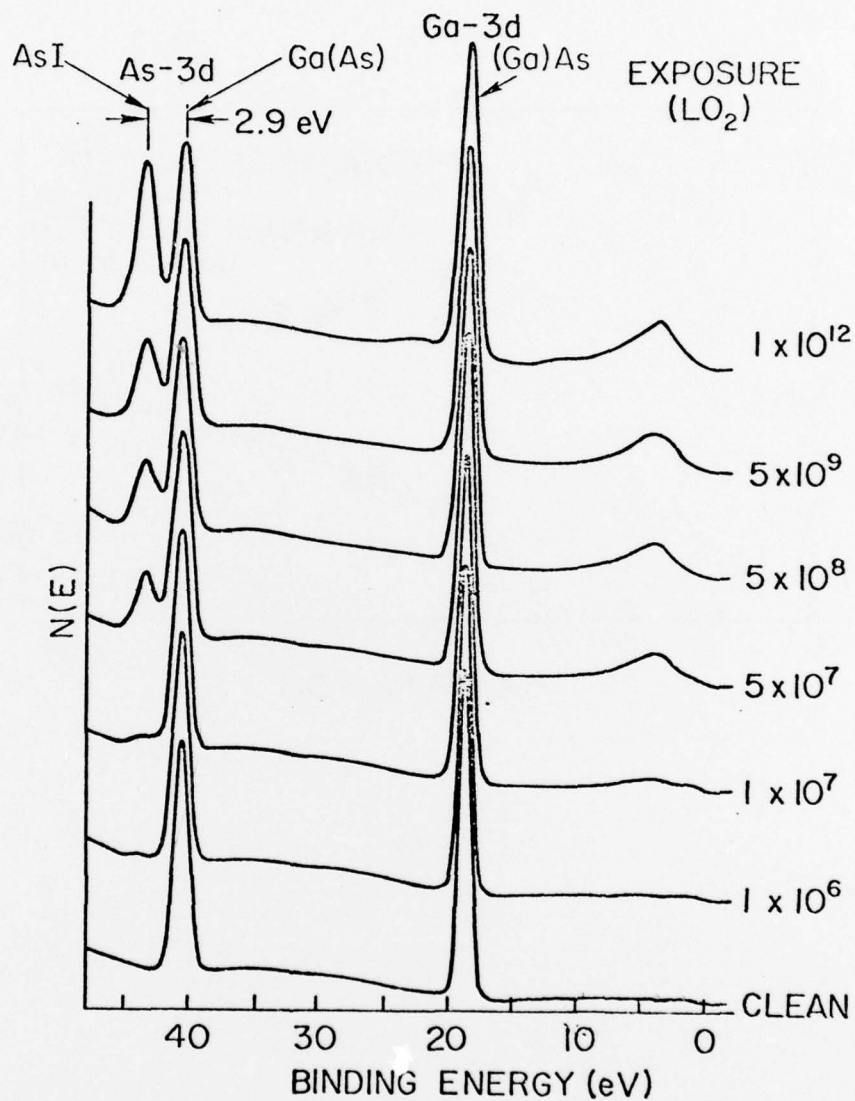


Fig. 5

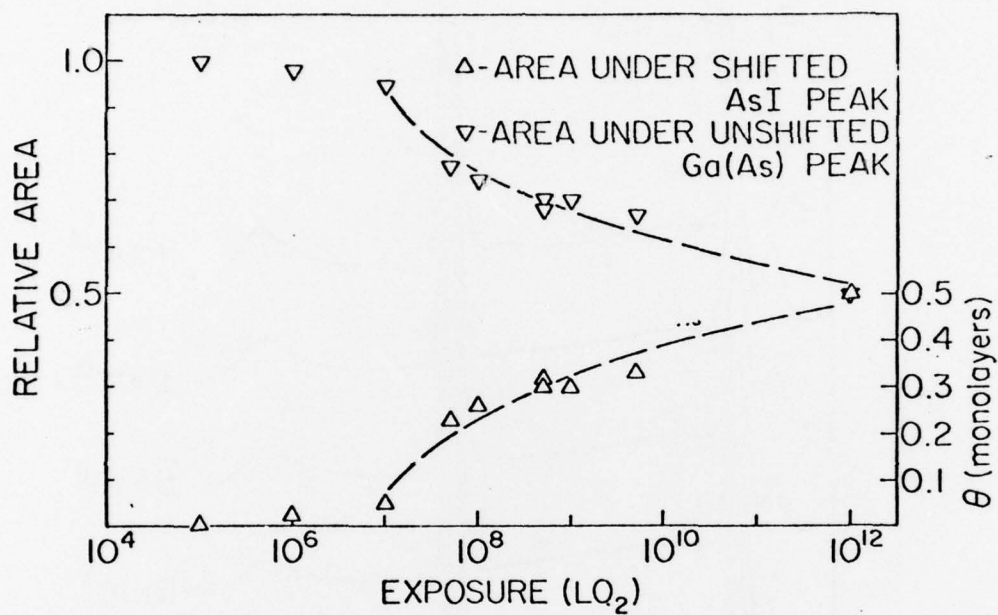


Fig 6

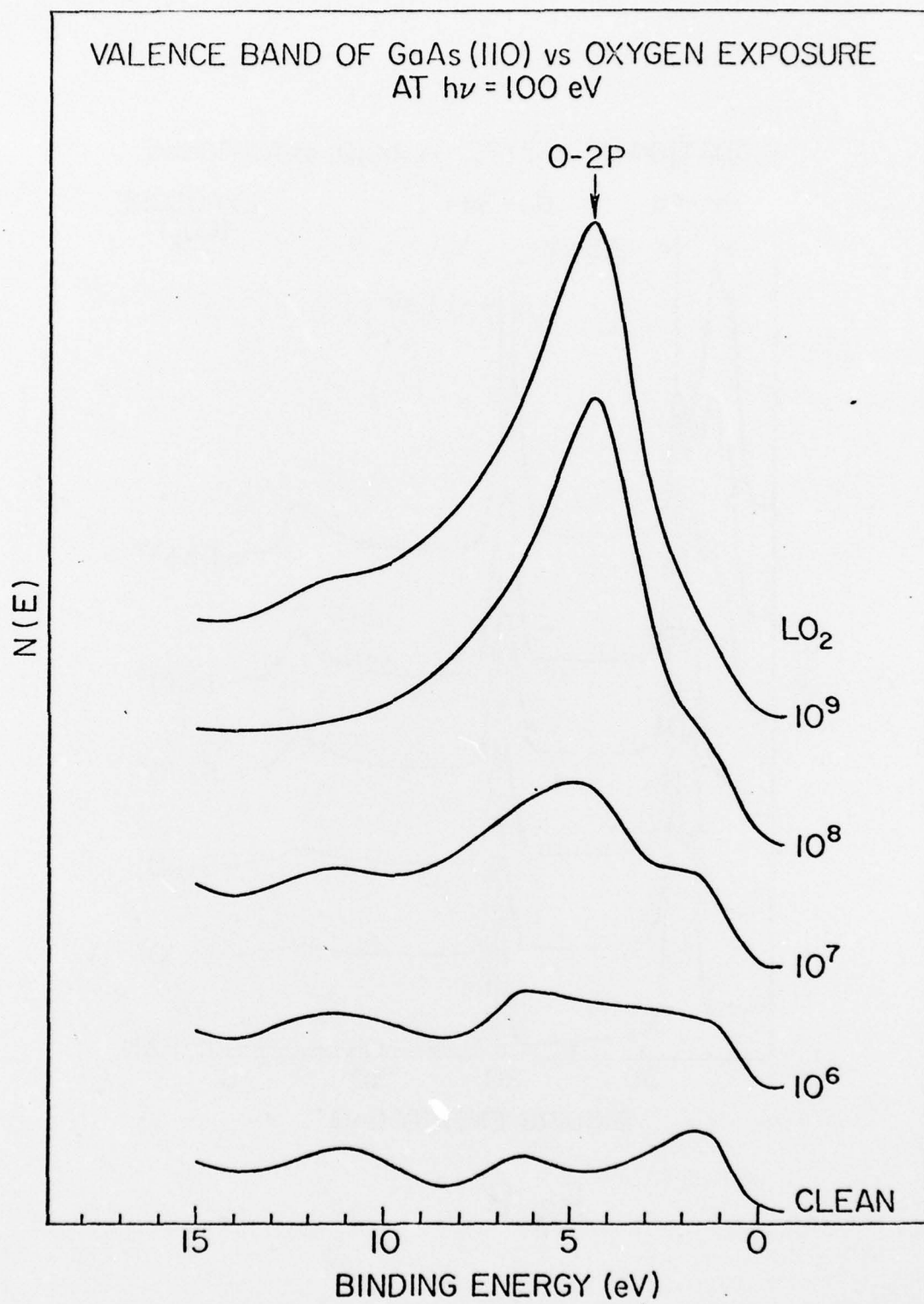


Fig 7

OXIDATION OF n-TYPE GaSb(110) at $\hbar\omega = 100\text{ eV}$

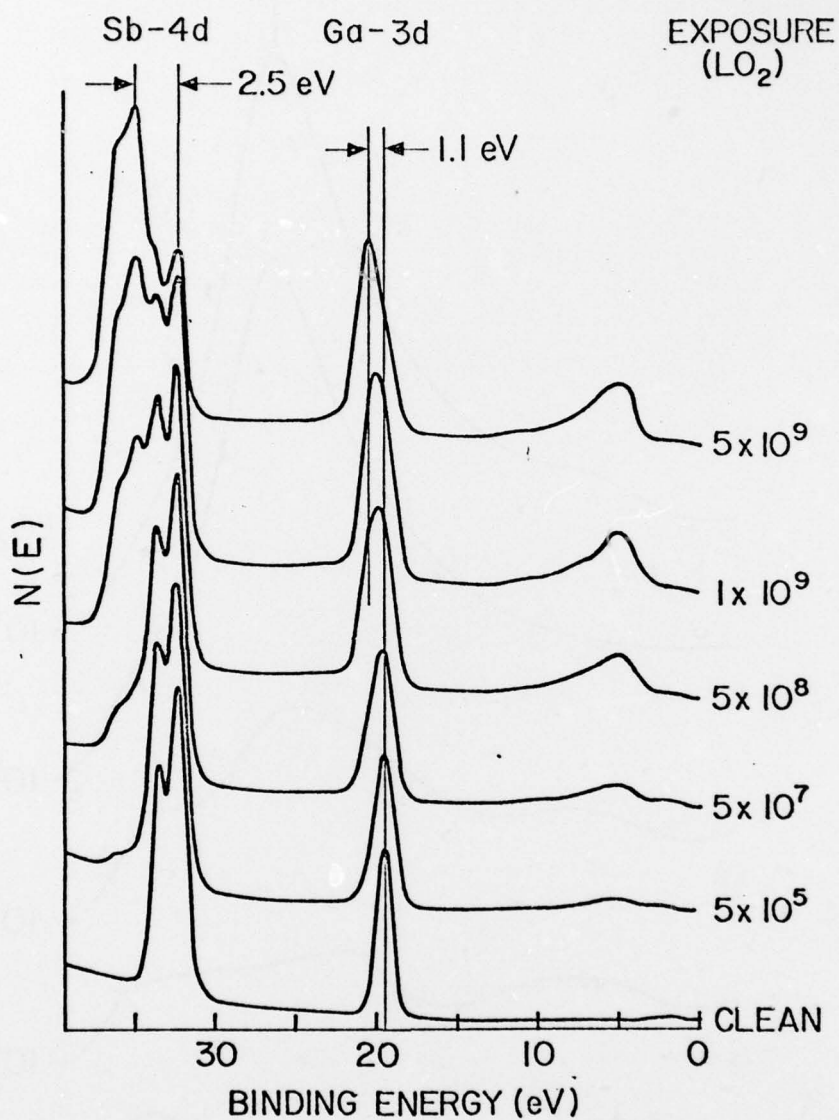


Fig 8

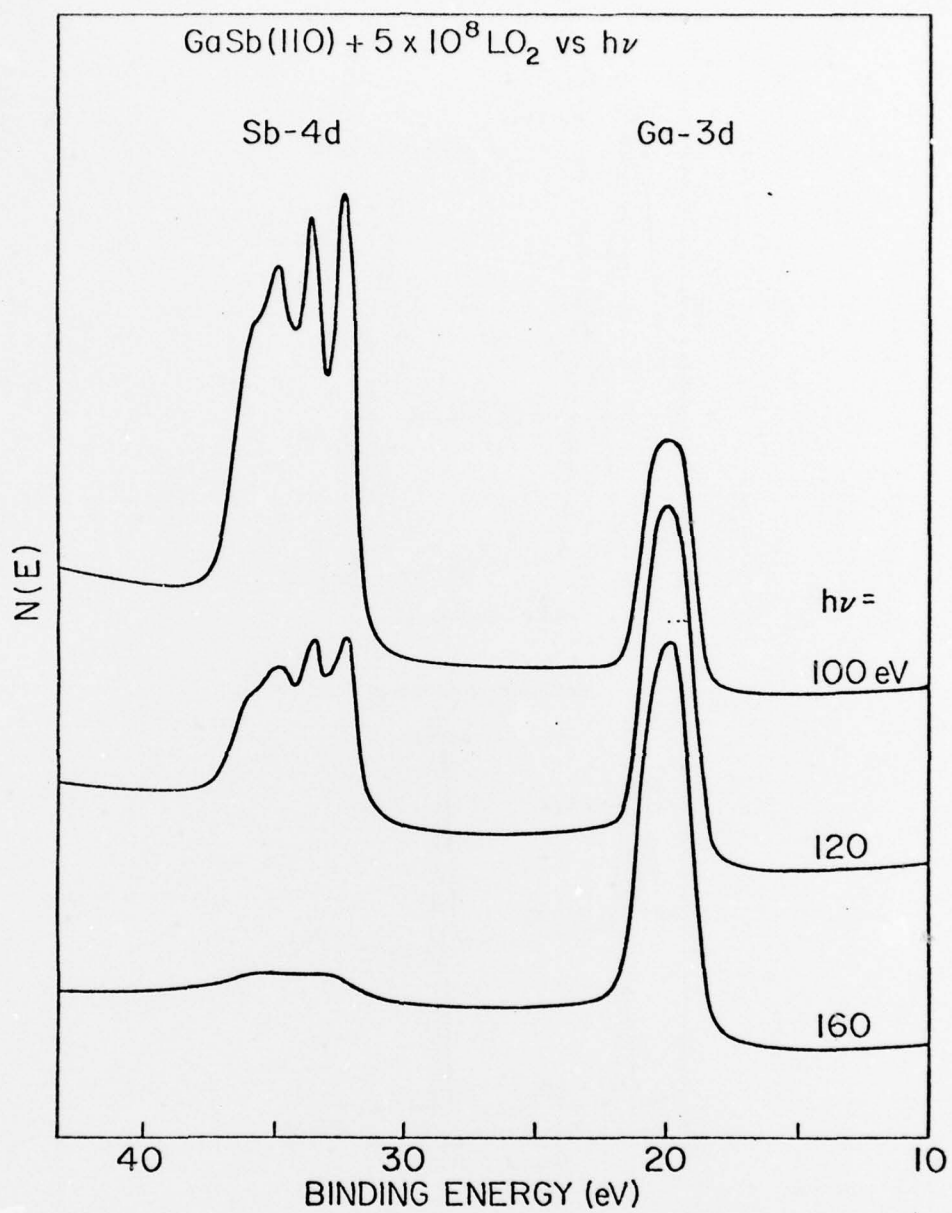


Fig 9

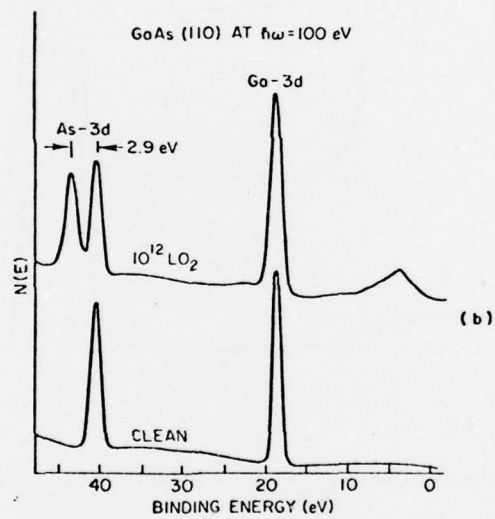
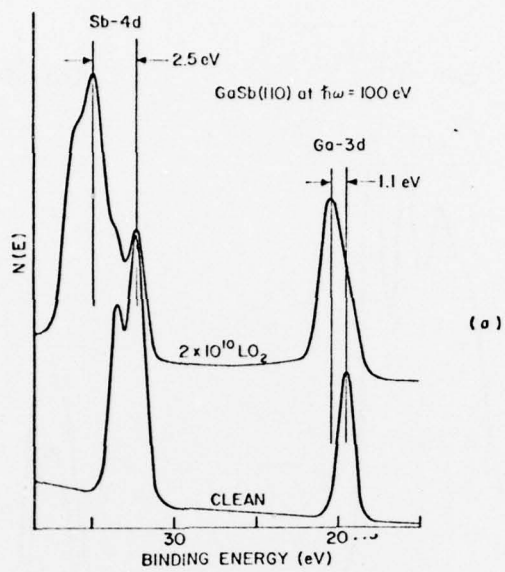


Fig. 10

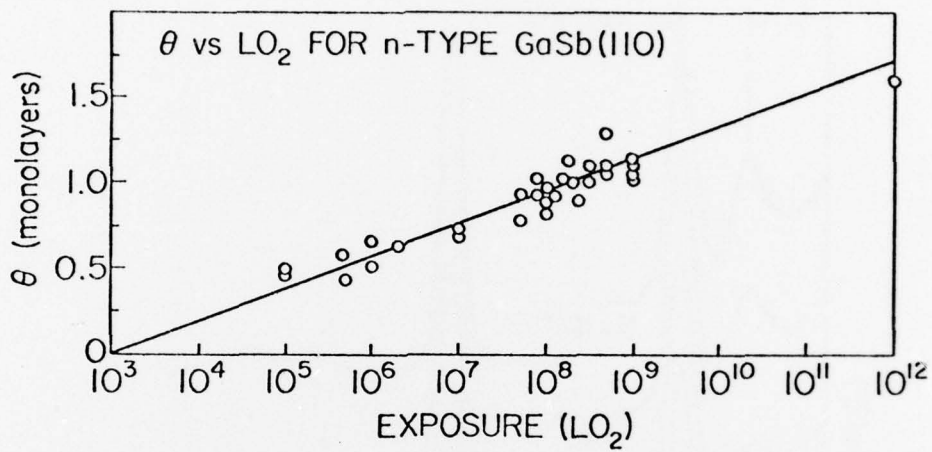


Fig. 11

OXIDATION OF p-type InP(110)
P-2p EXPOSURE In-4d
($\hbar\nu = 160\text{eV}$) (LO_2) ($\hbar\nu = 80\text{eV}$)

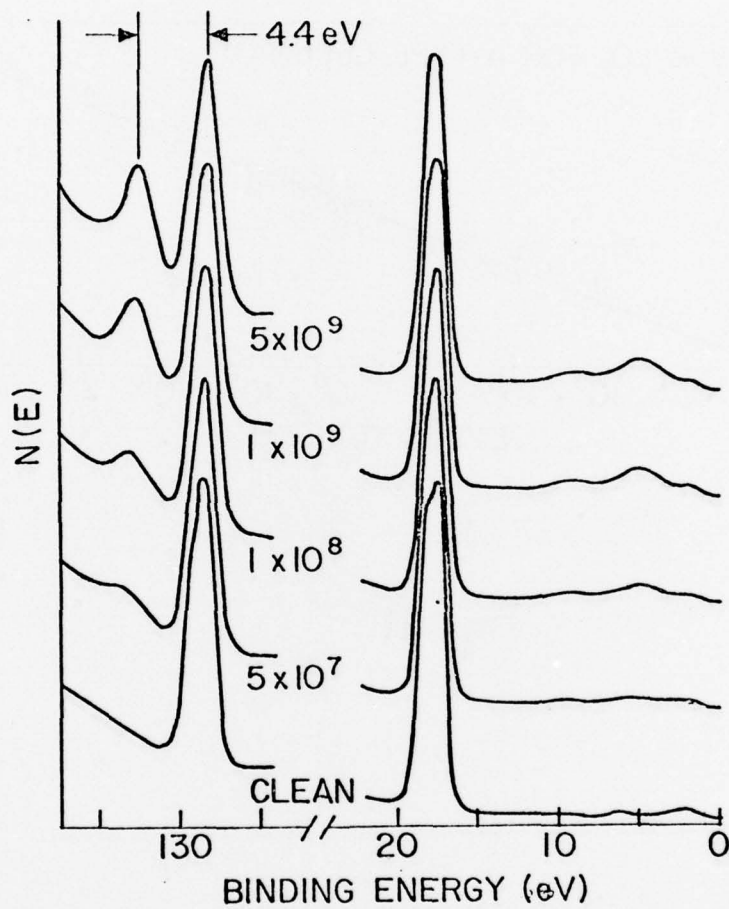


Fig 12

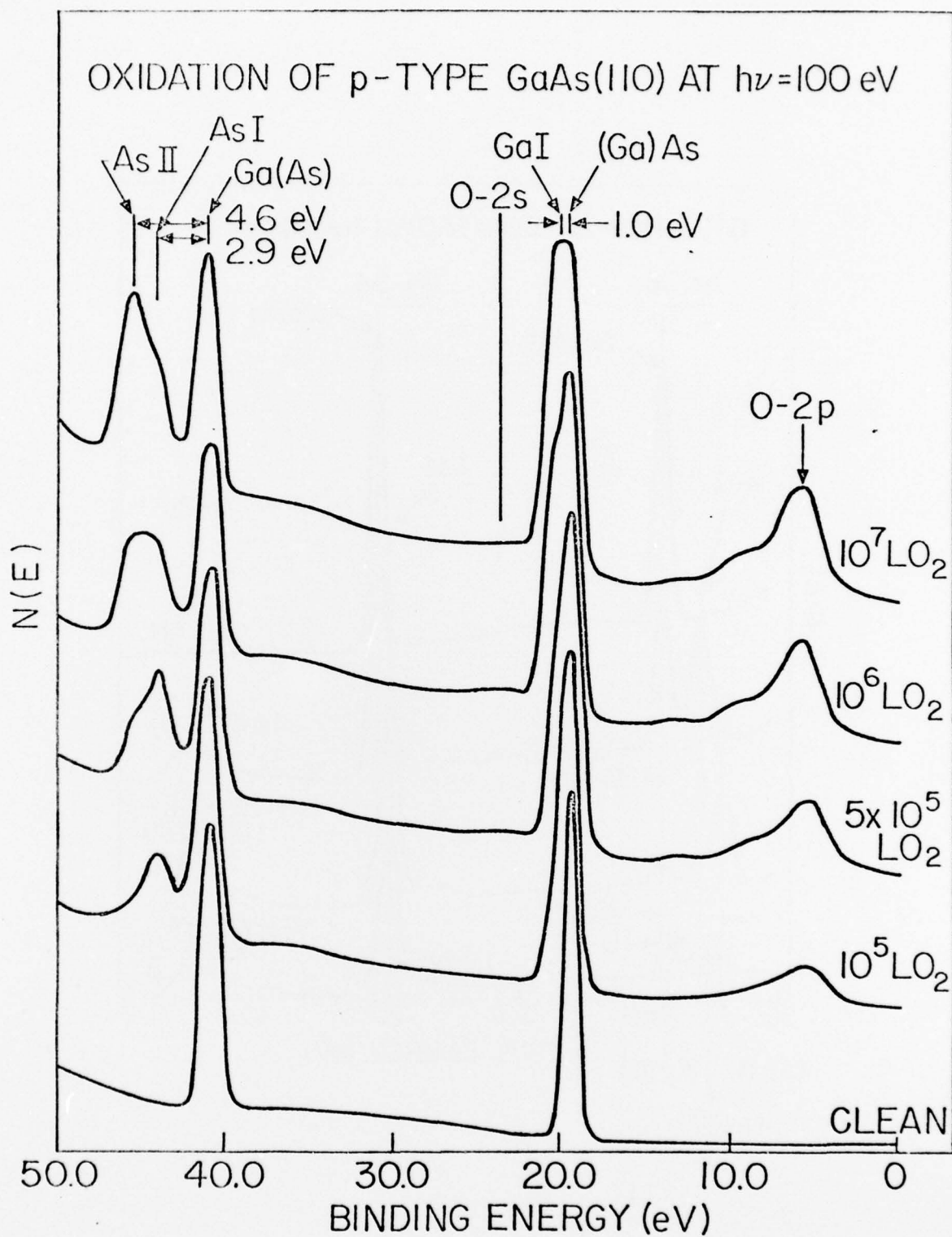


Fig 13

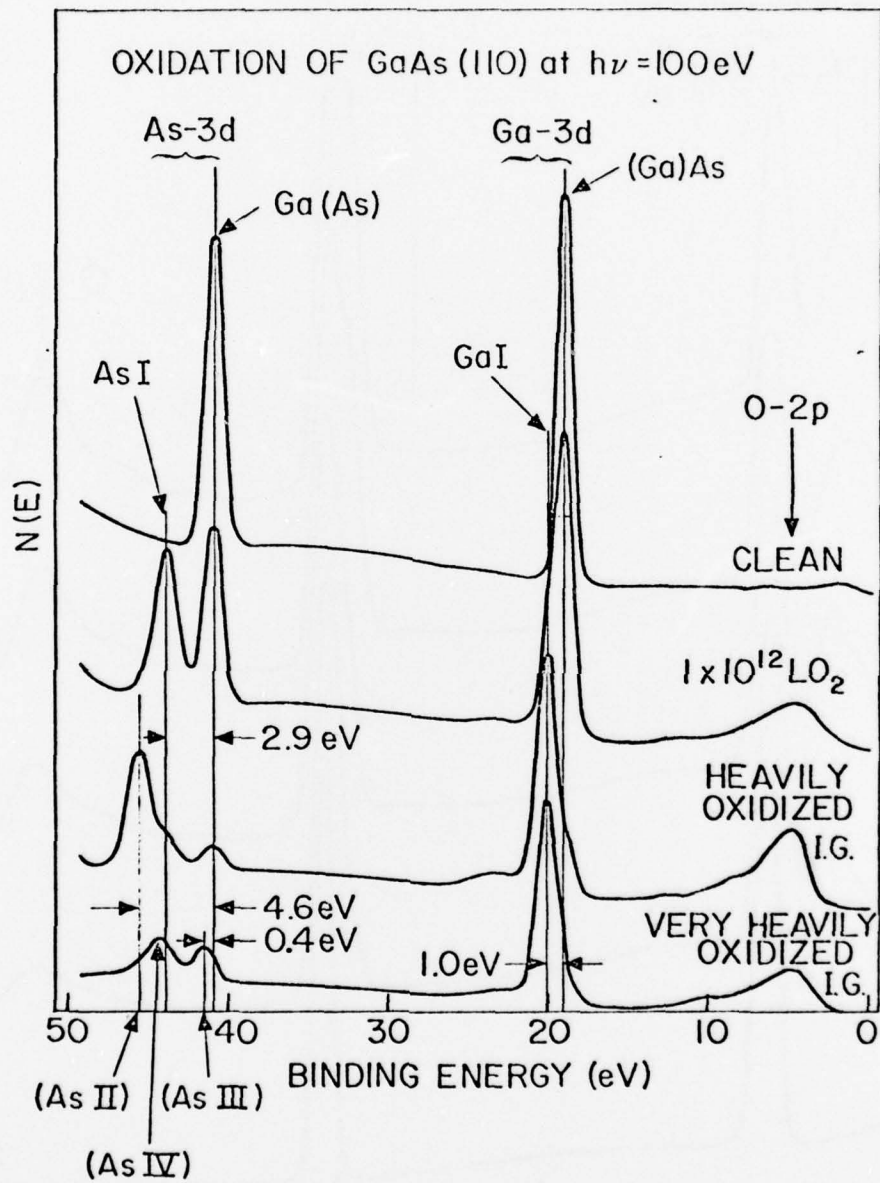
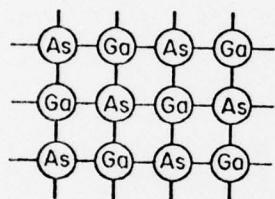
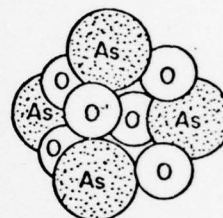


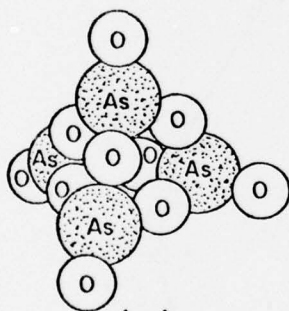
Fig 14



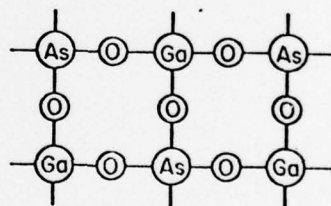
(a)



(b)



(c)



(d)

Fig 15

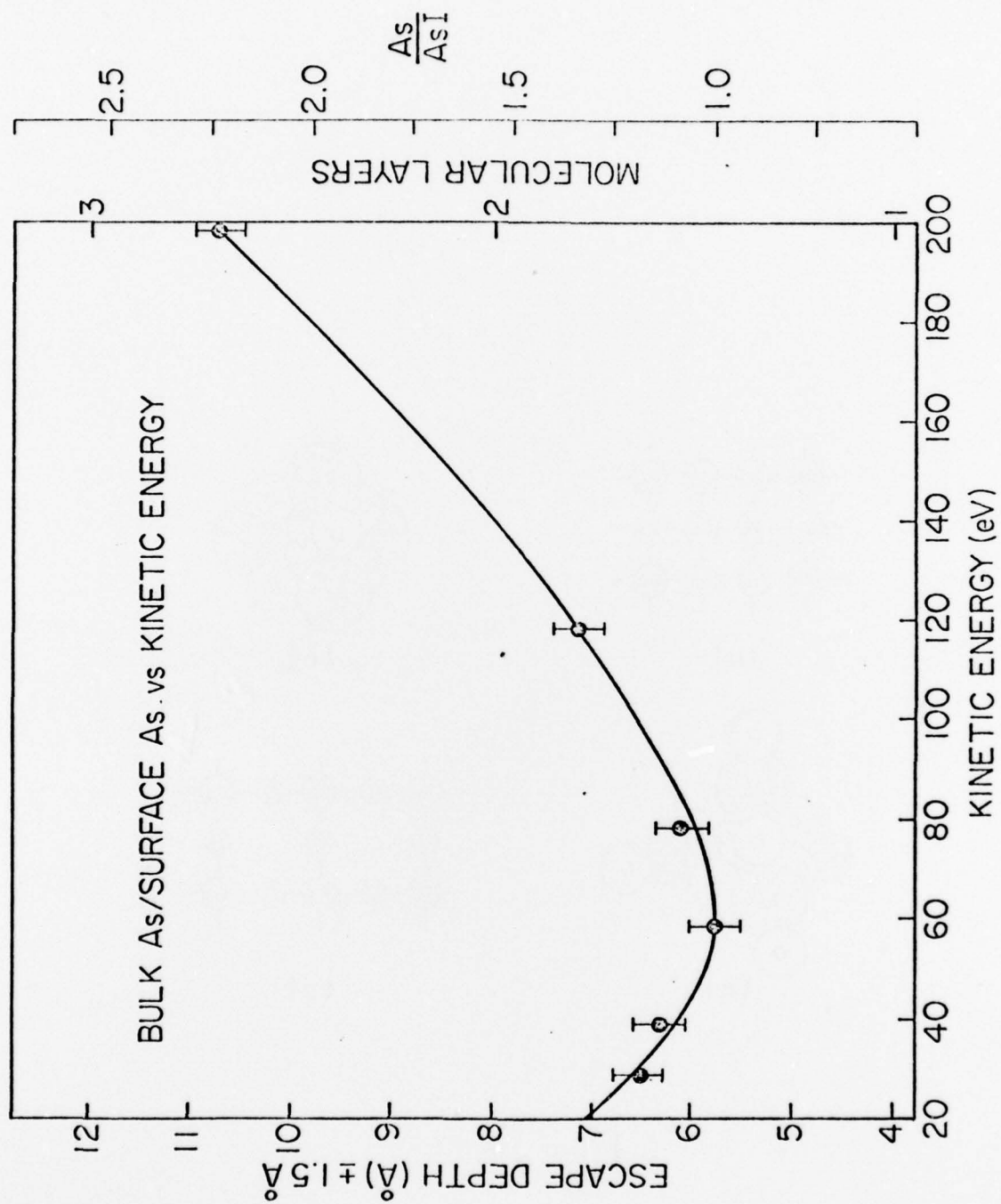


Fig 16

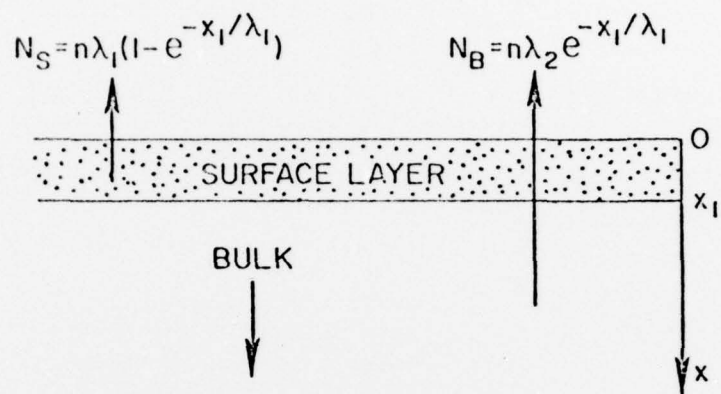


Fig 17